Global chromatin changes induced by altered tonicity interferes with DNA damage response signaling and DNA double-strand break repair

Inaugural-Dissertation

zur

Erlangung des Doktorgrades

Dr. rer. nat.

der Fakultät für Biologie

an der

Universität Duisburg-Essen

vorgelegt von

Lisa Marie Krieger

aus Castrop-Rauxel

August, 2018

Die der vorliegenden Arbeit zugrunde liegenden Experimente wurden am Institut für Medizinische Strahlenbiologie am Universitätsklinikum Essen durchgeführt.

1. Gutachter: Prof. Dr. George Iliakis

2. Gutachter: Prof. Dr. Stefan Westermann

Vorsitzender des Prüfungsausschusses: Prof. Dr. Christian Johannes

Tag der mündlichen Prüfung: 05. Dezember 2018

“Nucular. It’s pronounced nucular.“

Homer J. Simpson, 1998

Table of contents

1) List of abbreviations VII

2) List of figures XIV

3) List of tables XIX

4) Introduction 10

4.1) Ionizing radiation (IR) 12

4.1.1) Physical fundamentals of IR 13

4.1.2) DNA damage induction by IR 17

4.2) Mechanisms of DDR 17

4.2.1) Cell cycle checkpoint activation 18

4.3) DSB repair by homologous recombination 20

4.4) DSB repair by end joining processes 23

4.4.1) Classical non-homologous end joining 23

4.4.2) Alternative end joining 25

4.5) Single-strand annealing 27

4.6) Organization of DNA in chromatin 28

4.6.1) Histone modifications function as platform for DSB signaling and repair proteins 31

4.6.2) Chromatin dynamics upon DNA damage induction 33

4.6.3) Changes in extracellular tonicity globally alters chromatin 35

5) Aim of the thesis 38

6) Material and Methods 39

6.1) Material 39

6.2) Methods 43

6.2.1) Cell culture 43

6.2.2) X-ray irradiation 44

6.2.3) Hypotonic and hypertonic cell treatment 44
6.2.4) Histone extraction 45
6.2.5) SDS-PAGE and immunoblotting 45
6.2.6) Pulsed-field gel electrophoresis 46
6.2.7) Clonogenic survival assay 49
6.2.8) Confocal laser scanning microscopy 49
6.2.9) Flow cytometry 53
6.2.10) Cytogenetics 55
6.2.11) Quantification and statistics 56
7) Results 57
7.1) Retinal pigment epithelial cell line 57
7.2) Effects of global chromatin relaxation achieved by incubation in hypotonic medium 59
7.2.1) Chromatin is globally relaxed by decreased tonicity 59
7.2.2) Chromatin relaxation delays cell growth 65
7.2.3) Global chromatin relaxation inhibits cell division transiently 68
7.2.4) DDR signaling is inhibited in globally relaxed chromatin 71
7.2.5) Hypotonic treatment disturbs G2-checkpoint machinery 75
7.2.6) Global chromatin relaxation by hypotonic treatment shifts DSB repair from main repair pathways to SSA 80
7.2.7) Radiosensitivity to killing is minimally affected by global chromatin relaxation 90
7.2.8) Effects of globally relaxed chromatin on DDR signaling and cell proliferation are fully reversible 91
7.3) Global chromatin condensation induced by hypertonic treatment affects DDR signaling and DSB repair 96
7.3.1) Increase in extracellular NaCl concentration globally condenses chromatin 96

7.3.2) Global chromatin condensation inhibits cell growth 100

7.3.3) DNA damage checkpoint is masked after hypertonic treatment 103

7.3.4) DSB repair and signaling are disturbed upon global chromatin condensation 104

7.3.5) Cells get radiosensitized when chromatin is globally condensed ... 115

7.4) Radiosensitization after global chromatin condensation may result from recovery after transfer to normal growth conditions 117

8) Discussion 121

8.1) Global chromatin relaxation impairs DDR signaling and DSB repair, but reveals a pathway switch to SSA 121

8.2) Global chromatin condensation achieved by incubation in hypertonic medium arrests cells in G1-, G2- and M-phase and impairs resection-dependent DSB repair 130

9) Summary 134

10) Zusammenfassung 136

11) References 138

12) Supplementary data 151

12.1) Calculation of CCP 151

12.1.1) Image processing by ImageJ 151

12.1.2) MatLab codes for calculating CCP 152

12.2) Clonogenic survival assays 159

13) Acknowledgements 160

14) Curriculum vitae 161

15) Declarations 163

1) List of abbreviations

5'-dRP	5'-deoxyribose-5'-phosphate
53BP1	p53 binding protein
6-4PP	6-4 photoproduct
Ab	antibody
ADP	adenosine diphosphate
AFIGE	asymmetric field inversion gel electrophoresis
altEJ	alternative end joining
AP	apurinic/apyrimidinic
approx.	approximately
APS	ammonium persulfate
ARR	access-repair-restore
ATM	ataxia telangiectasia mutated kinase
ATP	adenosine triphosphate
ATR	ATM and Rad3 related kinase
BER	base excision repair
bidest.	double-distilled
BLM	Bloom syndrome RecQ like helicase
bp	base pair
BRCA1/2	breast cancer susceptibility protein 1/2
BrPBlue	bromophenol blue
BSA	bovine serum albumin
CCP	chromatin condensation parameter
CDC25A/C	cell division cycle 25A/C
CDK(s)	cyclin-dependent kinase(s)
CHD	chromodomain DNA helicase-binding
Chk1/2	checkpoint kinase 1/2

CLSM	confocal laser scanning microscopy
cm	centimeter
cm²	square centimeter
cNHEJ	classical non-homologous end joining
CPD	cyclobutane-pyrimidine dimer
CtBP	C-terminal binding protein
CtIP	CtBP interacting protein
d	day
DAPI	4’,6-diamidino-2-phenylindole
DDR	DNA damage response
DEQ	dose equivalent
D-loop	displacement loop
DMEM	dulbecco’s modified eagle’s medium
DMSO	dimethyl sulfoxide
DNA	deoxyribonulceic acid
Dna2	DNA replication ATP-dependent helicase/nuclease DNA2
DNA-PK	DNA-dependent protein kinase
DNA-PKcs	catalytic subunit of DNA-PK
DR	death receptor
DSB(s)	double-strand break(s)
DSBR	double-stranded break repair
dsDNA	double-stranded DNA
dsRNA	double-stranded RNA
DTT	dithiothreitol
EC	euchromatin
EDTA	ethylenediaminetetraacetic acid
EdU	5-Ethynyl-2’-deoxyuridine
e.g.	exempli gratia

EGFP	enhanced GFP
ERCC1	excision repair cross complementing 1
et al.	et alii
EtBr	ethidium bromide
etc.	et cetera
EtOH	ethanol
eV	electronvolt
Exo1	exonuclease 1
FBS	fetal bovine serum
FC	flow cytometry
FDR	fraction of DNA released
G1/2-phase	gap 1/2 phase
GFP	green fluorescent protein
Gy	Gray
h	hour
H1	histone H1
H2AK15ub	ubiquitylated lysine15 of histone H2A
H2AX	histone variant H2AX
H_2O	water
H_2O_2	hydrogen peroxide
H3	histone H3
H3K4/9/27/36/79	lysine4/9/27/36/79 of histone H3
H3K9ac	acetylated lysine9 of histone H3
H3K9me3	trimethylated lysine9 of histone H3
H3pS10	phosphorylated serine10 of histone H3
H4K20	lysine20 of histone H4
H4K20me2	dimethylated lysine20 of histone H4
HAT	histone acetyl transferase

HC	heterochromatin
HDAC1/2	histone deacetylase
HJ	Holliday junction
HP1	heterochromatin protein 1
HRR	homologous recombination repair
hTert	human telomerase catalytic subunit component
i	inhibitor
i.e.	id est
IF	immunofluorescence
IFMSB	Institut für Medizinische Strahlenbiologie
IR	ionizing radiation
IRIF	ionizing radiation induced foci
ISWI	imitation SWI
K	lysine
KAP1	KRAB-ZFP-associated protein 1
kb	kilobases
KCl	potassium chloride
keV	kilo electronvolt
kg	kilogram
KRAB	Krüppel-associated box
kV	kilovolt
LET	linear energy transfer
LIF	leica image format
Lig1/3/4	ligase 1/3/4
m	meter
mA	milliampere
MCPH1	microcephalin 1
MDC1	mediator of DNA damage checkpoint protein 1

MeOH	methanol
µg	microgram
MI	mitotic index
min	minute/s
mM	millimolar
µm	micrometer
µM	micromolar
MMEJ	microhomology mediated end joining
MMSET	multiple myeloma SET domain
M-phase	mitosis phase
Mre11	meiotic recombination 11
MRN complex	Mre11/Rad50/Nbs1 complex
NaCl	sodium chloride
NASA	National Aeronautics and Space Administration
Nbs1	nibrin
NER	nucleotide excision repair
NHEJ	non-homologous end joining
NLS	N-Lauroylsarcosine
nm	nanometer
nM	nanomolar
nt	nucleotide
NuRD	nucleosome remodeling and deacetylase
PAGE	polyacrylamide gel electrophoresis
pATM	phospho-ATM
PARP	poly-(ADP-ribose)-polymerase
PARylation	poly-ADP-ribosylation
PAXX	paralog of XRCC4 and XLF
PBS	phosphate buffered saline

PE	plating efficiency
PFA	paraformaldehyde
PFGE	pulsed-field gel electrophoresis
PI	propidium iodide
PI3K	phosphoinositide 3-kinase
PIKK	phosphoinositide 3-kinase-related protein kinase
Plk1	polo-like kinase 1
PMT	photomultiplier tube
pol μ/λ/θ	polymerase μ/λ/θ
PTM	posttranslational modification
puro	puromycin
RIF1	RAP1-interacting factor 1
RNA	ribonucleic acid
RNF8/168/169	ring finger protein 8/168/169
ROS	reactive oxygen species
RPA	replication protein A
RPE-1	retinal pigment epithelial cell line 1
rpm	revolutions per minute
RT	room temperature
RVD	regulatory volume decrease
RVI	regulatory volume increase
s	second
SD	standard deviation
SDS	sodium dodecyl sulfate
SDSA	synthesis dependent strand annealing
SE	standard error
Ser	serine
SET	Su(var)3-9-Enhancer-of-zeste-Trithorax domain

SETDB1	SET domain bifurcated 1
S-phase	synthesis phase
SSA	single-strand annealing
SSB(s)	single-strand break(s)
ssDNA	single-stranded DNA
SWI/SNF	switch/sucrose non-fermentable
TBE	tris, boric acid, EDTA
TBS	tris buffered saline
TBS-T	tris buffered saline and Tween 20
TCA	trichloroacetic acid
TdT	terminal deoxynucleotidyl transferase
TEMED	tetramethylethylenediamine
TNF	tumor necrosis factor
TRAIL	(TNF)-related apoptosis-inducing ligand
U2OS	human bone osteosarcoma epithelial cell line
UK	Universitätsklinikum
UV	ultra violet
XLF	XRCC4-like factor
XPF	Xeroderma Pigmentosum group F
XRCC1/2/3/4	X-ray cross-complementing protein 1/2/3/4
V	volt
WB	western blot
wt	wild type
γH2AX	phosphorylated H2AX at serine139
ZFP	zinc-finger protein

2) List of figures

Figure 1 Types of DNA damages and repair. 11

Figure 2 Spectrum of electromagnetic radiation. 13

Figure 3 Illustration of Compton process and photoelectric process. 15

Figure 4 Distribution of DNA damaging events after exposure to H_2O_2 or low and high LET radiation. 16

Figure 5 Illustration of DDR. 18

Figure 6 Cell cycle checkpoint activation in mammalian cells after IR. 19

Figure 7 Schematic mechanism of HRR. 22

Figure 8 Schematic drawing of cNHEJ mechanism. 24

Figure 9 Schematic drawing of altEJ mechanism. 26

Figure 10 Schematic drawing of SSA mechanism. 27

Figure 11 Multiple levels of DNA compaction. 29

Figure 12 PTMs of core histones. 30

Figure 13 Activation of ATM promotes signaling cascade on damaged chromatin. 32

Figure 14 Schematic model of relations between disordered mechanisms of cell volume regulation (RVD and RVI). 35

Figure 15 Representative PFGE gels and corresponding dose response and repair kinetics curves. 47

Figure 16 Principle of confocal microscopy. 50

Figure 17 Images representing different steps of processing in order to determine the CCP (Irianto, Lee, and Knight 2014). 52

Figure 18 Growth curve of RPE-1 cells. 58

Figure 19 Influence of 75 mM NaCl on RPE-1 cell diameter and cell volume. 59

Figure 20 CCP of RPE-1 cells treated with chromatin relaxing medium. 60

Figure 21 Representative images of metaphases formed in isotonically treated cells. 61

Figure 22 Representative images of metaphases formed in hypotonically treated cells. 62

Figure 23 Chromosome length quantification of metaphases formed in isotonically and hypotonically treated cells. 63

Figure 24 Global chromatin relaxation changes levels of histone H1 and EC/HC markers. 64

Figure 25 Cell number and corresponding cell cycle distribution of an asynchronous cell population after different treatment times at low concentrations of NaCl to induce global chromatin relaxation..... 66

Figure 26 Progression through the cell cycle of cells synchronized in G2-phase and treated with medium containing 75 mM NaCl. 68

Figure 27 Proportion of mitotic cells under chromatin relaxing conditions. 69

Figure 28 MI of RPE-1 cells treated with PIKK inhibitors when chromatin is globally relaxed. 70

Figure 29 Formation of γH2AX foci after incubation in hypotonic medium. 72

Figure 30 Formation of pATM foci under hypotonic conditions..... 73

Figure 31 Formation of 53BP1 foci after treatment in hypotonic medium. 74

Figure 32 MI of RPE-1 cells after 2 Gy of IR and subsequent isotonic or hypotonic treatment. 75

Figure 33 Cell cycle distribution of synchronized RPE-1 cells after treatment in hypotonic medium. 77

Figure 34 MI of RPE-1 cells under hypotonic conditions and treatment with PIKK inhibitors. 78

Figure 35 Formation of γH2AX and 53BP1 foci after IR in cells adapted to hypotonic medium..... 79

Figure 36 Global chromatin relaxation impairs DSB repair as measured by PFGE. 81

Figure 37 altEJ in RPE-1 cells remains unaffected by global chromatin relaxation. 82

Figure 38 DNA end resection and HRR in globally relaxed chromatin. 84

Figure 39 Cell viability and GFP expression in U2OS reporter cell lines. 85

Figure 40 Effects of global chromatin relaxation on HRR as measured by the U2OS DR-GFP reporter assay. 86

Figure 41 Schematic drawn of EJ5-GFP (A) and EJ2-GFP (B) (Moscariello et al. 2015). 87

Figure 42 Effects of global chromatin relaxation on end joining events measured using the U2OS EJ5-GFP (A) and U2OS EJ2-GFP (B) reporter cell lines. 88

Figure 43 Effects of global chromatin relaxation on SSA repair measured using the U2OS SA-GFP reporter cell line. 89

Figure 44 Clonogenic survival of RPE-1 cells when chromatin is globally relaxed. 90

Figure 45 Recovery of IRIF of γH2AX (A), pATM (B) and 53BP1 (C) after short incubation in hypotonic medium. 92

Figure 46 CCP of RPE-1 cells after either continuous treatment in hypotonic medium or 1 h treatment followed by return to normal conditions. 93

Figure 47 Representative images and length quantification of metaphases formed in hypotonically treated cells. 94

Figure 48 Cell cycle distribution of synchronous RPE-1 cells at different times after 1 or 4 h pretreatment in hypotonic medium. 95

Figure 49 Influence of 300 mM NaCl on RPE-1 cell diameter and cell volume. ... 96

Figure 50 CCP of RPE-1 cells treated in hypertonic medium. 97

Figure 51 Representative images of metaphases formed in hypertonically treated cells. 98

Figure 52 Chromosome length quantification in isotonically and hypertonically treated metaphases. 99

Figure 53 Changes in levels of linker histone H1 and HC/EC markers in globally condensed chromatin. 100

Figure 54 Cell number and cell cycle distribution of hypertonically treated RPE-1 cells. 101

Figure 55 Progression through the cell cycle of cells synchronized in G2-phase and treated in chromatin condensing medium. 102

Figure 56 Proportion of mitotic cells under chromatin condensing conditions. ... 103

Figure 57 Investigation of G2-checkpoint under hypertonic conditions. 104

Figure 58 Formation of γH2AX foci when chromatin is globally condensed. 105

Figure 59 Formation of pATM foci under hypertonic conditions. 106

Figure 60 Formation of 53BP1 foci after treatment in hypertonic medium. 107

Figure 61 Chromatin condensation impairs DSB repair as measured by PFGE. 109

Figure 62 altEJ in RPE-1 cells gets compromised upon global chromatin condensation. 110

Figure 63 Effects of global chromatin condensation on DNA end resection and Rad51 foci formation in RPE-1 cells. 111

Figure 64 Cell viability and GFP expression in U2OS reporter cell lines. 112

Figure 65 Effects of chromatin condensation on HRR. 113

Figure 66 Effects of chromatin condensation on end joining events measured using the U2OS EJ5-GFP (A) and U2OS EJ2-GFP (B) reporter cell lines. 114

Figure 67 Effects of chromatin condensation on SSA repair measured by U2OS SA-GFP reporter assay. 115

Figure 68 Clonogenic survival assay of RPE-1 cells. 116

Figure 69 Reversibility of γH2AX (A), pATM (B) and 53BP1 (C) foci effects after short incubation in hypertonic medium. 117

Figure 70 CCP of RPE-1 cells after either continuous incubation in hypertonic medium, or 1 h treatment in hypertonic medium followed by re-incubation under isotonic conditions. 118

Figure 71 Representative images and length quantification of metaphases formed in hypertonically treated cells. 119

Figure 72 Cell cycle distribution of synchronous RPE-1 cells at different times after 1 or 4 h pretreatment in hypertonic medium. 120

Figure 73 Survival of RPE-1 cells treated in isotonic medium for different times.159

3) List of tables

Table 1 Cell culture growth media 39

Table 2 Cell lines and corresponding growth media 39

Table 3 Antibodies for immunofluorescence (IF), FC and western blot (WB) 39

Table 4 Plasmids used for transfection 40

Table 5 EdU Click-iT reaction cocktail 40

Table 6 Chemicals 41

Table 7 Solutions for SDS-PAGE and immunoblotting 42

Table 8 Drugs 43

Table 9 Software 43

4) Introduction

The basis of life is the capability of cells to pass their genetic information to the next generation and thereby to conserve the species. This information is retained in the central macromolecule of the cell, the deoxyribonucleic acid (DNA) that should remain accessible as required. The accurate replication of DNA and its transcription and the following protein biosynthesis assure its biological function. The principle of complementary base pairing facilitates the creation of an exact copy of the original DNA molecule and ensures thereby the dissemination of the genetic material to the next generation. Precision of DNA replication is of highest importance and cells have evolved several mechanisms to avoid mistakes. However, not only faults during replication can cause changes in genomic material but also agents of endogenous and exogenous sources can endanger genomic integrity (Krieger and Iliakis 2017).

Each cell has to deal with ten thousands of DNA damages every day (Lindahl 1993). DNA lesions can block replication and transcription and in case they are not repaired, or repaired incorrectly, they can lead to mutations, or can interfere with cell viability. Physiological processes like DNA mismatches during replication or strand breaks caused by abortive topoisomerase I/II activity are sources for DNA lesions. Additionally, hydrolytic reactions and non-enzymatic methylations are responsible for a plenty of base lesions, while reactive oxygen species (ROS), that are by-products of oxidative respiration or redox-cycling events, as well, are attacking DNA leading to impaired base pairing (bulky lesions), blocking of DNA replication and transcription, base loss or to the formation of DNA single-strand breaks (SSBs) (see Figure 1). When two SSBs are formed in close proximity to each other or when DNA replication machinery encounters a SSB, the formation of double-strand breaks (DSBs) ensues. This form of DNA lesion is occurring infrequently compared to the above mentioned other forms of DNA damages, but is much more dangerous (Jackson and Bartek 2009; Khanna and Jackson 2001).

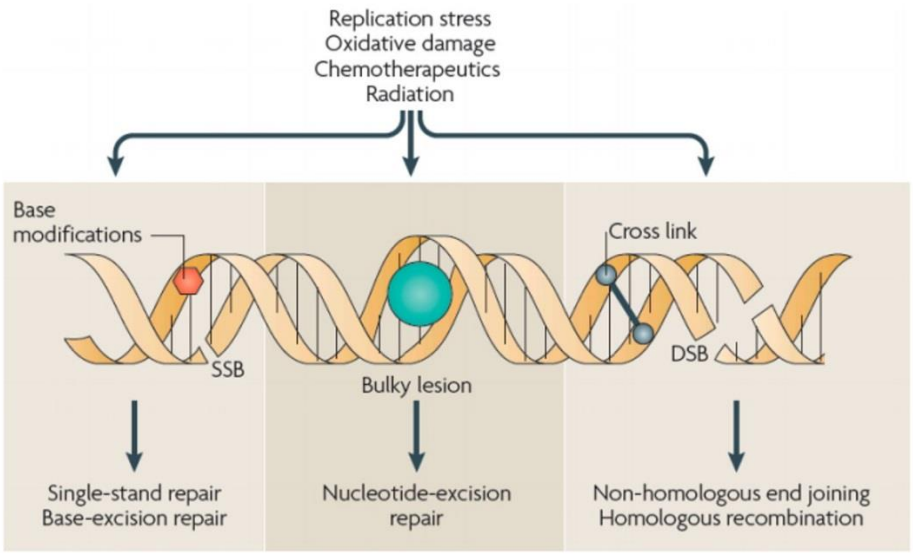

Figure 1 Types of DNA damages and repair.
Endogenous sources like replication stress and oxidative metabolism, but also exogenous sources like UV light, IR and chemotherapeutics can produce a variety of DNA damages which need to be repaired by distinct repair pathways (Arjunan, Sharma, and Ptasinska 2015).

Beside the endogenous sources for DNA lesions there are also several environmental agents with the potential to damage the DNA. Ultraviolet (UV) light is the most pervasive agent and induces DNA lesions like cyclobutane-pyrimidine dimers (CPDs) and 6-4 photoproducts (6-4PPs) (Sinha and Hader 2002). Another exogenous source causing DNA damages and especially DSBs is ionizing radiation (IR) which is the focus here. IR results from radioactive decay of natural compounds, like for example radioactive radon gas, which can accumulate in homes, as well as from cosmic radiation, which is constantly bombarding earth. These sources constitute the so called background radiation. In addition, human activities like medical X-rays, nuclear power plants etc. can cause exposure to IR (Khanna and Jackson 2001; Jackson and Bartek 2009).

Structural changes in DNA (referred to as DNA damages) can evoke mutations when they are not removed. Mutations can interfere with the viability of an organism and can also generate diseases. In many cases, after such genomic changes, cancer develops, or the cell cannot survive and undergoes mitotic death or apoptosis. Therefore, recognition and repair of DNA damages is imperative and DNA repair is considered fundamental process in DNA metabolism.

Considering the large number of DNA damages that occur every day in every cell, one might wonder how it is possible to stay healthy. The majority of DNA damages

are SSBs, base mispairing or base losses, which can be repaired easily. Repair mechanisms, like base excision repair (BER) and nucleotide excision repair (NER), can remove these damages and restore the original sequence and structure based on the complementary DNA strand, which is used as a template. As long as the SSB repair pathways are functional, SSBs are not compromising genomic stability, but when SSBs remain unrepaired and interfere with processes like DNA replication, fatal consequences can ensue.

In the case of DSBs no complementary strand functioning as template is available. Thus, repair of DSBs constitutes a serious problem for the cells and if they remain unrepaired, DSBs can lead to cell death or tumorigenesis. The cells have evolved different repair mechanisms to handle DSBs, each one with the ability to restore the DNA molecule structurally, but each operating with different fidelity and associated with different adverse consequences for genome stability. Homologous recombination repair (HRR) using the sister chromatid as a template is the only pathway which can restore the original sequence, while forms of end joining pathways and also single-strand annealing (SSA) can lead to sequence alterations. The mechanisms of these pathways will be described in detail later. The focus of this thesis is on the repair of DSBs, which are generated by X-rays. Therefore, the fundamental characteristics of IR are briefly outlined in the following section.

4.1) Ionizing radiation (IR)

As mentioned above, IR is omnipresent as it is a product of radioactive decay of natural compounds and is also reaching earth from space as cosmic radiation; both together are referred to as background radiation. In addition, there are several man-made sources of IR like X-ray devices used in medicine, nuclear power plants etc. IR is commonly used in the clinic, as it can be applied for diagnostic and therapeutic purposes. In addition, IR is also frequently used by researchers to induce random DNA damages. IR in the form of X-rays is inducing DSBs, and is therefore used in this thesis to investigate DSB repair and the DNA damage response (DDR). Using X-rays as an agent producing DSBs, allows a precise investigation of associated processes, as they can be applied in an accurate manner with regard to exposure time and dose administrated, and ensure a linear increase in generated lesions per

unit of dose. The physical basis of IR and how it generates DNA damages are outlined in the upcoming sections.

4.1.1) Physical fundamentals of IR

Radiation in general is defined as emitted energy traveling through a medium or through space, getting absorbed by matter and leading to excitation or ionization events in materials, including biological material. Usually radiations get classified as either electromagnetic or particulate. For electromagnetic radiation there is a whole panel of radiation forms that are classified by the frequency of their waves. The basis of this kind of radiation is the photon. The electromagnetic spectrum shows the different radiation forms from radio waves, microwaves, infrared radiation, visible light, UV radiation and X-rays to γ-rays; all differing in their properties and therefore in the energy of their photons. In general, photons of short wavelengths and high frequencies possess higher energy than those of long wavelengths and low frequencies (see Figure 2) (Hall and Giaccia 2006; Paul 2013).

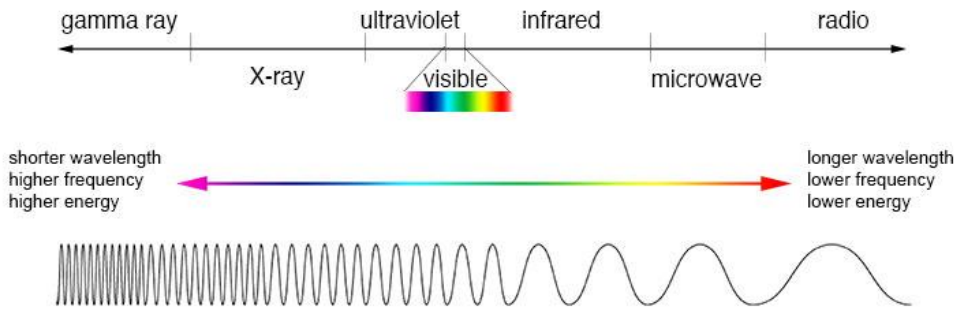

Figure 2 Spectrum of electromagnetic radiation.
Comparison of wavelength, frequency and energy of the different forms of radiation within the electromagnetic spectrum (source: NASA's Imagine the Universe).

During excitation the absorbed energy raises an electron in an atom or molecule to a higher energy level without actually ejecting the electron. But if the radiation energy is high enough one or more electrons can be ejected from the atom or molecule, an event called ionization. In order to break a strong chemical bond an energy of about 33 eV is needed which can easily be achieved by IR. An important characteristic of IR is the localized deposition of large amounts of energy. In the case of biological material, electromagnetic radiation is considered as ionizing radiation if its photon energy is above 124 eV. Thus, only radiation with shorter

wavelengths than 10^{-8} m, which includes X-rays and γ-rays, is considered as ionizing (Hall and Giaccia 2006).

Beside electromagnetic IR there are particulate radiations that are also often used in experimental approaches. These include electrons, protons, α-particles, neutrons and heavy charged particles.

The two kinds of IR, electromagnetic and particulate, also differ in their ionizing patterns. While charged particles directly ionize by disrupting the atomic structure of the absorber through which they pass, electromagnetic radiations (X-rays and γ-rays) ionize indirectly. They do not primarily produce damage by themselves but give up their energy to the material they pass to produce fast-moving electrons, which in turn can efficiently produce more ionizations and thus more biological damage (Hall and Giaccia 2006).

As already mentioned, in this thesis only X-rays are used as source of IR to produce DNA damage, thus only this form of radiation will be discussed in the following section.

In terms of X-ray irradiation there are two processes of photon absorption that can occur depending on the energy of the photons and the absorbing material. At high photon energies the Compton process dominates, in which the photon interacts with an electron from the outer shell possessing small binding energy. The energy of the photon is partly given to the electron as kinetic energy, while the photon continues with the remaining energy (see Figure 3 A). The result of this process is a fast electron and a photon of reduced energy. Fast electrons themselves can ionize other atoms and induce biological damage (Hall and Giaccia 2006).

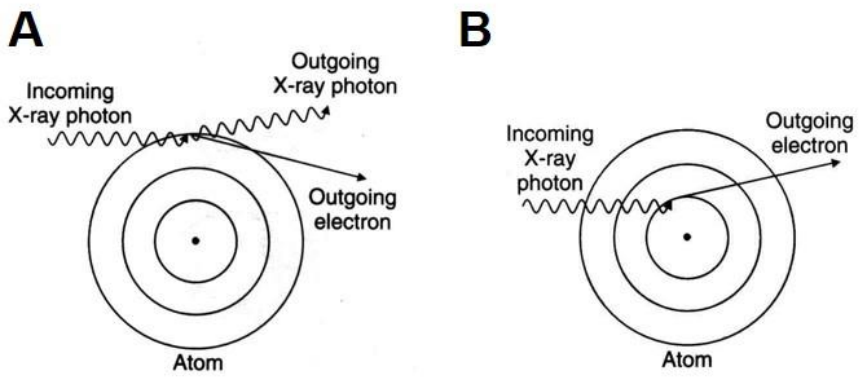

Figure 3 Illustration of Compton process and photoelectric process.
(A) In Compton process a photon interacts with a loosely bound electron from the outer shell and part of its energy is given to the electron as kinetic energy. (B) In photoelectric absorption the photon interacts with an electron in an inner shell giving up its entire energy. Thereby the electron gets ejected with a kinetic energy equal to the energy of the X-ray photon minus its binding energy (source: http://www.physics.hku.hk/~phys0607/lectures /chap06.html).

For X-rays with photons of lower energies the photoelectric absorption process becomes more important. During this process the photon interacts with an electron bound to an inner shell of the atom. Thereby all energy of the photon is given to the electron, partly to overcome the binding energy of the electron and partly as kinetic energy (see Figure 3 B). The resulting free space in the inner shell must be filled by another electron either from an outer shell or from outside the atom. This process leads to the emission of photons with low energy. Like in the Compton process, fast electrons are produced which in turn ionize other atoms and induce damage (Hall and Giaccia 2006).

The response of biological material to IR is analyzed as a function of the absorbed dose, which is defined as the energy that gets absorbed in a certain volume of the material divided by the mass of this volume. The radiation dose is normally expressed in Gray (Gy) which represents 1 Joule/kg (Allen, Borak, et al. 2011).

Ionization events during irradiation of biological material are not randomly distributed. Rather, they follow particle tracks and deposit their energy along them (see Figure 4) (Mladenov and Iliakis 2011). Different types of radiation are characterized by the density patterns of their ionization along the particle tracks. The density of ionization events is given as linear energy transfer (LET) and has dimensions of energy per unit length (e.g. keV/μm) (Allen, Ashley, et al. 2011). X-rays are only sparsely ionizing, hence they are considered as low LET radiation. In

contrast, neutrons and α-particles produce ionization events in close proximity to each other and are therefore considered to be of high LET.

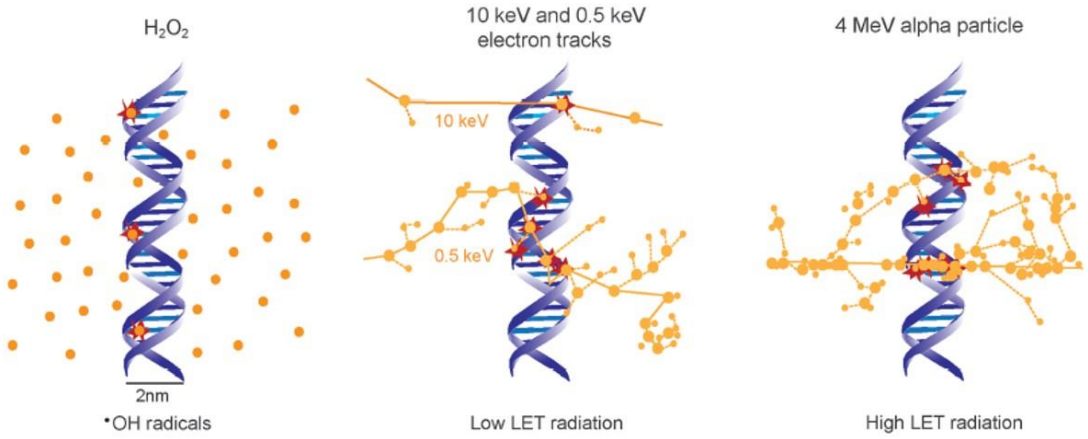

Figure 4 Distribution of DNA damaging events after exposure to H_2O_2 or low and high LET radiation.
Large dots represent ionization events while small dots indicate excitations along the tracks (Schipler and Iliakis 2013).

Especially the densely ionizing particles produce multiple damages in close proximity (referred to as clustering) and create thereby complex DNA damage. But also low LET radiation can produce complex damage by the electrons generated as they slow down, but also through indirect action mediated by ·OH radicals produced by interaction with water that further attack biological molecules like DNA (Mladenov and Iliakis 2011).

Cells consist of up to 80 % of water, which gets targeted by radiation as well. The interaction of photons or charged particles with water molecules produces ion radicals (see equation 1).

$$H_2O \rightarrow H_2O^+ + e^- \quad (1)$$

These ion radicals react with other water molecules and form highly reactive hydroxyl radicals (see equation 2).

$$H_2O^+ + H_2O \rightarrow H_3O^+ + \cdot OH \quad (2)$$

Highly reactive radicals can diffuse a short distance to reach a target in the cell. It is estimated that about two thirds of the X-ray damage to DNA is caused by ·OH (Hall and Giaccia 2006).

4.1.2) DNA damage induction by IR

Irradiation of biological material with IR causes damages to several components, like proteins and lipids. But the most critical target is DNA, as it is the carrier of genetic information. DNA can get damaged in direct ways (by photons or charged particles) and in indirect ways (by ·OH radicals) as it is described in the previous section.

X-rays, representative for low LET radiation, induces around 1,300 base lesions, 1,000 SSBs and 20 – 40 DSBs per Gy. SSBs and base lesions can be repaired easily if induced in an isolated manner (see introduction) and in contrast to DSBs do not correlate with cell killing. The number of damages caused by X-rays increase linearly with increasing dose (Hall and Giaccia 2006). Upon irradiation, in order to deal with all these damages, cells have evolved a huge machinery of signaling pathways and mechanisms which are partly explained (considering DSBs) in the next sections.

4.2) Mechanisms of DDR

Cells have evolved mechanisms to detect DNA lesions, signal their presence and promote their repair – collectively known as DDR. If parts of this network are not functional, cells show stringent sensitivity to DNA damaging agents and defects can cause severe human diseases (Jackson and Bartek 2009).

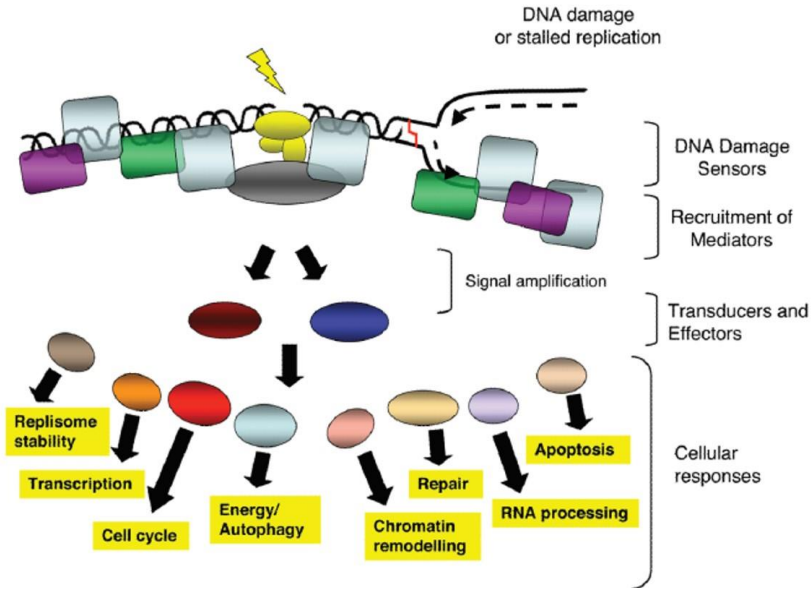

Figure 5 Illustration of DDR.
DNA lesions that can also lead to stalled replication forks are recognized by a variety of DNA damage sensors which recruit mediators, thereby initiating signaling pathways that impact several cellular processes (Jackson and Bartek 2009).

In the DDR several proteins participate that can be divided into different categories (see Figure 5): DNA damage sensors, transducers, mediators and effectors (Polo and Jackson 2011). DNA damage sensors like the MRN (Mre11, Rad50, Nbs1) complex sense structural changes in DNA upon damage induction and initiate the signaling response. The mediators and transducers amplify and pass this signal to effector proteins resulting in several cellular responses like cell cycle checkpoint activation, DNA repair and transcriptional inhibition (Bekker-Jensen and Mailand 2010; Polo and Jackson 2011). If the damage remains unresolved, the DDR activates apoptotic pathways or directs cells to senescence (Misteli and Soutoglou 2009).

4.2.1) Cell cycle checkpoint activation

The main purpose of DDR is to maintain genomic stability by coordinating DNA repair and cell cycle progression. Unrepaired DNA breaks can cause severe effects if they interfere with DNA replication or mitosis, which can lead to chromosomal aberrations and translocations. The DDR is therefore activating so called cell cycle checkpoints to arrest cells in their cell cycle phase until successful repair of the DNA damage took place.

Cyclin-dependent kinases (CDKs) in combination with cyclins, their regulatory subunits, control the progression through the cell cycle and are targeted by signaling cascades activated upon DNA damage (see Figure 6) (Löbrich and Jeggo 2007; Malumbres and Barbacid 2001).

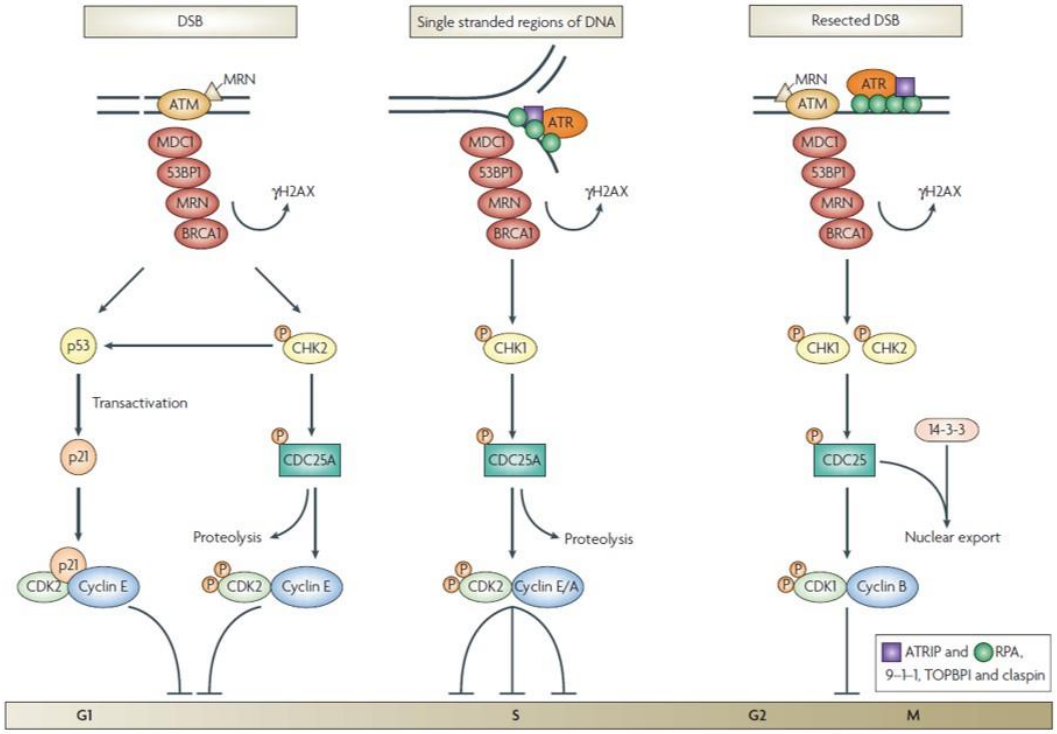

Figure 6 Cell cycle checkpoint activation in mammalian cells after IR.
Signal transduction pathways get activated by ATM and ATR kinases upon DSB formation and ssDNA, respectively. Upon damage induction by IR ATM and ATR activate mediator proteins (MDC1, 53BP1, MRN and BRCA1). The mediators amplify the signal via transducer kinases (Chk1 and Chk2) and effector proteins (Löbrich and Jeggo 2007).

Upon DNA damage, sensors like MRN complex, sensing DSBs, and replication protein A (RPA, binds to single-stranded DNA (ssDNA)), recruit the two phosphoinositide 3-kinase-like kinase (PIKK) family members ATM (ataxia telangiectesia mutated) and ATR (ataxia telangiectasia and RAD3-related). The signal generated by ATM and ATR is amplified by different mediators including MDC1 (mediator of DNA damage checkpoint 1), 53BP1 (p53-binding protein 1), MRN complex and BRCA1 (breast cancer susceptibility gene 1) targeting the transducer kinases Chk1 and Chk2 and effector proteins. Depending on the cell cycle phase in which the DNA damage occurs different proteins are targeted by the signaling pathways. A DSB in G1-phase leads to ATM activation and thereby to Chk2 phosphorylation and subsequent phosphorylation of the phosphatase CDC25A. This phosphorylation increases ubiquitylation and proteolytic degradation

of CDC25A and thereby prevents rapidly the activation of CDK2/cyclin E complex. In addition, a second, but delayed mechanism gets activated by ATM: the stabilization of p53 leading to the transcription of p21 which is an inhibitor of CDK2/cyclin E complex. While the signaling branch using Chk2 is rapidly transducing the signal, the p53 dependent pathway takes more time and is thought to maintain the G1-checkpoint upon DNA damage (Löbrich and Jeggo 2007; Sancar et al. 2004).

During S-phase stalled replication forks lead to ATR activation and subsequent Chk1 phosphorylation and CDC25A degradation. This slows down replication and stops cells in S-phase.

DSBs in G2-phase can activate ATM and indirectly ATR through generating single-stranded DNA by end resection. Similar to the above described mechanisms in G1- and S-phase, a rapid signal transduction involving phosphorylation of Chk2 and Chk1 and proteolytic degradation of CDC25 prevents the dephosphorylation of CDK1/cyclin B and inhibits the progression to mitosis (Sancar et al. 2004; Löbrich and Jeggo 2007).

The stop of the cell cycle engine persists until the DNA damage is repaired; in case of DSBs by one of the following repair pathways.

4.3) DSB repair by homologous recombination

In terms of faithful repair of DSBs there is only one pathway known which can restore the original sequence: HRR. In this process the DNA ends get resected forming 3'-ssDNA overhangs that are used for strand invasion during homology search on the sister chromatid. Due to the need of a sister chromatid for repairing the DSB this repair process is highly cell cycle regulated and HRR is only active during late S- and G2-phase.

In the initial process of DNA end resection several proteins are involved: MRN complex, CtIP (CtBP (carboxy-terminal binding protein) interacting protein), Exo1 (exonuclease 1), Dna2 and BLM (Bloom syndrome) helicase (Symington and Gautier 2011). Rad50 and Mre11 together form the core of MRN complex, providing DNA binding, single-strand endonuclease and 3'-5' exonuclease activities on ssDNA or dsDNA by Mre11 and regulatory ATPase and adenylate kinase activities

by Rad50. The third component of MRN complex, Nbs1, does not have any known enzymatic activity, but its recruitment to DSBs is essential for activation of ATM and thereby for activation of DDR. Nbs1 is also interacting with CtIP, which plays an essential role in activation of MRN complex and initiation of end resection (Mladenov et al. 2016). CtIP gets phosphorylated at serine327 and threonine847 upon CDK activation, which points out the cell cycle dependence of resection and facilitates the interaction with Nbs1 (Huertas and Jackson 2009). In addition, CtIP gets phosphorylated by activated ATM and activates thereby end resection (Wang et al. 2013). Upon the initial formation of single-stranded regions by MRN and CtIP, more processive nucleases (Exo1 and Dna2) generate long stretches of ssDNA overhangs (Sallmyr and Tomkinson 2018). In addition, the resection step is promoted by BLM helicase which helps to unwind the DNA.

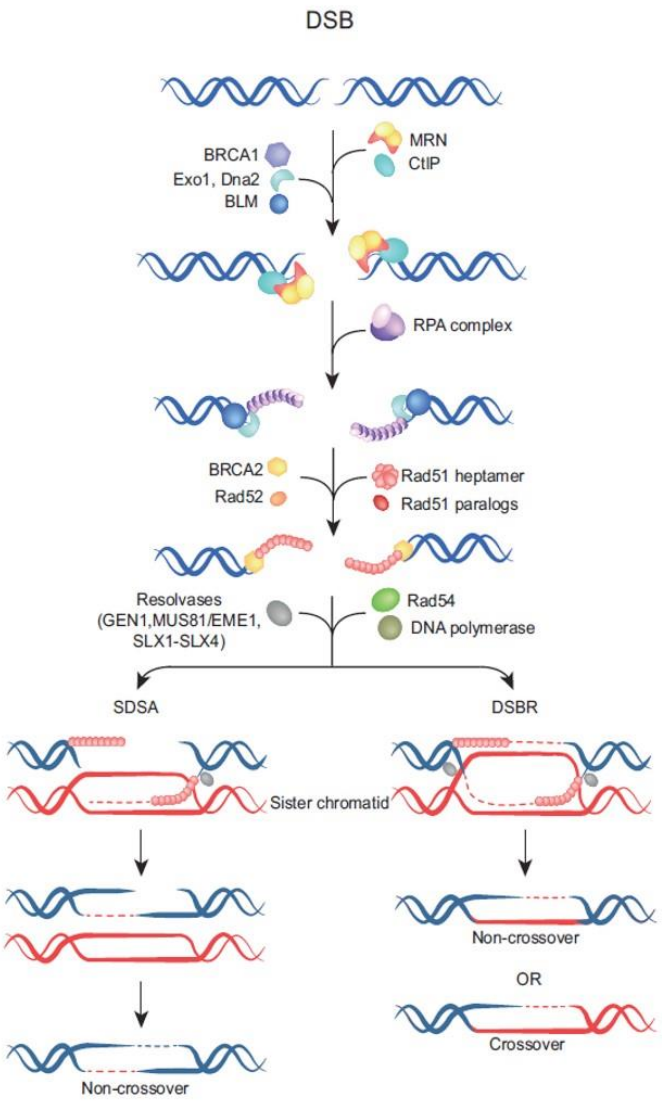

Figure 7 Schematic mechanism of HRR.
HRR is the only faithful repair pathway for DSBs and uses the homologous sister chromatid as template. Therefore, repair by HR is restricted to late S- and G2-phase of the cell cycle. Two possible outcomes occur after HRR: non-crossover and crossover products (Dueva and Iliakis 2013). For more details see text.

The arising single-stranded regions are promptly coated by RPA, which is a heterotrimeric complex consisting of RPA70, RPA32 and RPA14, preventing secondary structures and preparing the formation of Rad51 nucleoprotein filaments (see Figure 7). The replacement of RPA by the recombinase Rad51 is supported by the mediator protein BRCA2 and Rad51 paralogs (Rad51B, Rad51C, Rad51D, XRCC2 (X-ray cross complementing protein 2) and XRCC3). Subsequently, the Rad51 nucleoprotein filament invades the intact sister chromatid searching for homologous sequences and forms a structure called displacement loop (D-loop). As soon as homology is found, the elongation of the 3'-end of the invading strand

starts. In preparation for elongation Rad51 is removed by Rad54 and its paralog Rad54B (Mladenov et al. 2013; Mazin et al. 2010). At this point the repair of DSBs by HR branches into two different pathways (see Figure 7). In the process of synthesis-dependent strand annealing (SDSA) the invading 3'-end gets elongated over a limited distance, displaced from the template and re-ligated with the original DNA end. This event is the most frequent during HRR, forming one Holliday Junction (HJ) and resulting in non-crossover products. During double-stranded break repair (DSBR) a double HJ is formed and thereby non-crossover as well as crossover products can emerge. In resolving HJ several proteins, called resolvases, like GEN1, MUS81/EME1 and SLX1-SLX4 are involved (Mladenov et al. 2013; Dueva and Iliakis 2013; Ip et al. 2008; Mladenov et al. 2016).

4.4) DSB repair by end joining processes

As mentioned before, HRR is restricted to S/G2-phase of the cell cycle, so that there are other repair mechanisms that can also repair DSBs independently of cell cycle stages. Indeed, cells have evolved end joining repair processes, irrespective of the presence of a template, that operate throughout the cell cycle. cNHEJ, as main DSB repair pathway, and altEJ are described in detail in the next sections.

4.4.1) Classical non-homologous end joining

cNHEJ is not restricted to certain cell cycle phases and is a very fast process operating with half times of 10 – 30 min. As cNHEJ is simply rejoining free DNA ends and not restoring the original sequence, it is referred to as an error-prone repair mechanism (Dueva and Iliakis 2013). In order to rejoin the broken DNA the ends need to be clean and ligatable, which is not the case for IR-induced DSBs. Most of them are associated with damage to the sugar-phosphate backbone and/or the bases of the terminal nucleotides. Therefore, limited or extensive additions and deletions of nucleotides arise during cNHEJ (Mladenov and Iliakis 2011). In addition to the inability of restoring the original sequence, cNHEJ has no build-in mechanism that ensures the rejoining of the original DNA molecule. In principle it can ligate the DNA ends of any DNA molecule irrespective of its origin and thereby result in chromosomal translocations. It is assumed that its operational speed is associated with limited sequence alterations and translocation formation to sustain genomic

stability and suppress carcinogenesis (Dueva and Iliakis 2013; Ferguson et al. 2000; Iliakis et al. 2004; Burma, Chen, and Chen 2006).

The first molecule binding to free ends of DSBs is Ku. The core domains Ku70 and Ku80 form a ring-shaped heterodimer that binds around the DNA ends (see Figure 8). So far no enzymatic activity has been associated with Ku, but recently it was reported that binding of Ku to the DNA ends stimulates 5'-deoxyribose-5'-phosphate (5'-dRP) and abasic, apurinic/apyrimidinic (AP) lyase activities excising damaged nucleotides in close proximity to DNA ends (Mladenov et al. 2016; Roberts et al. 2010). However, the most important role of Ku is recruiting the catalytic subunit of DNA-dependent protein kinase (DNA-PKcs). DNA-PKcs belongs to the PIKK family, like ATM and ATR, and together with Ku it is forming the holoenzyme complex DNA-PK, which activates the repair by cNHEJ (Meek et al. 2004).

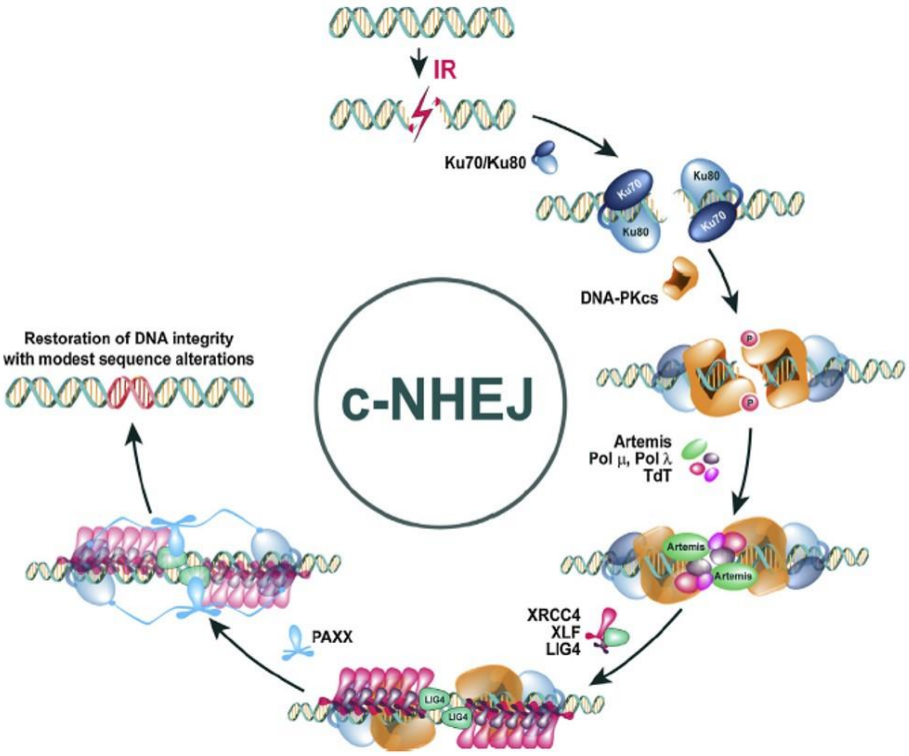

Figure 8 Schematic drawing of cNHEJ mechanism.
The main DSB repair pathway cNHEJ is active throughout the whole cell cycle, but is considered to be error-prone as it is not using a template and thus not restoring the original sequence (Mladenov et al. 2016). See text for more details.

Active DNA-PK phosphorylates many proteins participating in DDR and regulates cNHEJ and DSB processing, but of high importance is its autophosphorylation, which further regulates its activity. Further downstream, DNA-PK phosphorylates and recruits Artemis nuclease that, together with other DNA end processing

activities (e.g. polymerase (pol) μ, pol λ and TdT (terminal deoxynucleotidyl transferase)), prepares DNA ends for the upcoming ligation step (Mladenov et al. 2016).

After DNA end processing a ligation complex consisting of ligase 4 (Lig4), XRCC4 and XLF (XRCC4-like factor), which is recruited by DNA-PK as well, helps to rejoin the DNA ends. Recently, a new factor called PAXX (paralog of XRCC4 and XLF) has been identified. It provides structural similarity to XRCC4 and XLF and is participating in the formation of a filament structure bridging the DNA ends and thereby promoting DNA ligation (see Figure 8) (Mladenov et al. 2016; Andres et al. 2012; Ochi et al. 2015; Xing et al. 2015).

4.4.2) Alternative end joining

In addition to the two main DSB repair pathways, cNHEJ and HRR, a third mechanism repairing DSBs was reported, functioning also on end joining principles: altEJ (Wang et al. 2003). In altEJ there are multiple ways of DSB processing which impede the full elucidation of its mechanism. In the following it is described what is known so far.

One of the first proteins involved in altEJ is poly-(ADP-ribose)-polymerase 1 (PARP1) which has DNA end binding affinity and may compete with Ku for DSBs (Cheng et al. 2011; Paddock et al. 2011; Wang et al. 2006). In biochemical approaches it was shown that histone H1 has a role in stabilizing the DNA ends (Rosidi et al. 2008). In contrast to cNHEJ the mechanism of altEJ requires end resection, which is facilitated by MRN complex and CtIP (see Figure 9). Under normal conditions end resection is only observed in S- and G2-phase, where CDK-mediated phosphorylation is activating CtIP. Nevertheless, under certain conditions, like for example when 53BP1 is depleted, which is known to promote cNHEJ, Mre11 and CtIP-dependent resection can be observed in G1-phase (Bakr et al. 2016). This process initiates the repair by altEJ and emphasizes its backup role. The dependency on resection is reflected by the increased activity of altEJ during G2-phase, where it is also functioning as a backup pathway to HRR (Wu et al. 2008).

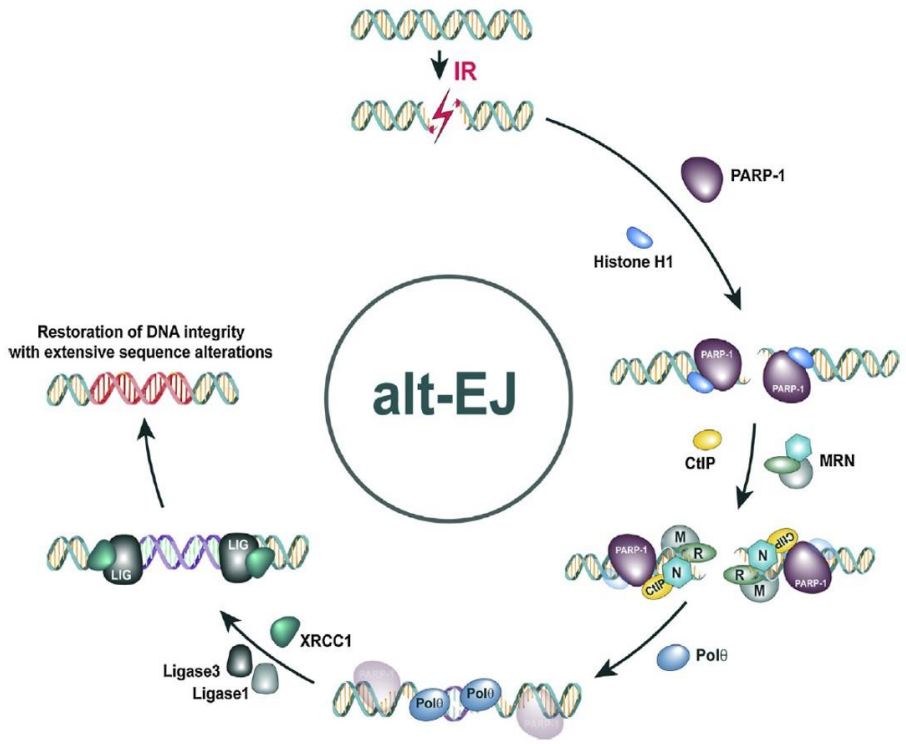

Figure 9 Schematic drawing of altEJ mechanism.
altEJ functions as a backup repair mechanism to cNHEJ and also HRR. The underlying mechanisms are not completely understood, but the scheme here shows what is known so far (Mladenov et al. 2016). See text for more details.

As altEJ does not require homology for repairing DSBs, like HRR and SSA, it is occasionally facilitated by microhomologies (2 - 4 nt) found at the DNA ends, especially after resection and the generation of ssDNA. This form of repair is also termed microhomology mediated end joining (MMEJ) (Dueva and Iliakis 2013). In the next step pol θ is binding to resected DNA and promotes altEJ by filling-in remaining gaps from end alignment based on microhomology (Ceccaldi et al. 2015). The ligation step is then performed by Lig1 and Lig3/XRCC1 (Paul et al. 2013).

Although altEJ is removing DSBs and functions as a backup mechanism in situations where the main repair pathways cannot be active, it is a highly mutagenic pathway leading to large alterations at the junctions and to the formation of chromosomal translocations (Mladenov et al. 2016; Soni et al. 2015). In addition to its fluctuating activity throughout the cell cycle, a suppression of altEJ in G0-phase cells was reported (Singh et al. 2011; Singh et al. 2012). Considering that most of the cells in the human body are in a differentiated, non-proliferating state, a suppression of a DSB repair pathway leading to genomic instability appears very reasonable.

4.5) Single-strand annealing

Another DSB repair pathway in addition to HRR and end joining processes is SSA. Usually its activity is restricted to DSBs that are flanked by direct sequence repeats. Upon DNA damage the ends undergo extensive resection, most probably performed by MRN complex and CtIP, until complementary sequences are completely exposed (Valerie and Povirk 2003; Bhargava, Onyango, and Stark 2016; Morrical 2015). The homologous DNA stretches are then annealed by the Rad52 undecamer and the protruding ends are trimmed by the ERCC1 (excision repair cross complementing 1) / XPF (Xeroderma Pigmentosum group F) nuclease (see Figure 10). Resulting nicks are then ligated by DNA Lig1 (Symington 2002; Mladenov et al. 2016).

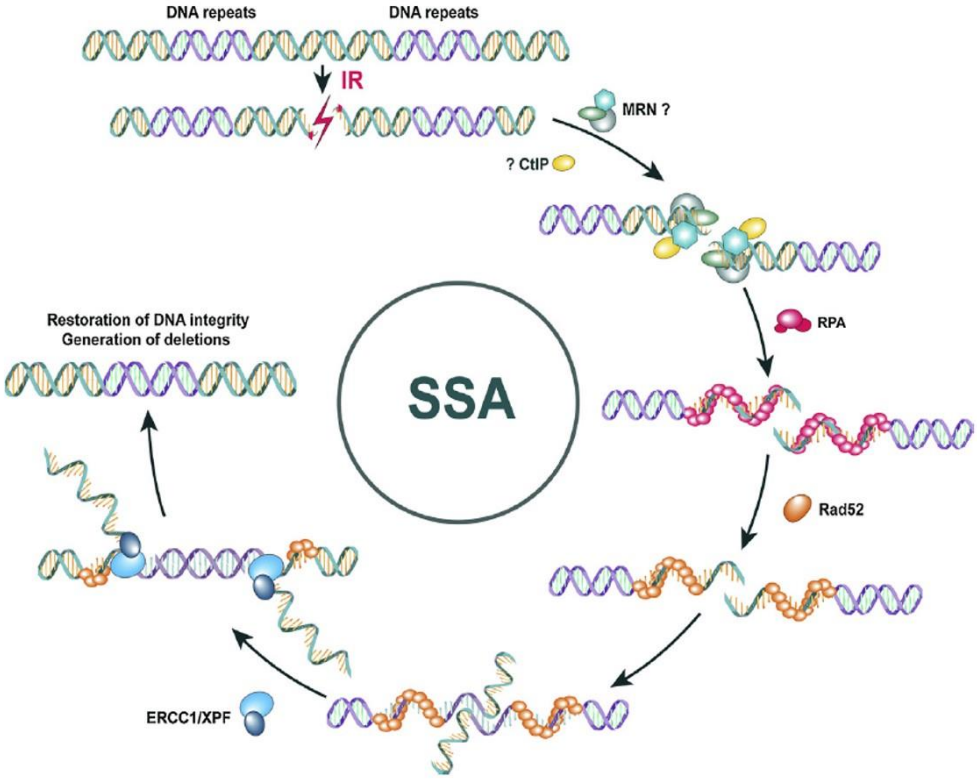

Figure 10 Schematic drawing of SSA mechanism.
SSA is a mutagenic repair pathway as it deletes long stretches of DNA. It can function as a backup mechanism for HRR (Mladenov et al. 2016). See text for more details.

However, SSA is a very mutagenic repair pathway leading to the deletion of the sequence between two repeats and one repeat itself and thereby resulting in loss of genetic information. SSA shows a cell cycle dependence similar to HRR as it is dependent on end resection by CtIP. Notably, SSA is strongly suppressed by HRR and vice-versa, as it was shown that SSA activity is enhanced upon loss of Rad51,

Rad54 or BRCA2. This kind of regulation suggests a backup role for SSA to HRR (Mladenov et al. 2016; Bhargava, Onyango, and Stark 2016; Mansour et al. 2008).

4.6) Organization of DNA in chromatin

In this thesis we focus on signaling and repair of DNA damages in the context of chromatin structure. In mammalian cells DNA is not naked but organized in a very specific manner. Thus, this section will elucidate the structural characteristics of DNA in chromatin and how this structure gets affected upon introduction of DNA DSBs and vice versa how it influences DSB repair.

Higher eukaryotic organisms have evolved special ways of packaging their DNA into chromosomes to accommodate the 3.2 billion base pairs (bp) of DNA in the nucleus. During the cell cycle the chromosome compaction level changes; it has its highest compaction level in mitosis (10,000-fold) and is much less condensed during interphase (500-fold). The chromosome structure is highly dynamic and can get decondensed when cells need access to specific DNA regions for gene expression, DNA repair and replication. This type of packaging is made possible by specialized proteins called histones and nonhistone chromosomal proteins. The complex of these proteins and DNA is called chromatin (Alberts et al. 2008).

An octamer of four positively charged core histones (H2A, H2B, H3 and H4) and 147 bp of genomic DNA wrapped around forms a protein-DNA complex called nucleosome core particle (see Figure 11). In order to build a histone octamer first H3-H4 and H2A-H2B dimers are formed, of which the H3-H4 dimers combine to form a tetramer. Together with two H2A-H2B dimers the compact octamer core is built. Between DNA and histones 142 hydrogen bonds are formed in each nucleosome core particle. In addition numerous hydrophobic interactions and salt linkages hold DNA and histones together. Two nucleosome core particles are separated from each other by so called linker DNA, which can vary in length from a few nucleotide pairs up to about 80 bp. Linker DNA together with a core nucleosome particle composes the nucleosome (see Figure 11). These nucleosomes can be visualized by electron microscopy and appear as a “beads on a string” filament. Further packaging of DNA requires, beside core histones, the linker histone H1. It binds approx. 10 bp of DNA at the entry and exit site of the nucleosome core particle and the whole complex is referred to as chromatosome (see Figure 11) (Fyodorov

et al. 2018). Higher chromatin compaction levels remain unclear, as the hitherto assumed 30 nm fiber structure could not be experimentally observed.

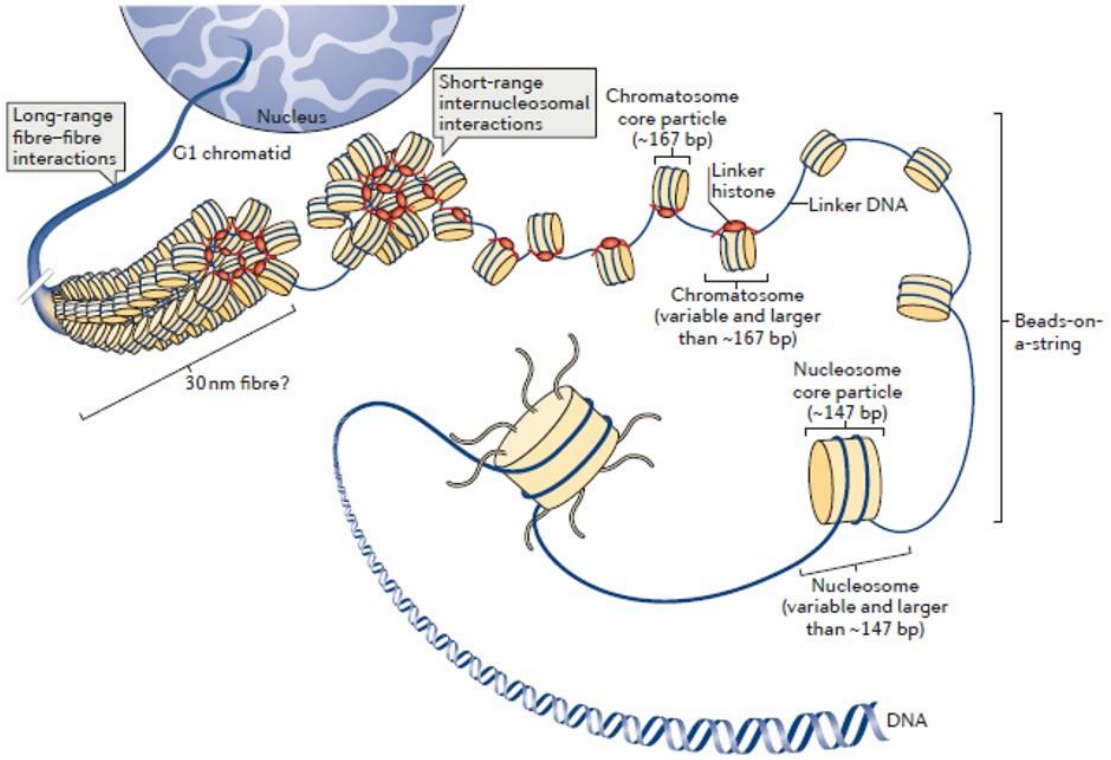

Figure 11 Multiple levels of DNA compaction.
The organization of DNA compaction within an interphase nucleus can be depicted at several levels. In combination with histone proteins a nucleosome is formed. A chromatosome particle is built with the help of linker histone H1. The interaction of several chromatosomes leads to the formation of higher order fibers which eventually produce tertiary structures (Fyodorov et al. 2018).

Core histones are globular proteins except for their N-terminal tails which are unstructured and exposed to the outside of the nucleosomes. These tails possess a large number of residues that are known to get modified, thereby facilitating different processes the DNA is involved in. The best studied histone modifications are acetylation, methylation, phosphorylation and ubiquitylation (see Figure 12).

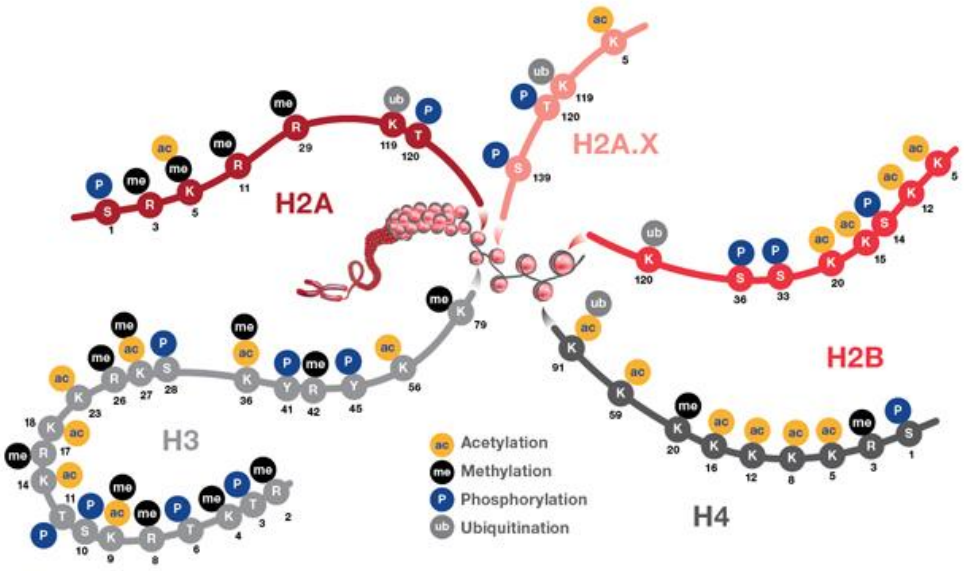

Figure 12 PTMs of core histones.
Nucleosomes are represented by red spheres wrapped by DNA (shown in gray). Positions of PTMs located on histone proteins H2A, H2AX, H2B, H3 and H4 are shown (Source: https://www.thermofisher.com/de/de/home/life-science/protein-biology/protein-biology-learning-center/protein-biology-resource-library/pierce-protein-methods/overview-post-translational-modification.html).

Chromatin can be divided in two distinct domains: silent heterochromatin (HC) and active euchromatin (EC), which are both characterized by different posttranslational modifications (PTMs) on their N-terminal histone tails. In HC low levels of acetylation and high levels of methylation at certain sites (H3K9, H3K27 and H4K20) are observed. Therefore, trimethylated H3K9 (H3K9me3) can be used as a HC marker. In addition, the heterochromatin protein 1 (HP1) helps to maintain the condensed chromatin state (Zhang and Reinberg 2001).

However, EC regions, which presents the larger proportion of the genome, are more flexible. Typically, actively transcribed EC harbors high levels of acetylation (e.g. H3K9ac marks EC) and is trimethylated at H3K4, H3K36 and H3K79. DNA damage occurs in the context of EC as well as of HC, challenging the repair processes in different ways.

4.6.1) Histone modifications function as platform for DSB signaling and repair proteins

Upon DNA damage induction, several histone modifications become necessary to create a platform for recruitment and binding of repair proteins.

One of the earliest events occurring upon DNA damage is the ATM-mediated phosphorylation of H2AX on serine139 (referred to as γH2AX, see Figure 13). Simultaneously, the neighboring tyrosine142 gets dephosphorylated which is required for recognition of γH2AX by MDC1 (Cook et al. 2009). Together with MRN complex, MDC1 recruits more ATM proteins to the break site to facilitate the bidirectional spreading of γH2AX for hundreds of kilobases (kb) along the chromatin fiber emanating from the DSB (Melander et al. 2008; Bonner et al. 2008).

Besides MDC1, as the main sensor of γH2AX, MCPH1 (microcephalin 1) also binds to γH2AX independently of MDC1 and recruits the chromatin remodeler complex SWI/SNF (Peng et al. 2009). However, also MDC1-γH2AX recruits many chromatin modifying, DDR signaling and DNA repair proteins, e.g. RNF8. The ubiquitin E3 ligase RNF8 catalyzes K63-linked poly-ubiquitylation of H1, which subsequently mediates recruitment of the E3 ligase RNF168 (see Figure 13). Both ligases together catalyze mono- and poly-ubiquitylation of histones H2A and H2AX at lysine13-15 (Doil et al. 2009; Pan et al. 2011; Thorslund et al. 2015; Mattiroli et al. 2012). These ubiquitin modifications recruit the effector proteins 53BP1 and BRCA1 which are likely to regulate the repair pathway choice between cNHEJ and HRR (Doil et al. 2009; Sirbu and Cortez 2013). The cNHEJ mediator 53BP1 provides two recruitment mechanisms upon DNA damage: on the one hand it binds via its tandem Tudor domain to H4K20me2 and on the other hand via an ubiquitin binding motif to H2AK15ub (Fradet-Turcotte et al. 2013) (see Figure 13).

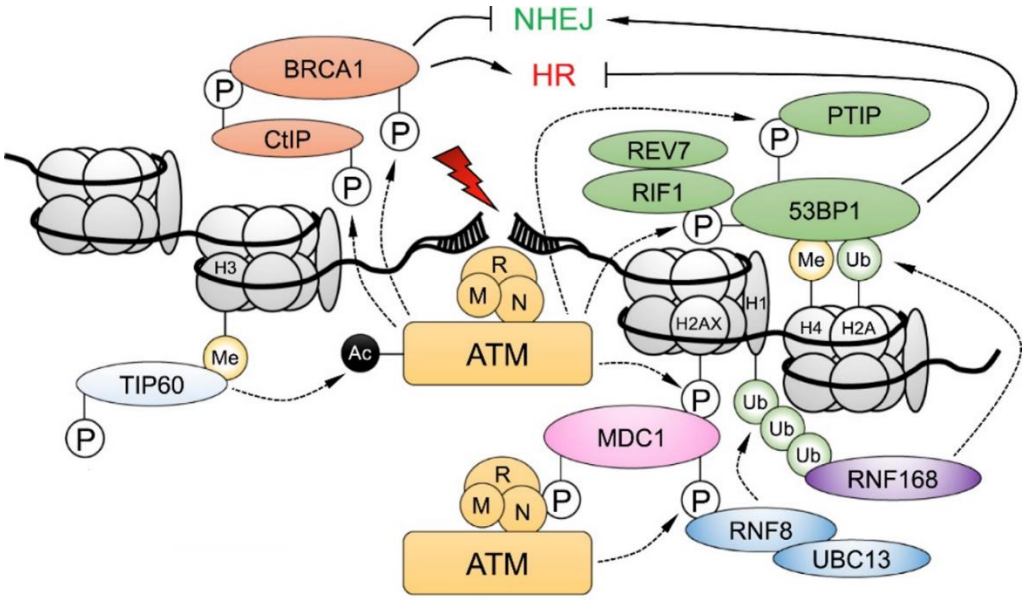

Figure 13 Activation of ATM promotes signaling cascade on damaged chromatin. ATM is recruited and activated by the MRN complex at DSBs. A phosphorylation-acetylation cascade sustains ATM activation by chromatin-bound TIP60. ATM phosphorylates H2AX and MDC1 to activate a phosphorylation-ubiquitylation signaling cascade mediated by RNF8 and RNF168 that results in 53BP1 recruitment. ATM phosphorylates 53BP1 to promote recruitment of its effectors, which are counteracted by BRCA1 and CtIP, also ATM substrates. p, phosphorylation; Me, methylation; Ub, ubiquitylation; Ac, acetylation. Adapted from (Blackford and Jackson 2017).

Another PTM, occurring very quickly at damage sites, is poly-ADP-ribosylation (PARylation), catalyzed by PARPs, which recruits NuRD complex (Chou et al. 2010). This complex harbors ATP-dependent chromatin remodeling and histone deacetylase activities and promotes transcriptional silencing to support the repair process by minimizing the likelihood of DNA breakage caused by collisions of advancing RNA polymerases (Larsen et al. 2010).

Considering acetylation as another chromatin influencing PTM, two further proteins come into play: histone deacetylases HDAC1 and HDAC2 (also part of NuRD complex). They deacetylate lysine56 of histone H3 (H3K56) and lysine16 of histone H4 (H4K16) and seem to stimulate DSB repair via cNHEJ. The transient removal of acetyl marks from histones close to DNA ends might facilitate the DSB tethering by preventing spreading of Ku away from DNA ends as Ku shall prevent the dissociation of DNA ends after chromosomal breakage (Lukas, Lukas, and Bartek 2011).

Recruitment of repair factors to methylated histone residues also seems to be regulated by MDC1. The methyltransferase MMSET gets activated by ATM-

phosphorylation, binds to the phosphate-binding module of MDC1 and methylates H4K20, which is also needed for 53BP1 accumulation. Another methyltransferase, SET8 (SET-domain-containing protein 8), is contributing to this methylation event and thereby promoting 53BP1 accumulation and shunting breaks to cNHEJ repair.

In addition, several chromatin alterations in response to DSBs are reported; ranging from relaxation in order to allow access of the repair proteins mentioned above to transcriptional repression of the surrounding chromatin and are described more in detail in the following section.

4.6.2) Chromatin dynamics upon DNA damage induction

Upon DSB induction the characteristics of the surrounding chromatin structure determine further processing of DNA damage. The more open the chromatin structure, the more efficient the ensuing DDR seems to be. Chemical inhibitors of HDACs globally relaxing chromatin, or genetic reduction of linker histone H1, usually causing a more compact chromatin structure by connecting neighboring nucleosome core particles, lead to hyperresistance to DNA damage. In contrast, hypercondensed chromatin domains are associated with lower DNA repair efficiency. Thus, the chromatin modifier KAP1 (KRAB (Krüppel-associated box)-ZFP (zinc finger protein)-associated protein 1) is required for repair in such domains regulating heterochromatin structure through binding histone methyltransferase SETDB1, HDAC1 and HDAC2 and the nucleosome remodeling factor CHD3 (chromodomain DNA helicase-binding 3) (Lukas, Lukas, and Bartek 2011; Iyengar and Farnham 2011). Thus, major structural remodeling was reported to be required for heterochromatic DSB repair (Goodarzi et al. 2008; Jakob et al. 2011).

In general, DSB repair is associated with local chromatin relaxation in order to allow access to repair proteins (Schwertman, Bekker-Jensen, and Mailand 2016; Shi and Oberdoerffer 2012; Smeenk and van Attikum 2013). The processes of chromatin relaxation, as well as its re-condensation after the breaks are repaired are highly regulated by chromatin remodelers, which can be classified into four subfamilies: the imitation switch (ISWI), the CHD, the switch/sucrose non-fermentable (SWI/SNF) and the INO80 subfamily (Stadler and Richly 2017).

Upon DSB induction local chromatin relaxation is achieved by the NuA4 remodeling complex β subunit TIP60, which is one of the most important acetyltransferases

during DSB repair and catalyzes acetylation of histones H2A and H4. The N-terminal tail of H4 can interact with the surface of H2A-H2B dimers of adjacent nucleosomes via ionic interactions. Acetylation of H4 disrupts this interaction and causes thereby chromatin decompaction (Price and D'Andrea 2013; Luger, Dechassa, and Tremethick 2012). TIP60 binds via its chromodomain to H3K9me3, which is transiently released by HP1 in the vicinity of DNA damage, and together with MRN complex it activates ATM by acetylation (see Figure 13) (Sun et al. 2009; Sun et al. 2005). Another subunit of NuA4 complex, a motor ATPase p400 (member of INO80 subfamily), further increases the accessibility of DNA for repair proteins by destabilizing histone-DNA interactions (Xu et al. 2010).

On the other hand, although there is substantial evidence for chromatin relaxation upon DNA damage induction, there are also some studies reporting chromatin condensation in DSB repair (Shi and Oberdoerffer 2012). So it was found, that HP1 variants accumulate at DSB sites (Luijsterburg et al. 2009). Suppression of RNA Polymerase II activity and following abrogation of transcription-coupled decondensation are further marks for condensed chromatin in the vicinity of DSBs (Shanbhag et al. 2010), as well as gene silencing mediated by hypermethylation at CpG islands (O'Hagan, Mohammad, and Baylin 2008). Condensation of chromatin during DSB repair could provide positional stability within the nucleus, as loss of local positional restrain can result in increased genomic instability and translocation formation (Soutoglou et al. 2007; Shi and Oberdoerffer 2012). Further, in addition to local chromatin reorganization, global chromatin condensation has been reported (Hamilton et al., 2011), suggesting a protective role for genome compaction upon DNA damage induction.

In summary, chromatin structure, especially after break induction, is highly dynamic. Rearrangements are additionally regulated in a cell cycle specific manner, as there was a complete disruption of nucleosomes around DSBs observed in asynchronous cells but only partial disruption in G1-arrested cells (Goldstein et al. 2013). The different responses might reflect the distribution of DSB repair pathways across the cell cycle, as cNHEJ is predominantly active in G1-phase, while HRR is restricted to S/G2-phase (Dabin, Fortuny, and Polo 2016). This transient disruption of nucleosomes shall facilitate the access of repair proteins to the damage sites. When

the break sites are repaired new core histones are binding the restored DNA, finishing the DDR.

4.6.3) Changes in extracellular tonicity globally alters chromatin

As the above mentioned reports about chromatin reorganization upon DSB induction are opposing, we wanted to further investigate the influence of chromatin structure on DSB signaling and repair. Therefore, we utilized cell culture medium with low and high concentration of NaCl to globally induce chromatin relaxation and condensation, respectively.

An increase in inorganic ions in the extracellular fluid generates a concentration gradient between the inside and outside of the cell, which the cell will try to counterbalance immediately. Thus, water moves out of the cell and thereby increases its inner concentration of ions. During this process the cell volume decreases. The opposite is true for a lower concentration of inorganic ions in the extracellular fluid. The cell takes up water decreasing its inner ion concentration aiming for an equilibrium. During this process the cell swells. As a response to this volume change swollen cells release KCl, nonessential organic osmolytes and cell water during a process called regulatory volume decrease (RVD). On the contrary, regulatory volume increase (RVI) is responsible for gaining cell volume of osmotically shrunken cells by taking up KCl and cell water (see Figure 14) (Hoffmann, Lambert, and Pedersen 2009).

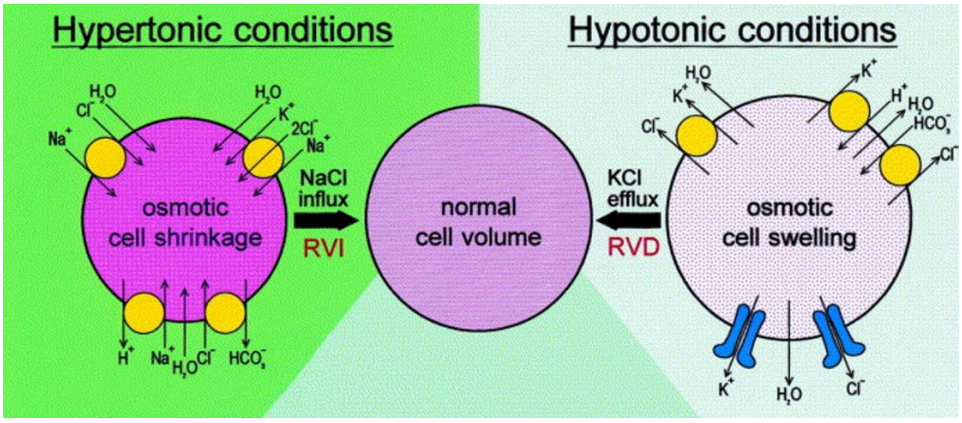

Figure 14 Schematic model of relations between disordered mechanisms of cell volume regulation (RVD and RVI).
See text for more detail. Adapted from (Okada and Maeno 2001).

While cell volume is restored relatively quickly, the intracellular ionic strength remains low (after RVD) or high (after RVI), respectively. The altered ion concentration perturbs macromolecules within the cell and gets replaced by compatible organic osmolytes which do not interfere with cellular processes (Dmitrieva and Burg 2005; Burg, Kwon, and Kultz 1997).

Normally, the tonicity of extracellular fluids is kept constant but under certain circumstances the osmolarity can change and perturb the regulation of cell volume. Water or hypotonic food intake reduces osmolarity of the extracellular environment of intestinal epithelial cells, while on the other hand antidiuresis can lead to an exposure to very high tonicity for kidney medullar cells. In addition to medullar cells, recent studies demonstrate that hypertonic environments also occur upon bacterial skin infections causing cutaneous Na^+ accumulation and that high dietary salt intake can result in hyperosmolality in skin, muscle and other tissues (Jantsch et al. 2015; Nikpey et al. 2017; Fischereder et al. 2017). Furthermore there are several pathophysiological conditions causing changes in cell volume such as hypoxia/ischemia, hypo-/hypernatremia and increases or decreases in extracellular K^+ concentration (Hoffmann, Lambert, and Pedersen 2009).

Incubation of cells in hypertonic cell culture medium results in chromatin condensation and large reductions in nuclear size (Finan, Leddy, and Guilak 2011; Albiez et al. 2006). Treatment with high salt concentration was also shown to sensitize cells to chromosomal damage and killing by IR and to inhibit tumor growth (Falk, Lukásová, and Kozubek 2008; Dettor et al. 1972; Lin et al. 2005). DNA repair seems to be inhibited by high NaCl concentrations, as measurements of DSB rejoining performed by pulsed-field gel electrophoresis (PFGE) showed a decrease in the fast repair component under hypertonic conditions (Iliakis et al. 1993). It was reported that Mre11 exonuclease is caused to move from the nucleus to the cytoplasm and cannot initiate repair. Additionally, Chk1 is not phosphorylated in response to DNA breaks induced by exposure to hypertonic medium (Dmitrieva, Bulavin, and Burg 2003; Dmitrieva, Cai, and Burg 2004). Another study showed an 3 - 4 fold increase in γH2AX foci size upon hypertonic treatment immediately following irradiation indicating disturbed DSB repair (Reitsema et al. 2005).

Chromatin decondensation can be achieved by lowering ionic strength using hypotonic treatment. Similar to hypertonic treatment, incubation of cells in medium

with low NaCl concentration impairs DSB repair efficiency (Falk, Lukásová, and Kozubek 2008).

However, the underlying mechanisms how variations in ionic strength influence and disrupt repair of DSBs and in general the activation of DDR and cell cycle checkpoints is not completely understood, yet. Therefore we utilize hypo- and hypertonic treatment in order to investigate DSB signaling and repair.

5) Aim of the thesis

In this thesis the contribution of chromatin structure to DDR signaling and DSB repair and repair pathway choice is investigated. From the literature contrary roles of relaxed and condensed chromatin are suggested for successful DSB processing. Our approach of utilizing changes in tonicity to globally relax or condense chromatin should help to elucidate the role of chromatin environment in the evolution and maintenance of complex signaling cascades of DDR elicited by the induction of DSBs.

Therefore our first attempt is the quantification of changes in chromatin structure evoked by extracellular changes in tonicity. In addition to a mathematical approach based on intensity changes in fluorescently stained nuclei, also optical evaluation of chromatin compaction is performed with the help of cytogenetics and helps to elucidate the chromatin altering effects of hypotonic and hypertonic treatment.

The choice between HRR and cNHEJ is the focus of several studies and chromatin structure is often implicated in promoting the one or the other repair pathway. Thus, investigation of initial DDR signaling and several downstream DDR outcomes (e.g. DNA damage checkpoint activation and DSB repair) shall help to characterize the role of chromatin in the overall response. Visualization of IR-induced foci (IRIF) by immunofluorescent staining allows the study of initial DDR signaling in an environment of either relaxed or condensed chromatin. Another endpoint of DDR function is the activation of G2-checkpoint, which helps in maintaining genomic stability and is here also investigated under conditions of changed tonicity.

Furthermore DSB repair is investigated at several levels utilizing not only analysis of IRIF by confocal microscopy, but also PFGE to investigate repair of the physical DSBs. Associated processes of cell cycle redistribution and arrest are analyzed by flow cytometry (FC). Finally, the usage of reporter assay cell lines helps to elucidate the influence of chromatin structure on DSB repair pathway choice.

For all experiments the human retinal pigment epithelial (RPE-1) hTert cell line is used that provides a non-transformed, repair proficient genetic background for the investigation of diverse endpoints of DDR signaling and DSB repair in the context of altered chromatin structure.

6) Material and Methods

6.1) Material

Table 1 Cell culture growth media

growth medium	supplier
Dulbecco's Modified Eagle Medium (DMEM)	Sigma-Aldrich
McCoy's 5A medium	Sigma-Aldrich

Table 2 Cell lines and corresponding growth media

cell line	cell type	origin	growth medium	serum
RPE-1 hTert	retina pigmented epithelium	human	DMEM	10 %
U2OS 279A EJ2-GFP	osteosarcoma	human	McCoy's 5A	10 %
U2OS 280A EJ5-GFP	osteosarcoma	human	McCoy's 5A	10 %
U2OS 282C DR-GFP	osteosarcoma	human	McCoy's 5A	10 %
U2OS 283C SA-GFP	osteosarcoma	human	McCoy's 5A	10 %

Table 3 Antibodies for immunofluorescence (IF), FC and western blot (WB)

antibody	host / type	dilution	incubation time	supplier
53BP1 (H300)	rabbit / polyclonal	1:1,000 (IF)	1.5 h	Santa Cruz Biotechnology
anti-goat IRDye 800	donkey / polyclonal	1:10,000 (WB)	1 h	Li-COR Biosciences
anti-mouse Alexa Fluor 488	goat / polyclonal	1:400 (IF/FC)	1 h	Invitrogen
anti-mouse Alexa Fluor 568	goat / polyclonal	1:400 (IF)	1 h	Invitrogen
anti-mouse Alexa Fluor 647	goat / polyclonal	1:400 (IF)	1 h	Invitrogen
anti-mouse IRDye 680LT	goat / polyclonal	1:10,000 (WB)	1 h	Li-COR Biosciences
anti-rabbit Alexa Fluor 488	goat / polyclonal	1:400 (IF/FC)	1 h	Invitrogen
anti-rabbit Alexa Fluor 568	goat / polyclonal	1:400 (IF)	1 h	Invitrogen

anti-rabbit Alexa Fluor 647	goat / polyclonal	1:400 (IF/FC)	1 h	Invitrogen
anti-rabbit IRDye 800LT	goat / polyclonal	1:10,000 (WB)	1 h	Li-COR Biosciences
CyclinB1 (H-433)	rabbit / polyclonal	1:400 (IF)	1.5 h	Santa Cruz Biotechnology
Histone H1	goat / polyclonal	1:1,000 (WB)	overnight	Santa Cruz Biotechnology
Histone H3	rabbit / polyclonal	1:2,000 (WB)	overnight	Merck Millipore
H3pS10	rabbit / polyclonal	1:5,000 (FC)	1.5 h	Abcam plc
H3K9ac	mouse / monoclonal	1:1,000 (WB)	overnight	Abcam plc
H3K27me3	mouse / monoclonal	1:1,000 (WB)	overnight	Abcam plc
pATM	mouse / monoclonal	1:500 (IF)	1.5 h	Cell Signaling Technology
Rad51 (14B4)	mouse / monoclonal	1:400 (IF)	1.5 h	GeneTex
RPA70B	mouse / monoclonal	1:500 (FC)	1.5 h	IFMSB, UK Essen
γH2AX	mouse / monoclonal	1:500 (IF)	1.5 h	Abcam plc

Table 4 Plasmids used for transfection

plasmid	description
pCMV-3xnls-ISceI	I-SceI expressing plasmid
pEGFP-N1	EGFP expressing plasmid

Table 5 EdU Click-iT reaction cocktail

stock solutions	working concentration
1 M Tris pH 7.4	100 mM
1X PBS	
10 mM $CuSO_4$	1.25 mM
1 mM Azide dye (Alexa Fluor 647)	1.25 µM
500 mM Ascorbic Acid	12.5 mM

Table 6 Chemicals

chemicals	supplier
4’,6-diamidino-2-phenylindole (DAPI)	SERVA
5-Ethynyl-2’-deoxyuridine (EdU)	SERVA
Acetic acid	Roth
Acetone	J.T. Baker
Ammonium persulfate (APS)	Sigma-Aldrich
Ascorbic acid	Roth
Boric acid	Roth
Bovine serum albumin (BSA) fraction V	Roth
Bromophenol blue (BrPBlue)	Sigma-Aldrich
Colcemid	Calbiochem, Merck Millipore
Copper(II) sulfate pentahydrate ($CuSO_4$)	Sigma-Aldrich
Crystal violet	Merck
Dimethyl sulfoxide (DMSO)	Sigma-Aldrich
Dithiothreitol (DTT)	Roth
Ethanol (EtOH)	Sigma-Aldrich
Ethidium bromide (EtBr)	SERVA
Ethylenediaminetetraacetic acid (EDTA)	Roth
Fetal bovine serum	Sigma-Aldrich
Gelatin	Sigma-Aldrich
Glycerol	Sigma-Aldrich
Glycine	Roth
HEPES (4-(2-hydroxyethyl)-1-piperazineethansulfonic acid)	Roth
KU55933	Haoyuan ChemExpress
Magnesium chloride ($MgCl_2$)	Sigma-Aldrich
Methanol (MeOH)	J.T. Baker
N-Lauroylsarcosine (NLS)	Merck
Non-fat dry milk	Roth
NU7441	Haoyuan ChemExpress
Paraformaldehyde (PFA)	Roth
Potassium chloride (KCl)	Roth
PromoFluor antifade reagent	PromoKine
Propidium iodide (PI)	Sigma-Aldrich
Protease inhibitor	Roche
Proteinase K	Sigma-Aldrich
RNase A	Applichem
Rotiphorese® Gel 30 (37.5:1)	Roth
Sodium chloride (NaCl)	Roth
Sodium dodecyl sulfate (SDS)	Roth
Sodium hydrogen carbonate ($NaHCO_3$)	Roth
Sulfo-cyanine5 azide	Lumiprobe
Sulfuric acid (H_2SO_4)	Merck

Tetramethylethylenediamine (TEMED)	Roth
Trichloroacetic acid (TCA)	Roth
TRIS Pufferan®	Roth
Triton X-100	Roth
Trypsin	Biochrom
Tween 20	Roth
VE-821	Haoyuan ChemExpress

Table 7 Solutions for SDS-PAGE and immunoblotting

solutions	compounds
10X running buffer	0.025 M Tris-HCl 0.192 M glycine 0.1 % SDS
4X stacking gel buffer	0.5 M Tris-HCl, pH 6.8 0.4 % SDS
4X resolving gel buffer	1.5 M Tris-HCl, pH 8.8 0.4 % SDS
2X sample loading buffer	0.065 M Tris-HCl, pH 6.8 0.01 M EDTA 20 % glycerol 3 % SDS 0.02 % BrPBlue 5 % DTT
5 % stacking gel	16.8 % Rotiphorese® Gel 30 bidest. H_2O 0.125 M 4X stacking gel buffer 0.1 % SDS 0.1 % APS 0.2 % TEMED
15 % resolving gel	50 % Rotiphorese® Gel 30 bidest. H_2O 0.37 M 4X resolving gel buffer 0.1 % SDS 0.1 % APS 0.1 % TEMED
4X electrode buffer	0.1 M Tris-HCl, pH 8.3 0.7 M glycine
western blot transfer buffer	25 % 4X electrode buffer 20 % MeOH

Table 8 Drugs

drug	description	working concentration
KU55933	specific inhibitor of ATM	10 µM
NU7441	specific inhibitor of DNA-PK	5 µM
VE-821	specific inhibitor of ATR	5 µM

Table 9 Software

software	provider
EndNote X8	Thomson Reuters, USA
ImageJ	Image Processing and Analysis in Java, USA
ImageQuant 5.2	GE Healthcare, Sweden
ImarisXT 8.0.2	Bitplane AG, Switzerland
Isis Fluorescence Imaging Platform	MetaSystems, Germany
Kaluza 1.2	Beckman Coulter, USA
LasAF	Leica Microsystems, Germany
MatLab R2017b	MathWorks Inc. USA
Microsoft Office 2013	Microsoft, USA
MultiCycle AV DNA Analysis	Phoenix Flow Systems, USA
Odyssey® Infrared Imaging System	LiCor Biosciences USA
Adobe Photoshop CS5	Adobe Systems Inc. USA
SigmaPlot 12.5	Systat Software Inc. USA

6.2) Methods

6.2.1) Cell culture

Cells are cultivated at 37 °C in a humidified incubator with 5 % CO_2. All growth media are supplemented with 100 µg/ml penicillin and 100 µg/ml streptomycin. Cells are maintained in 100 mm cell culture dishes with 15 ml growth medium containing 10 % fetal bovine serum (FBS). The cell lines and media used are listed in Table 1 and Table 2.

Cell lines are regularly passaged to avoid overgrowing and to ensure a stable reproducible source of cells to setup experiments. In order to passage or collect cells, cells are washed with 1X phosphate buffered saline (PBS) and incubated in 1 ml of a 0.05 % trypsin/EDTA solution for 2 - 5 min on a warm plate (42 °C) to detach from dish surface. Afterwards, cells are collected and resuspended in 5 -

7 ml growth medium containing 10 % FBS. Cell numbers are measured in a Beckman Coulter Counter (Multisizer Z2).

For experiments, cells are plated in either 35 or 60 mm cell culture dishes with 2 and 5 ml medium, respectively. Cells used for experiments are in exponential growth phase.

6.2.2) X-ray irradiation

Irradiation of cells is carried out using an X-ray machine (X-ray tube: MXR320 (Comet), X-ray generator: ISOVOLT Titan (General Electrics), control unit: Xrad320 (PXi)) operating at 320 kV and 12.5 mA with 1.65 aluminum filter. Cells are exposed to X-rays at room temperature (RT) in standard cell culture dishes at distances according to the dish sizes and while rotating the irradiation table to avoid intensity fluctuations within the irradiation field. Cells in 30 - 60 mm diameter cell culture dishes are irradiated at a distance of 50 cm and a dose rate of 3.6 Gy/min. Performing G2-checkpoint assays and PFGE experiments, cells in 25 cm^2 flasks and cells in 60 mm dishes, respectively, are irradiated on a thin-walled aluminum box filled with pre-warmed water to avoid temperature fluctuations at a distance of 66 cm and a dose rate of 3.2 Gy/min. Controls are treated similarly but are not irradiated.

6.2.3) Hypotonic and hypertonic cell treatment

For hypotonic and hypertonic treatment, the osmotic concentration of the standard cell growth medium is increased or decreased by a factor of two. Osmotic concentration is decreased by adding equal volume of bidest. sterile water to yield approx. 75 mM NaCl end concentration. For hypertonic conditions an equal amount of a 450 mM NaCl solution is added to increase the NaCl concentration to 300 mM. For control experiments an equal volume of a 150 mM NaCl solution is added to maintain isotonic conditions.

For experiments, cells are plated in standard growth medium for 1 or 2 days. Immediately after irradiation, sterile water, 150 mM NaCl solution or 450 mM NaCl solution is added to establish hypotonic, isotonic or hypertonic conditions during DSB repair. Cells are kept in these conditions until collection.

6.2.4) Histone extraction

In order to investigate histone PTMs, that are characteristic for EC and HC, histones are extracted from RPE-1 cells using the following protocol adapted from (Shechter et al. 2007).

For histone extraction approx. 0.5 x 10^6 RPE-1 cells are seeded in 100 mm cell culture dishes in 10 ml DMEM + 10 % serum and are incubated at 37 °C and 5 % CO_2. After two days of growth 10 ml of sterile water, 150 mM NaCl solution or 450 mM NaCl solution is added to achieve global chromatin relaxation or condensation, respectively. After 1 h of incubation cells are trypsinized, collected and centrifuged at 1,500 rpm for 5 min at RT. The supernatant is aspirated and cell pellet is resuspended in 500 µl 1X PBS. The cells are transferred to a 1.5 ml Eppendorf tube and centrifuged at 10,000 rpm for 5 min. Afterwards the supernatant is aspirated and cell pellet is stored at -20 °C until further procession.

In order to lyse cells the pellet is resuspended in 1 ml hypotonic solution (1.5 mM $MgCl_2$, 1 mM KCl, 10 mM Tris-HCl, 1 mM DTT in bidest. H_2O) containing protease inhibitor. After 30 min of incubation on a shaker at 4 °C, samples are centrifuged at 9,500 rpm and 4 °C for 10 min to separate intact nuclei from cell debris. The supernatant is discarded and nuclei are resuspended in 400 µl of 0.4 N H_2SO_4. Samples are incubated on shaker for 2 h at 4 °C. Nuclear debris is separated from histones by centrifugation at 9,500 rpm at 4 °C for 10 min. The supernatant containing extracted histones is transferred to a new 1.5 ml Eppendorf tube and 132 µl TCA is added in order to precipitate histones. The samples are incubated on ice for 1 h before centrifugation at 12,000 rpm and 4 °C for 10 min. The supernatant is aspirated and histone pellet is washed with ice-cold acetone twice to remove acidic rests. After another centrifugation step at 12,000 rpm and 4 °C for 10 min the acetone is removed and histone pellets are allowed to air-dry for 20 min at RT. Afterwards histones are dissolved in 60 µl bidest. H_2O and stored in -20 °C until further use.

6.2.5) SDS-PAGE and immunoblotting

Immunoblotting is applied to detect proteins of interest by separating them according to their molecular weight. In this thesis only histones are loaded onto gels. After

histone extraction (see 6.2.4) 5 µl of samples are mixed 1:1 with 2X sample loading buffer (see Table 7) and denatured for 5 min at 96 °C. Before loading samples are spun down for few seconds at 13,000 rpm. During SDS polyacrylamide gel electrophoresis (SDS-PAGE) histones are resolved on 15 % SDS polyacrylamide gel with a constant voltage of 120 V for 105 to 120 min.

For western blotting, the separated histones from the SDS polyacrylamide gel are transferred onto an Odyssey® 0.22 µm nitrocellulose membrane for 1 h at 120 V by the help of a wet transfer apparatus. During the transfer the temperature is constantly kept at 4 °C. Afterwards the membrane is blocked with 5 % non-fat dry milk in 1X TBS (25 mM Tris-HCl, pH 7.6, 150 mM NaCl) for 1 h at RT while gently shaking. Incubation with primary antibodies, which are diluted (see Table 3) in 5 % non-fat dry milk in TBS-T (1X TBS with 0.05 % Tween-20), is performed overnight at 4 °C. Before incubation with secondary antibodies (diluted in TBS-T, see Table 3), membranes are washed with TBS-T three times for 10 min. After 1 h of incubation with secondary antibodies at RT and three additional washing steps in TBS-T for 10 min, the membrane is allowed to dry. For detecting histones the Odyssey® Infrared Imaging System (LI-COR Biosciences) is used.

6.2.6) Pulsed-field gel electrophoresis

The technique of asymmetric field inversion gel electrophoresis (AFIGE) which was developed by Stamato and Denko in 1990 is used with minor modifications to analyze IR-induced DSBs in mammalian cells (Stamato and Denko 1990; Iliakis et al. 1991). DSBs cause the fragmentation of DNA that can be measured by the size-dependent migration of DNA fragments in an agarose gel under the influence of a pulsed electric field. This fragmentation of chromosomal DNA leads to a linear, dose dependent increase in the fraction of DNA which becomes released (FDR) from the plug into the lane (see Figure 15 A). As dose responses may vary from cell line to cell line, or due to the cell cycle phase (Iliakis et al. 1991), the repair kinetics are expressed as DEQ (dose equivalent) instead of FDR to facilitate comparison. DEQ is the equivalent dose reflecting remaining DSBs and calculated from the FDR of every repair time point on the basis of the corresponding dose response curve (see Figure 15 B) (Paul et al. 2013).

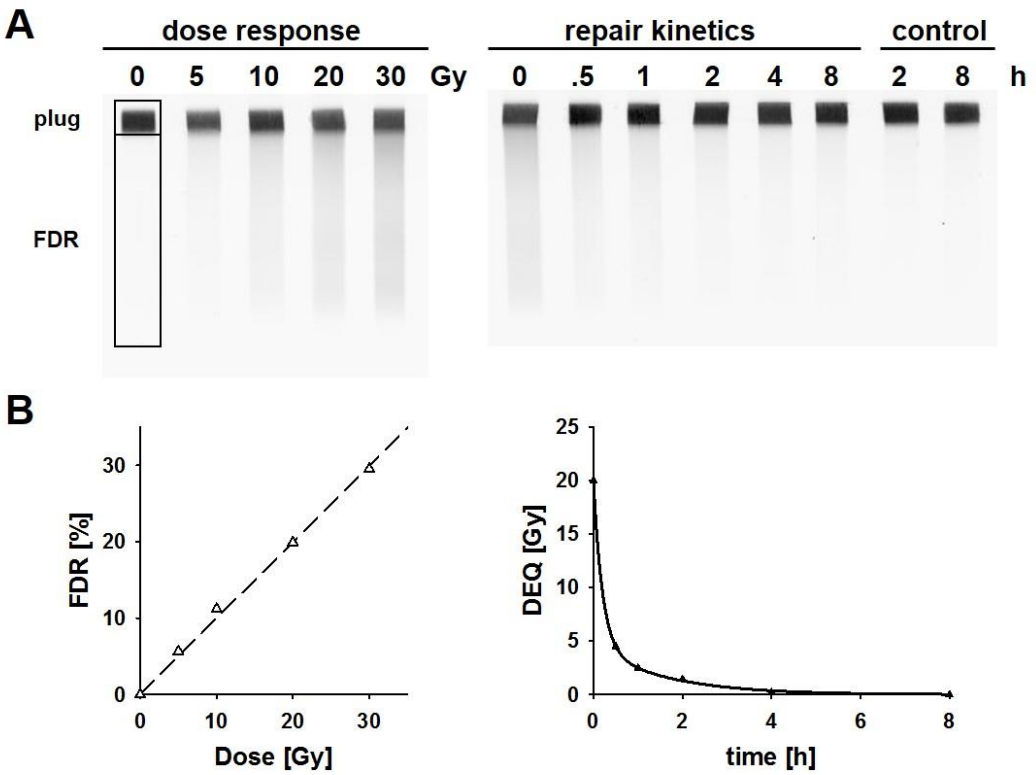

Figure 15 Representative PFGE gels and corresponding dose response and repair kinetics curves.
(A) Images of EtBr stained gels, which are used to evaluate the FDR from the plugs. For repair kinetics cells are irradiated with 20 Gy and collected at indicated time points. (B) Dose response curve is plotted from intensity values of FDR versus the corresponding doses. Using the equation of the regression line from the dose response curve, DEQ values are calculated and plotted against repair times.

For PFGE experiments approx. 2 x 10^5 cells are plated in 60 mm dishes and incubated at 37 °C and 5 % CO_2. After two days of growth, cells are differently treated for dose response and repair kinetics.

In order to evaluate the induction of DSBs at different IR doses cells are trypsinized and collected. Cell number is counted in a Beckman Coulter Counter and the cells are centrifuged at 1,500 rpm for 5 min at 4 °C. The supernatant is aspirated and cells are washed with 1X PBS and centrifuged again. The cell pellet is then resuspended in serum-free medium containing 5 mM $NaHCO_3$ and 20 mM HEPES in a way that yielded a concentration of 6 x 10^6 cells per ml. Afterwards the same amount of prewarmed (50 °C) serum-free medium containing 1 % low melting agarose is added to obtain a final concentration of 3 x 10^6 cells per ml. This solution is pipetted into glass tubes (Ø 3 mm) and placed on ice to allow the agarose to solidify. The solid agarose containing the cells is extruded from the glass tubes and

cut into 5 mm long pieces (plugs) with every plug containing approx. 10^5 cells. The plugs are then placed into a 35 mm dish (containing 2 ml of serum-free HEPES buffered medium) which is placed into a 100 mm dish filled with ice in order to irradiate the cells in the plugs under cold conditions. After irradiation the plugs are put into lysis solution (10 mM Tris, 100 mM EDTA, 50 mM NaCl, 2 % NLS, pH 7.6 and freshly added 0.2 mg/ml proteinase K) and incubated on ice for approx. 30 min before incubation at 50 °C for 18 h.

In order to analyze the repair kinetics of IR-induced DSBs cells are irradiated with 20 Gy on a warm plate and collected at certain time points after IR. The collection of cells and preparation of plugs is the same as described above. The plugs are incubated in lysis solution for 18 h at 50 °C. In case of analysis of altEJ repair efficiency cells are pretreated with DNA-PKi (see Table 8) for 1 h prior IR.

After the lysis in hot buffer the plugs are washed in washing buffer (10 mM Tris, 100 mM EDTA, 50 mM NaCl, pH 7.6) for 1 h at 37 °C. The washing buffer is then replaced by fresh washing buffer containing 0.1 mg/ml RNase A and plugs are incubated for 1 h at 37 °C.

Beside dose response and repair kinetics, cells that are equally treated but not irradiated are processed in the same way at certain time points (2 and 8 h control, see Figure 15) to determine and subtract in the analysis background signals generated in non-irradiated cells.

PFGE is performed in 0.5 % agarose gels in 0.5X TBE buffer (44.5 mM Tris, 44.5 mM boric acid, 1 mM EDTA). Plugs are loaded onto gels and sealed with 1 % agarose to avoid floating during the PFGE run. For electrophoresis, chambers are filled with 2 l of 0.5X TBE, which is cooled to 8 °C. The run is operated by a switching unit in alternating cycles changing from 50 V for 900 s in the direction of DNA migration to 200 V for 75 s in reverse direction. After 40 h the run is stopped and the gel is stained with 5 mg/ml EtBr for 4 h. Afterwards the gel is washed in bidest. H_2O for several hours, replacing the water 2 - 3 times. The gel is then scanned using Typhoon 9410 scanner and FDR is analyzed with ImageQuant 5.2 (GE Healthcare).

To determine FDR values the intensity of stained DNA in the lane below the plug is divided by the total intensity of the plug and the released DNA (total DNA in the sample). FDR levels of controls are subtracted from FDR values of irradiated

samples. The dose response curve is generated by plotting FDR values against dose. With the equation of the dose response regression line, the DEQ for every sample of repair kinetics is calculated. The repair kinetics curves are fitted by using a non-linear regression analysis of SigmaPlot 12.5.

6.2.7) Clonogenic survival assay

Clonogenic survival assays are preformed to estimate the cell radiosensitivity to killing. Therefore approximately 10^5 cells were seeded in 60 mm and incubated at 37 °C and 5 % CO_2. After two days of growth, cells are irradiated and either treated with isotonic, hypotonic and hypertonic medium for 6, 9, 16 and 24 h or directly collected and seeded in low numbers aiming towards 30 - 150 colonies/dish in 60 mm dishes. After 11 days of growth at 37 °C and 5 % CO_2, colonies are stained with 1 % crystal violet in 70 % EtOH and counted.

6.2.8) Confocal laser scanning microscopy

For the quantification of foci formation, confocal laser scanning microscopy (CLSM) is performed. In order to generate high resolution optical images, a LEICA TCS-SP5 confocal microscope is used. With this kind of microscopy images with much higher resolution than conventional wide-field fluorescence microscopy can be produced. The region-of-interest is illuminated by a laser beam, which is focused by a pinhole placed in front of the source. The laser beam is focused by an objective lens onto the specimen and the emitted light is focused by a second objective lens at a second pinhole, which has the same focus as the first pinhole that is confocal with it (see Figure 16).

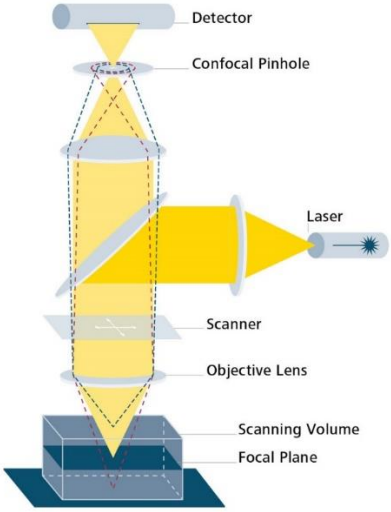

Figure 16 Principle of confocal microscopy.
Figure obtained from www.zeiss.com "The Confocal Principle".

The light passing through the second pinhole is then detected by a photomultiplier (PMT) detector and analyzed by appropriate software. The key principle of confocal microscopy is that the second pinhole prevents light from above or below the focus plane from reaching the detector. With this technique the generation of much sharper images is possible by eliminating out-of-focus fluorescent light (Paddock 2000). A scanning device excites the specimen in X and Y directions and optical sectioning in steps of 0.5 µm in Z direction allows a three-dimensional reconstitution of the sample.

6.2.8.1) Immunofluorescence staining for microscopic samples

For immunofluorescence experiments approximately 10^5 cells are plated in 35 mm dishes containing Ø 20 mm glass coverslips. After two days of growth, cells are irradiated (1 - 16 Gy) and incubated at 37 °C, 5 % CO_2 until the time points at which the formation of IRIF has to be examined (30 min - 8 h). To identify cells which are in S-phase during irradiation, cells are additionally incubated before irradiation with 10 µM of the thymidine analogue EdU for 30 min at 37 °C, 5 % CO_2. After IR cells are washed with 1X PBS and standard growth medium is added.

For fixation the medium is removed, cells are washed with 1X PBS and incubated in 2 ml of 2 % PFA (+ 2 % sucrose, optional) in 1X PBS for 15 min at RT. PFA-solution is removed and cells are washed with 1X PBS. For permeabilization, 2 ml

of P-solution (100 mM Tris pH 7.4, 50 mM EDTA in bidest. H_2O) containing 0.5 % Triton X-100 is added for 7 min at RT. After removing P-solution and another washing step with 1X PBS, cells are incubated in 2 ml of PBG (0.2 % gelatin, 0.5 % BSA fraction V in 1X PBS) at 4 °C overnight.

After blocking, cells are incubated with primary antibodies (diluted in PBG, Table 3) for 1.5 h at RT. The coverslips are washed with 1X PBS three times for 5 min. Secondary antibodies with conjugated Alexa Fluor dyes (Table 3) are diluted 1:400 in PBG and incubated with cells for 60 min at RT in the dark. The coverslips are washed with 1X PBS three times for 5 min. In case of prior EdU incorporation, EdU is labeled with Click-iT reaction cocktail (see Table 5) incubating cells in 90 µl of EdU labeling solution for 30 min at RT. Afterwards coverslips are washed with 1X PBS three times for 5 min before the cells are incubated with DAPI (50 ng/ml) for 10 min at RT in the dark to stain the DNA.

Finally, cells are washed with 1X PBS (three times for 5 min) and mounted on microscopic slides using PromoFluor Antifade Reagent. After solidification of the mounting media in the dark at RT, 3D-images are scanned using a confocal microscope.

6.2.8.2) Determination of chromatin condensation parameter

In order to determine the chromatin condensation parameter (CCP) of cell nuclei treated with different NaCl concentrations, 10^5 cells are plated in 35 mm dishes containing Ø 20 mm glass coverslips and 2 ml standard cell culture medium. After two days of growth, 2 ml of isotonic, hypotonic or hypertonic H_2O is added and cells are incubated at 37 °C, 5 % CO_2 until the time points at which the status of chromatin condensation is examined (1 – 24 h).

Fixation, permeabilization and blocking are performed as described in 6.2.8).

In order to stain the DNA, cells are incubated in 2 ml 1X PBS containing 50 ng/ml DAPI for 10 min at RT in the dark. After incubation coverslips are washed with 1X PBS three times for 5 min before mounting onto slides using PromoFluor Antifade reagent.

The nuclei are imaged by CLSM using a 63.0 x 1.4 Oil UV objective at a resolution of 1024 x 1024 pixels per image. Per time point 132 - 275 cells are scanned. Using

ImageJ software, images in gray scale containing single nuclei are generated using a macro described in supplementary information.

The quantification of CCP is performed following the instructions in Irianto et al. that are explained in an upcoming section (Irianto, Lee, and Knight 2014). The different steps of processing the images are shown in Figure 17.

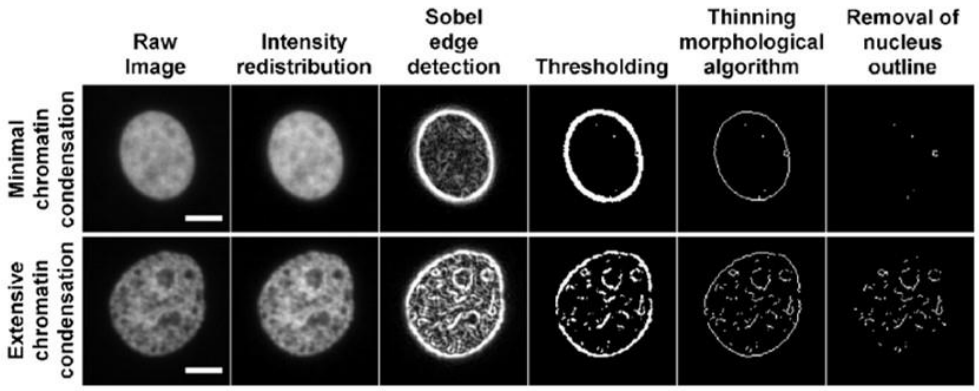

Figure 17 Images representing different steps of processing in order to determine the CCP (Irianto, Lee, and Knight 2014).
Images of two separate nuclei with minimal (top) and extensive (bottom) chromatin condensation, showing the results of each image processing step leading to the calculation of the CCP (bar: 5 μm).

In order to standardize the images the intensity profiles are redistributed by dividing each pixel intensity by the maximum intensity of the image and multiplying by 255 which is the maximum intensity for 8-bit images. In the next step a Sobel edge detection algorithm is used. This detection uses 3 x 3 kernels to approximate the gradients between a pixel and the eight surrounding pixels (described in equation 3):

$$S_x = \begin{bmatrix} +1 & 0 & -1 \\ +2 & 0 & -2 \\ +1 & 0 & -1 \end{bmatrix} \quad \text{and} \quad S_y = \begin{bmatrix} -1 & -2 & -1 \\ 0 & 0 & 0 \\ +1 & +2 & +1 \end{bmatrix} \tag{3}$$

S_x is Sobel kernel for the approximation of gradient in X direction and S_y is Sobel kernel for the approximation of gradient in Y direction. Further the gradient magnitude is used to represent the processed pixel of interest in the target image and is calculated by the following equations:

$$G_x = S_x \times I \tag{4}$$

$$G_y = S_y \times I \quad (5)$$

$$G = \sqrt{G_x^2 + G_y^2} \quad (6)$$

G_x is the approximated gradient in X direction, G_y is the approximated gradient in Y direction and I is the target image.

The calculation of the gradient magnitude G is repeated for every pixel in the target image and the new image is then showing the level of edges based on the gradient magnitude (see Figure 17 third column). The more the chromatin in the imaged nuclei is condensed the stronger edges are produced by the Sobel edge detection algorithm. In addition the image is thresholded to acquire the strong edges. The produced image is then undergoing a thinning algorithm which transforms an entity within the image into a single pixel thickness entity. As there is a natural high difference in intensity between the imaged nucleus and the background, the Sobel edge detection algorithm is generating an artificial boundary edge which needs to be removed. In the end the number of edges within the nucleus is divided by the nuclear area and determines the edge density which is defined as CCP.

All calculations are performed using MatLab and the codes provided in supplementary files from Irianto et al. and adapted for our purposes. The used MatLab codes can be seen in supplementary materials.

6.2.9) Flow cytometry

FC is performed using a Beckman Coulter Gallios flow cytometer. It is used to analyze cell cycle distribution, to determine the mitotic index (MI) by H3pS10 labeling and to measure DNA end resection.

In order to determine the cell cycle distribution the fluorescence signal of the intercalating agent PI is analyzed. PI has a red fluorescence which is excited by an Argon laser (488 nm). As it binds to double-stranded nucleic acids, RNase is added to avoid signal from dsRNA. The measured fluorescent signal intensity is proportional to DNA amount and is used to determine G1-, S- and G2/M-phase percentage. PI is not membrane permeable, so cells have to be permeabilized before PI staining. In order to analyze cell cycle distribution, cells are collected, fixed

in cold 70 % EtOH and stored at 4 °C. Before FC, cells are centrifuged at 4 °C for 5 min at 1,500 rpm. EtOH is removed and the cell pellet is resuspended and incubated for 30 min at 37 °C in PI staining solution (40 µg/ml PI, 62 µg/ml RNase A in 1X PBS). During FC 30,000 cells per condition are analyzed. In order to only measure cells of interest, gating is monitored based on the forward and side scattering (single cells). Cell cycle analysis is carried out using MultiCycle AV DNA Analysis software.

6.2.9.1) Immunofluorescence staining for FC

For three parametric FC measurements of DNA end resection approx. 10^5 cells are plated in 60 mm dishes and allowed to grow for two days at 37 °C in a 5 % CO_2 atmosphere. Cells are then pulse-labeled with EdU for 30 min prior to IR (see 6.2.8). In order to collect cells at certain time points trypsinization and collection of cells are performed before centrifugation at 2,000 rpm for 5 min at 4 °C. The supernatant is removed and cells are incubated in 500 µl of cold 1X PBS containing 0.2 % Triton X-100 for 2 min on ice. After another centrifugation step cells are fixed in 500 µl 2 % PFA solution containing 2 % sucrose for 15 min at RT. Another centrifugation step follows and cells are then incubated in 1 ml PBG overnight at 4 °C.

In order to prepare for antibody labeling, cells are centrifuged at 2,000 rpm for 5 min at 4 °C and the supernatant is removed. 150 µl of primary antibodies diluted in PBG (see Table 3) are added and cells are incubated for 1.5 h at RT while shaking. For washing, 1 ml of 1X PBS is added to the samples before centrifugation and removal of supernatant. This step is repeated once. Afterwards cells are incubated in 100 µl of secondary antibodies diluted 1:400 in PBG for 1 h at RT (see Table 3) while shaking in the dark. Another washing step follows before cells are incubated in 90 µl of EdU ClickiT reaction cocktail (see Table 5) for 30 min at RT while shaking in the dark. Cells are washed again with 1X PBS and then incubated in PI staining solution for 30 min at RT.

Measurement is performed by Beckman Coulter Gallios flow cytometer. In order to determine the proportion of DNA end resection only single G2-phase cells that are negative for EdU are analyzed.

6.2.9.2) Determination of mitotic index

In order to determine the proportion of cells that are in mitosis, a two parameter FC approach is applied. As cells in M-phase have the same amount of DNA as G2-phase cells, staining of phospho-Serine10 of histone H3 (H3pS10) is used as a marker of mitotic cells, in addition to normal PI staining.

For MI determination approx. 10^5 cells are plated in 25 cm² cell culture flasks. After one day of growth at 37 °C and 5 % CO_2 caps of the flasks are closed to ensure steady state of CO_2 atmosphere and the flasks are relocated to a warm room with constant temperature of 37 °C. As temperature fluctuations can influence the MI, all further steps are performed in the warm room at 37 °C. An exception is the irradiation, which is then performed on a warm plate to minimize temperature fluctuations.

Mitotic cells are rounded up and can easily detach from flask surface. So the growth medium is not aspirated but collected in 15 ml tubes before cells are washed with prewarmed 1X PBS, which is collected in the tubes as well. Cells are detached by trypsinization and collected in prewarmed medium in the same tubes. After centrifugation at 1,200 rpm for 5 min at 4 °C the supernatant is removed, cells are fixed in cold 70 % EtOH and stored overnight at -20 °C.

For immunofluorescent staining cells are incubated in 500 µl of cold 1X PBS containing 0.25 % Triton X-100 for 5 min on ice before centrifugation at 1,500 rpm for 5 min at 4 °C. After removing the supernatant, cells are incubated in 1 ml PBG overnight at 4 °C. In case of treatment with PIKK inhibitors, ATMi, ATRi (concentrations see Table 8) and DMSO (equal volume as control) are added 1 h prior to IR.

6.2.10) Cytogenetics

For cytogenetic experiments approx. 10^5 cells are plated in 60 mm dishes. After two days of growth, cells are washed with 1X PBS, isotonic, hypotonic or hypertonic medium is added and cells are incubated at 37 °C, 5 % CO_2 until collection (1 - 24 h). Metaphases are accumulated by adding colcemid (0.1 µg/ml) 30 min before time point collection, which leads to the disruption of the spindle fibers and thereby prevents cells from proceeding to anaphase. Cells are collected by trypsinization

and resuspension in isotonic, hypotonic and hypertonic trypsin solution and medium. Subsequently, samples are centrifuged for 5 min at 1,200 rpm at 4 °C. The supernatant is discarded and hypotonic solution (75 mM KCl) is added dropwise to the cells up to a final volume of 7 ml. In this solution, cells are resuspended and incubated for 14 min at RT. Afterwards an equal volume of MeOH - acetic acid (3:1 ratio) is added before centrifugation for 7 min at 1,200 rpm at 4 °C. The supernatant is removed and cells are resuspended in 7 ml MeOH - acetic acid for fixation and stored overnight at 4 °C. The fixation procedure is repeated 3 times on the next day. Metaphase spreads are then prepared by dropping 15 µl of cell suspension onto clean wetted glass microscope slides, which are then allowed to air dry overnight.

After drying, slides are fixed for 15 min at RT in 2 % PFA solution. After washing with 1X PBS slides are counterstained with 50 ng/ml DAPI for 10 min in the dark at RT. After staining the slides are rinsed with MilliQ water and allowed to air dry for several hours. In the end slides are mounted using PromoFluor Antifade reagent and covered with coverslips.

Slides are scanned with a predefined protocol using MetaSystems working station and analyzed using the Isis Fluorescence Imaging Platform. For length quantification of metaphase chromosomes Adobe Photoshop CS5 ruler tool is used.

6.2.11) Quantification and statistics

For quantitative analysis mean values are calculated by Microsoft Excel using the "=AVERAGE" function. In cases of combination of two experiments the standard deviation (SD) function "=STDEV.P" is used which is based on the following formula:

$$SD = \sqrt{\frac{\sum(x - \bar{x})^2}{n}} \qquad (7)$$

In this calculation *x* is the sample mean and *n* is the number of repeats.

When three or more experiments are combined the standard error (SE) is calculated based on the following equation:

$$SE = \frac{SD}{\sqrt{n}} \qquad (8)$$

In this formula *SD* is the standard deviation (see equation 7) and *n* is the number of experiments.

7) Results

7.1) Retinal pigment epithelial cell line

Radiation biology studies the action of IR on living organisms and its consequences on human health. Radiation therapy is a widely used method to treat cancer. More than 80 % of malignant tumors are carcinomas, cancer that develops from epithelial cells. Therefore, we choose a normal epithelial cell line to investigate the repair of IR-induced DNA damage, in an effort to facilitate transfer of our findings to cancer research. In this study the human RPE-1 cell line expressing telomerase catalytic subunit component (hTert) is used. Expression of hTert in RPE-1 cells reconstitutes telomerase activity and extends their replicative lifespan without compromising the DDR or causing abnormal cell growth control or oncogenic transformation (Jiang et al. 1999). The hTert RPE-1 cell line is derived by transfecting the RPE-340 cell line with the pGRN145 hTert-expressing plasmid (ATCC® CRL-4000™) (Matsunaga et al. 1999; Bodnar et al. 1998).

In order to identify optimal growth conditions for the experiments described here, an initial number of 10^5 cells is seeded in 60 mm dishes with 5 ml growth medium and cell number is recorded over several days (see Figure 18 A). In addition, the cell cycle distribution at different stages of growth is determined by PI staining and FC analysis (see Figure 18 B).

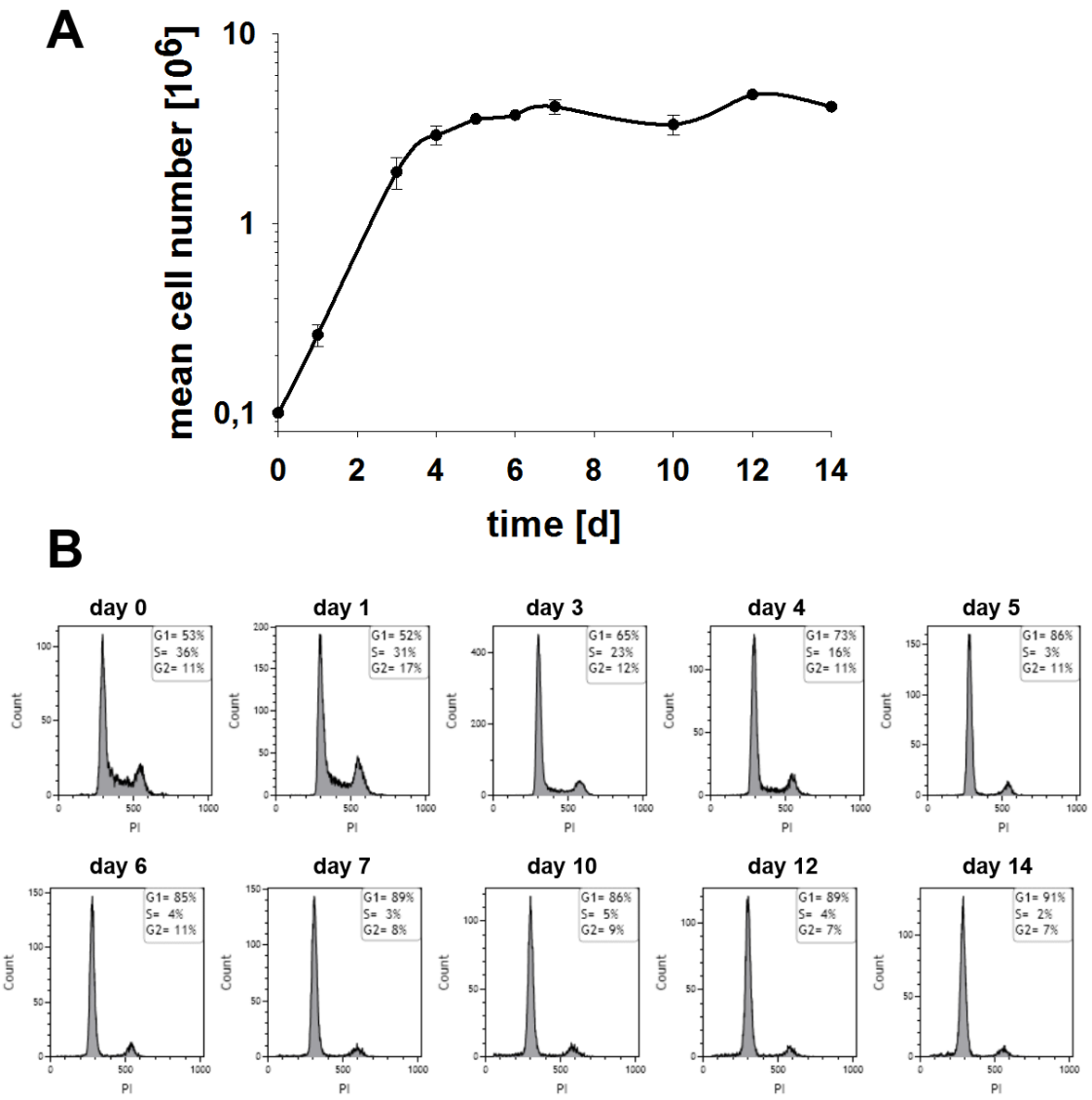

Figure 18 Growth curve of RPE-1 cells.
(A) Number of RPE-1 cells after plating 10^5 cells per dish and allowing growth for several days. Data shown here represents means ± SD from two independent experiments. (B) Cell cycle distribution of representative cultures at the indicated times measured by FC (PI staining).

RPE-1 cells grow exponentially for three days and then enter a plateau-phase of growth that is stable for 14 days. The percentage of cells in G1-phase is between 85 and 91 % after five days of growth and remains relatively constant for up to day 14.

7.2) Effects of global chromatin relaxation achieved by incubation in hypotonic medium

The purpose of this study is to investigate how chromatin organization is influencing DSB signaling and repair. As there are several reports about local chromatin relaxation upon DNA damage induction (see introduction), we are interested in how global chromatin relaxation achieved by incubation in medium containing only 75 mM of NaCl (referred to as hypotonic) affects the mechanisms of DDR and DSB repair.

7.2.1) Chromatin is globally relaxed by decreased tonicity

First, we want to establish that incubation in hypotonic medium is relaxing chromatin. First hints are given by measurements of cell diameter and cell volume that show a small increase after few minutes of incubation, but also a fast adaptation, as these parameters reverse and even decrease under their original values within 60 min (Figure 19 A and B).

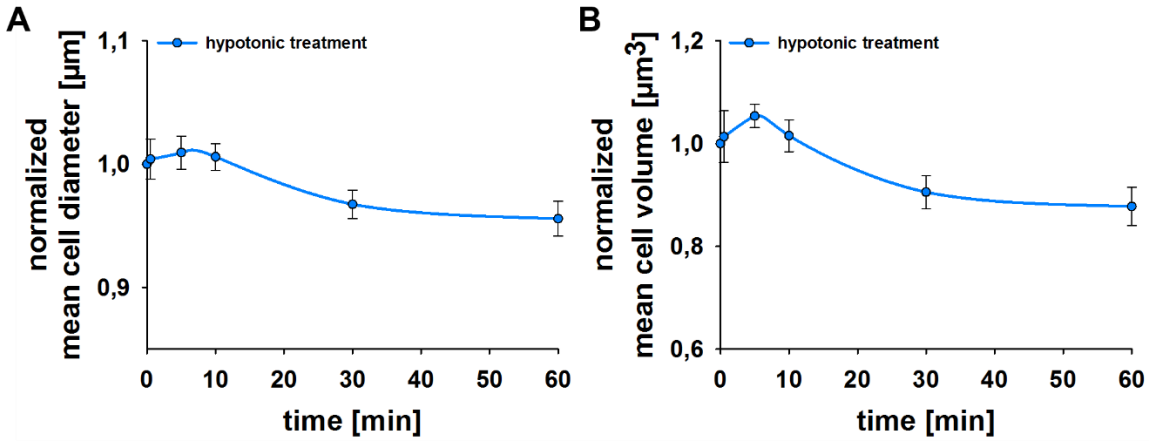

Figure 19 Influence of 75 mM NaCl on RPE-1 cell diameter and cell volume.
Mean cell diameter (A) and mean cell volume (B) of hypotonically treated RPE-1 cells at different times as measured in a Beckmann Coulter Counter. Data is normalized to cell diameter and volume at starting point of experiment (0 h), respectively. Means ± SE from four independent experiments are plotted.

Upon incubation in medium containing low concentrations of sodium and chloride ions, cells have to deal with decreased osmotic pressure. By taking up inorganic ions and water, the cell volume is increased. As cells rapidly activate RVI processes the cell volume is normalizing quickly (see Figure 19 B).

In order to determine if hypotonic treatment leads to a change in chromatin condensation level, DAPI stained nuclei are imaged after incubation in medium containing 75 mM NaCl by CLSM (see Figure 20 A).

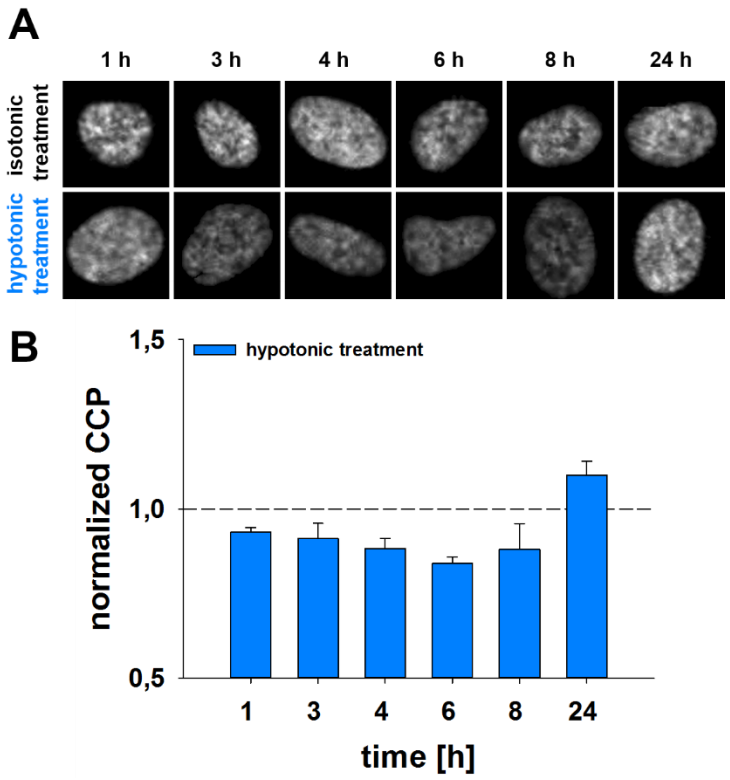

Figure 20 CCP of RPE-1 cells treated with chromatin relaxing medium.
(A) Images taken by CLSM of DAPI stained RPE-1 nuclei after different times of treatment with isotonic or hypotonic medium. (B) Mean CCPs of RPE-1 cells treated with hypotonic medium for different durations. Values are normalized to isotonic controls (represented by black dashed line) at each time point. Means and SD are calculated from two independent experiments.

The mean CCP is calculated (see 6.2.8.2) for each condition and normalized to the isotonic control. After incubation in medium with 75 mM NaCl global chromatin relaxation is observed, represented by a decreased CCP relatively to controls (see Figure 20 B). While volume regulation upon changes in osmolarity recovers very quickly (within 1 h), chromatin condensation status is still reduced after 6 to 8 h (see Figure 20 B). As described in the introduction, the changed intracellular ionic strength need longer time to become restored and perturb the organization of several macromolecules. The quantification of CCP represents exactly this proposition. However, after 24 h of treatment cells adapt and recondense chromatin.

During mitosis the DNA reaches its highest condensation state and the individual chromosomes become visible under the microscope. As we can show that low

osmotic pressure induces global chromatin relaxation, the following question arises: how do metaphase associated processes operate under these conditions? Therefore, cells are treated with media containing 75 mM NaCl for different durations before adding colcemid for 30 min. Colcemid depolymerizes microtubuli and blocks mitosis at the stage of metaphase. Using a classical cytogenetics protocol for the preparation of metaphases and a MetaSystems workstation, metaphases of the different samples are imaged.

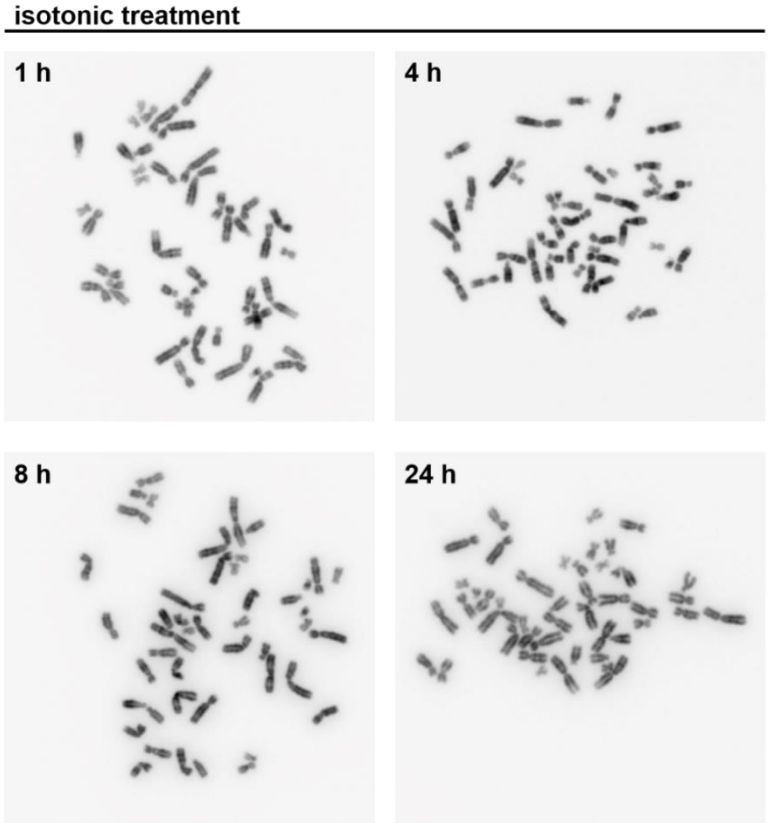

Figure 21 Representative images of metaphases formed in isotonically treated cells. Cells are incubated in isotonic control medium for the times indicated before a 30 min treatment with colcemid. DNA is stained by DAPI and is shown in inverted gray scale. The scale is the same in all images.

Metaphases of samples taken 1, 4, 8 and 24 h after incubation in normal cell culture medium show normally shaped chromosomes (see Figure 21) and serve as a control for treated samples.

In comparison to control metaphases, chromosomes of cells treated with hypotonic medium appear longer and less condensed as indicated by the less intense DAPI staining. Notably, chromatids seem to be more separated from each other (see Figure 22).

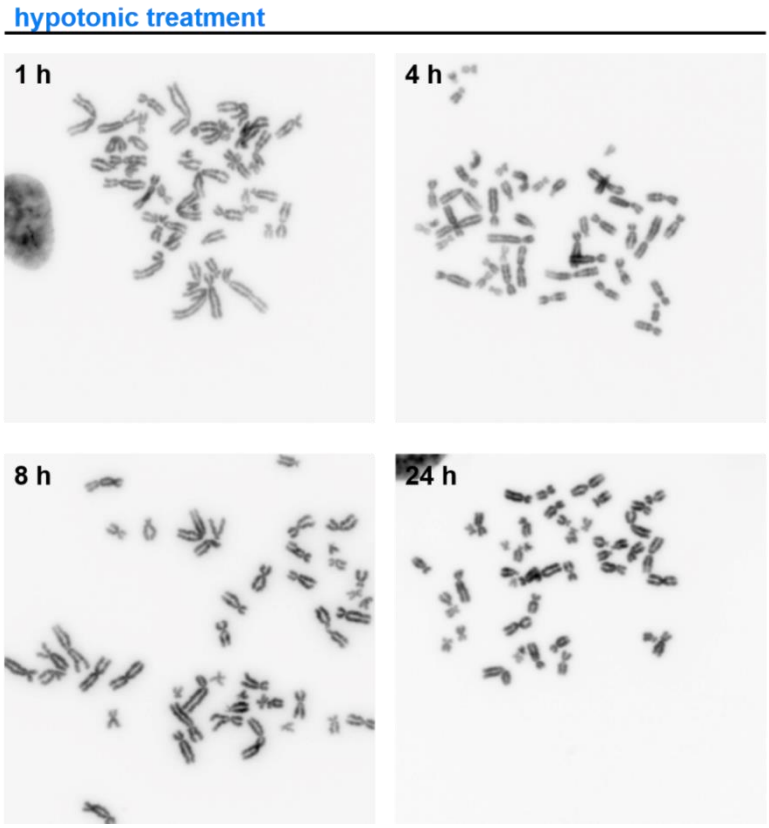

Figure 22 Representative images of metaphases formed in hypotonically treated cells. Cells are incubated in hypotonic medium for different times as indicated before a 30 min treatment with colcemid. DNA is stained by DAPI and is shown in inverted gray scale. The scale is the same in all images.

When chromosome lengths are quantified for the different metaphases shown, there is no big change in mean values from isotonic and hypotonic treated cells observed (see Figure 23). While the mean chromosome length doesn't change, the spreading in hypotonically treaded samples show increased lengths of long chromosomes.

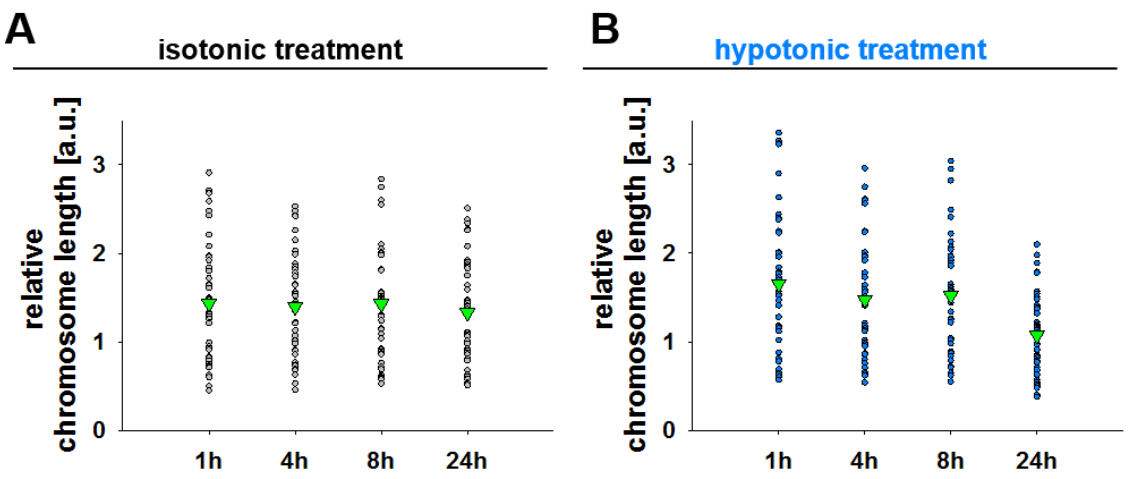

Figure 23 Chromosome length quantification of metaphases formed in isotonically and hypotonically treated cells.
Lengths of chromosomes at metaphase stage measured by ruler tool in Adobe Photoshop CS5 from representative images of isotonically (A) and hypotonically (B) treated cells. Images are shown in Figure 21 and Figure 22 and are processed at the same scale. X-axis indicates treatment times and green triangles represent means calculated for every metaphase.

After long hypotonic treatment times (24 h) the mean chromosome length even decreases in comparison to control (see Figure 23 B), which represent activated processes that counteract the relaxing effect of hypotonic treatment and overshoot the goal of regulation. Similar results have been obtained by determining the CCP, which is also slightly higher than in controls after 24 h of hypotonic treatment (see Figure 50).

Another effect contributing to chromatin relaxation is seen by greater separation of sister chromatids, which are usually held together with the help of cohesins that need to be removed for proper segregation during mitosis. Global chromatin relaxation seems to affect this connection and to interfere with the preservation of cohesins on chromosomes. This effect is still seen after 8 h of incubation in medium containing 75 mM NaCl (see Figure 22). After 24 h the cells seem to have transited to a different state and chromatids appear to be close together.

Chromatin harbors discriminative PTMs on N-terminal histone tails that are characteristic for different compaction states or that can serve as binding sites for proteins. As described in the introduction, open and relaxed EC exhibits high levels of acetylation. Thus, we test how the levels of H3K9ac (a common EC marker) and how levels of marker for HC regions (H3K27me3) change upon global chromatin relaxation induced by hypotonic treatment.

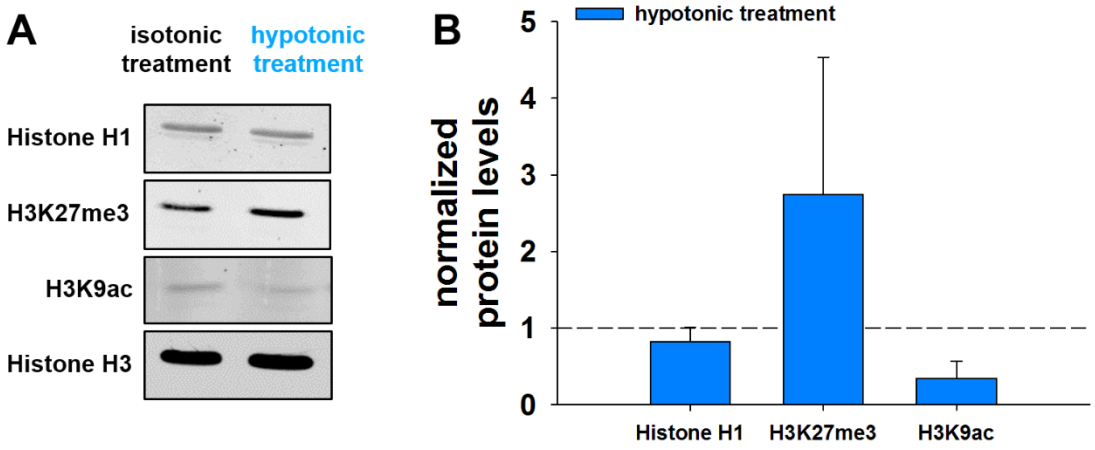

Figure 24 Global chromatin relaxation changes levels of histone H1 and EC/HC markers.
(A) WB analysis of histone H1, H3K27me3 and H3K9ac. RPE-1 cells are treated in isotonic (control) or hypotonic medium for 1 h before histone extraction. Histone H3 serves as loading control. (B) Levels of histone H1 and EC/HC markers are normalized to loading control and then normalized to isotonic samples (represented by black dashed line). Data represent means ± SD from two independent experiments.

The levels of HC marker H3K27me3 is almost three times elevated when chromatin is globally relaxed in comparison to controls (see Figure 24 B), while H3K9ac (marks decondensed chromatin) levels decrease by 66 %. Although we show that chromatin is globally relaxed when cells are incubated in hypotonic medium (see CCP in Figure 20), the changes in typical HC and EC markers do not support this finding. However, changes in chromatin induced by incubation in medium containing 75 mM NaCl occur due to altered ionic interactions, so that the definition of condensed HC and relaxed EC cannot be combined with the global chromatin relaxation achieved by our treatment. Nevertheless, the modifications of histone tails serve as binding sites for several proteins and changes upon hypotonic treatment could interfere with protein recruitment to chromatin.

In contrast to changes in histone PTMs, the decreased levels of histone H1 fits to a relaxed chromatin status. Usually histone H1 further compacts chromatin and is more abundant in condensed regions. However, disturbed binding abilities of H1 due to altered ionic strength would be a possible explanation for lowered H1 levels.

Taken together, hypotonic treatment relaxes chromatin in a less defined way than we know from processes defining EC regions, but changes histone PTM levels and with them the binding of proteins to chromatin.

7.2.2) Chromatin relaxation delays cell growth

As changing the salt concentration of the cell culture medium may not only influence chromatin structure but also the overall behavior of the cells, we analyze cell growth, as well as cycle distribution to check if the cells are still proliferating. Therefore, cells are incubated in hypotonic medium and cell numbers and cell cycle distribution is analyzed by PI staining and FC measurement.

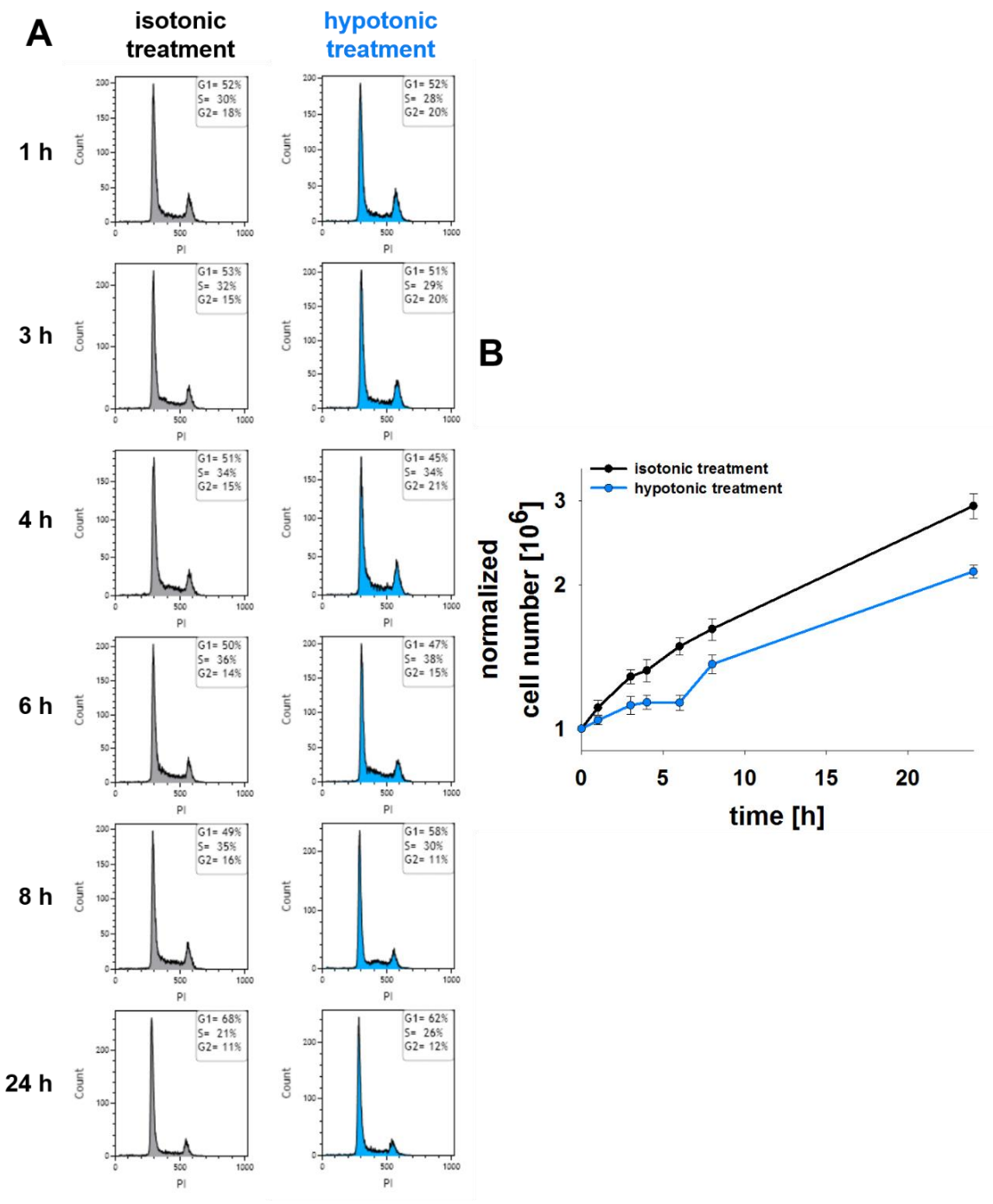

Figure 25 Cell number and corresponding cell cycle distribution of an asynchronous cell population after different treatment times at low concentrations of NaCl to induce global chromatin relaxation.
(A) Representative PI histograms measured by FC of RPE-1 cell populations that are treated with isotonic (grey histograms) or hypotonic medium (blue histograms) for different times. (B) Numbers of RPE-1 cells after growing in isotonic (black line) or hypotonic medium (blue line) for different times. Values are normalized to values measured at 0 h (start of treatment) and represent means ± SE from three independent experiments.

Hypotonic treatment seems to be a shock for cells, as cell numbers initially only slightly increase after starting treatment (see Figure 25 B). However, after 6 h cells

adapt to the new condition and start dividing normally. After 24 h of exposure to hypotonic medium cell numbers are still lower, due to the initial delay, in comparison to the controls, but overall the graph shows a similar rate of cell growth. Regarding the percentage of cells in S-phase, we see a slight increase at 4 and 6 h (from 28 to 38 %), which also represents the initial shock and subsequent adaptation of hypotonically treated cells. After 24 h there are still 26 % of the cells in S-phase, while in controls the proportion starts to decrease, indicating a transition into a plateau-phase.

Requirement for proliferation is cell division. During mitosis chromatin gets compacted 10,000-fold. Inducing global chromatin relaxation may interfere with chromatin condensation during M-phase and may explain the initial delay in cell growth observed in Figure 25 B.

In order to further investigate cell division under conditions of globally relaxed chromatin, cells are synchronized in G2-phase by treatment with CDK4/6 inhibitor PD0332991 followed by a thymidine block. When cells are released from the thymidine block and are allowed to progress to G2-phase (4 h after release) the NaCl concentration is reduced to 75 mM and cell cycle distribution is measured by PI staining and FC analysis (see Figure 26 A and B).

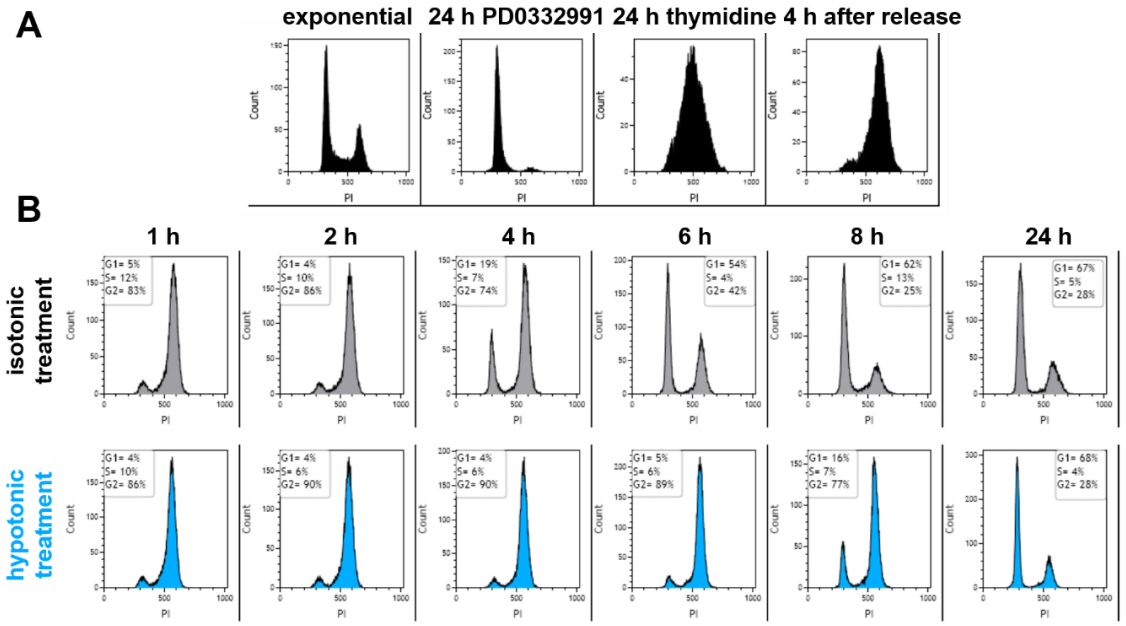

Figure 26 Progression through the cell cycle of cells synchronized in G2-phase and treated with medium containing 75 mM NaCl.
(A) PI histograms of cells at different steps of synchronization measured by FC. Exponentially growing cells are first arrested in G1-phase by a treatment with 500 nM CDK4/6 inhibitor PD0332991 for 24 h. Subsequently they are treated with 2 mM thymidine to accumulate in early S-phase. At 4 h after release of thymidine block the majority of the population is in G2-phase. (B) Cell cycle distribution of synchronized cells treated with isotonic or hypotonic medium for different times starting at 4 h after thymidine block release.

At 4 h after incubation in hypotonic medium, controls start to divide and to progress to G1-phase (19 % in G1) and after 6 h more than half of the cell population passes through mitosis (see Figure 26 B). When cells are treated with hypotonic medium cell cycle progression is delayed (16 % in G1 after 8 h); this confirms previous results also showing delayed cell growth (see Figure 25). After 24 h of global chromatin relaxation the distribution of cells in different phases of the cell cycle is similar to that measured in untreated control cultures. However, the percentage of S-phase cells is very low (4 - 5 %) in both cases, which indicates stress tentatively generated by synchronization procedure or transition of cells to a plateau-phase.

This experiment reveals that entry into mitosis is prevented under conditions of global chromatin relaxation until cells adapt to this new condition.

7.2.3) Global chromatin relaxation inhibits cell division transiently

To further investigate the interference of global chromatin relaxation achieved by hypotonic treatment on mitosis, we examine the MI of RPE-1 cells as a function of

incubation time. This parameter examines specifically the fate of cells irradiated in G2-phase of the cell cycle. In asynchronous cells, the percentage of cells in mitosis is measured at different times of incubation in medium containing 75 mM NaCl by H3pS10 staining and FC analysis.

In contrast to controls, which show only small fluctuations in MI, global chromatin relaxation induced by incubation in hypotonic medium decreases the number of cells in mitosis down to almost 0 % after 1 h of treatment (Figure 27 A). This result confirms our previous assumption that entry into mitosis is stopped when chromatin is globally relaxed, which is exactly antagonizing the strong condensation occurring during mitosis. Later cells adapt to hypotonic conditions and start progressing to mitosis again. After 4 h of treatment, MI is at the initial level and further increases with time.

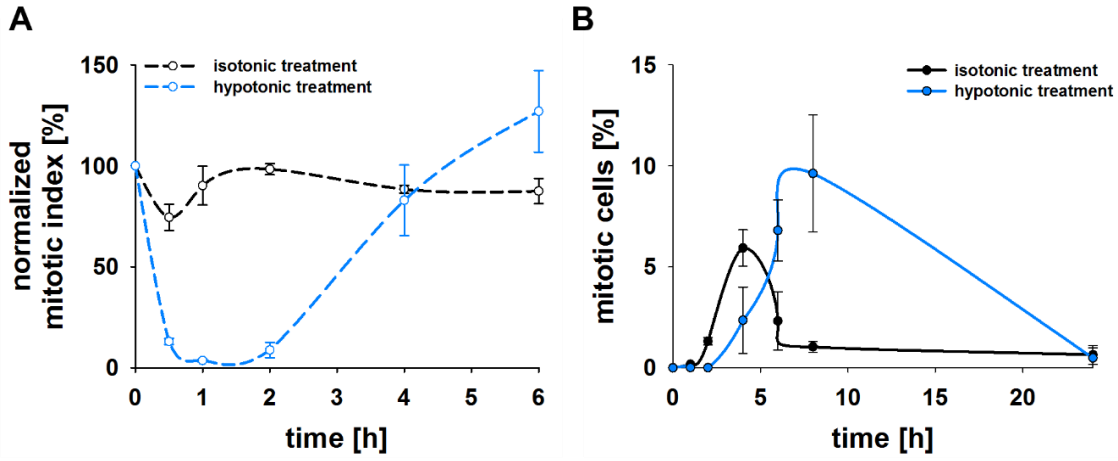

Figure 27 Proportion of mitotic cells under chromatin relaxing conditions.
(A) MI is measured by FC and H3pS10 staining. Percentages are normalized to 0 h control. Asynchronous cells are treated with isotonic (black dashed line) or hypotonic (blue dashed line) medium and fixed at different times. Data represent means and SE calculated from three (isotonic) and five (hypotonic) independent experiments. (B) Cells are synchronized in G2-phase as described in Figure 26 A. At 4 h after release of thymidine block (marks starting point: 0 h) cells are incubated in isotonic (black line) or hypotonic (blue line) medium. Graph shows percentage of cells in mitosis determined by FC and H3pS10 staining at different time points after beginning of treatment. Means and SD calculated from two independent experiments are plotted.

Using cells synchronized in G2-phase confirms this finding. At 4 h after release from thymidine block (see Figure 26 A) the majority of cells are in G2-phase and are then incubated in isotonic or hypotonic medium. The MI starts to increase within 2 h in the controls (see Figure 27 B); however, it needs longer times (4 h) to reach the same levels when cells are treated hypotonically. Notably, the maximum amount of

cells in mitosis is nearly twice as high as in controls; this suggests that under hypotonic conditions cells arrest before mitosis and accumulate there until they adapt and start dividing again. It seems that in this stage of the cell cycle, hypotonic treatment acts as a synchronizing agent. After 24 h of treatment the percentage of mitotic cells returns to control levels again.

In order to further investigate the mitotic block under hypotonic conditions, we use specific inhibitors of the PIKKs ATM and ATR. Both kinases play central roles in activation of G2-checkpoint response upon DNA damage induction. Their activation also results in a decreased MI and is reminiscent to the above shown findings of cells with globally relaxed chromatin (see Figure 27 A).

In cells treated with hypotonic medium, inhibition of ATM has no effect on the development of MI in comparison to DMSO control. However, inhibition of ATR attenuates the effect of hypotonic treatment so that after 1 h the number of cells in mitosis does not decrease down to 0 % but to 25 %. Also the recovery takes place much faster and reaches almost 100 % of MI after 2 h (see Figure 28).

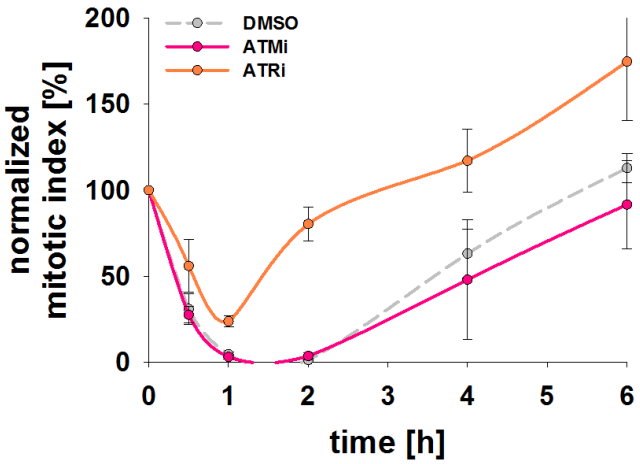

Figure 28 MI of RPE-1 cells treated with PIKK inhibitors when chromatin is globally relaxed.
Cells are pretreated with ATMi (10 µM KU55933) or ATRi (5 µM VE-821) for 1 h before applying hypotonic conditions. MI is measured by FC and H3pS10 staining. Percentages are normalized to 0 h control and means ± SE from three independent experiments are plotted.

The finding that inhibition of ATM and/or ATR does not prevent an initial decrease of MI upon hypotonic treatment is not surprising as there is no damage induced; but it clarifies that the drop in MI when cells are incubated in medium containing 75 mM NaCl is not due to a G2-checkpoint-like response, but is most probably a result of

chromatin relaxation, which is opposing chromatin condensation in preparation for mitosis. However, it seems that ATR plays a role in this inhibition of mitosis upon hypotonic treatment as its inhibition leads to a faster recovery from the drop in MI seen in Figure 28.

7.2.4) DDR signaling is inhibited in globally relaxed chromatin

Chromatin serves as a binding platform for several components of DDR and its constitution can influence a variety of activating signaling cascades. Several PTMs of histones, introduced upon DNA damage, are known (see introduction) but the most common marker for DSBs is γH2AX. ATM is the main responsible kinase for phosphorylation of H2AX, which spreads bidirectionally from the break sites and provides a binding site to signal transducers. Here we investigate how global chromatin relaxation achieved by hypotonic treatment is influencing the initial signaling of DDR measured by the formation of γH2AX, pATM and 53BP1 foci.

Under control conditions the analysis of γH2AX foci shows a maximum of approx. 40 foci after 1 h post 2 Gy of IR. After 6 h more than 50 % of foci are resolved, which represents ongoing DSB repair. Treating cells in 75 mM NaCl to relax chromatin, causes a 50 % reduction in the number of DSBs that develop γH2AX foci 1 h after IR (see Figure 29 B). Yet, the number of residual γH2AX foci at 6 h is similar to that measured in control cells.

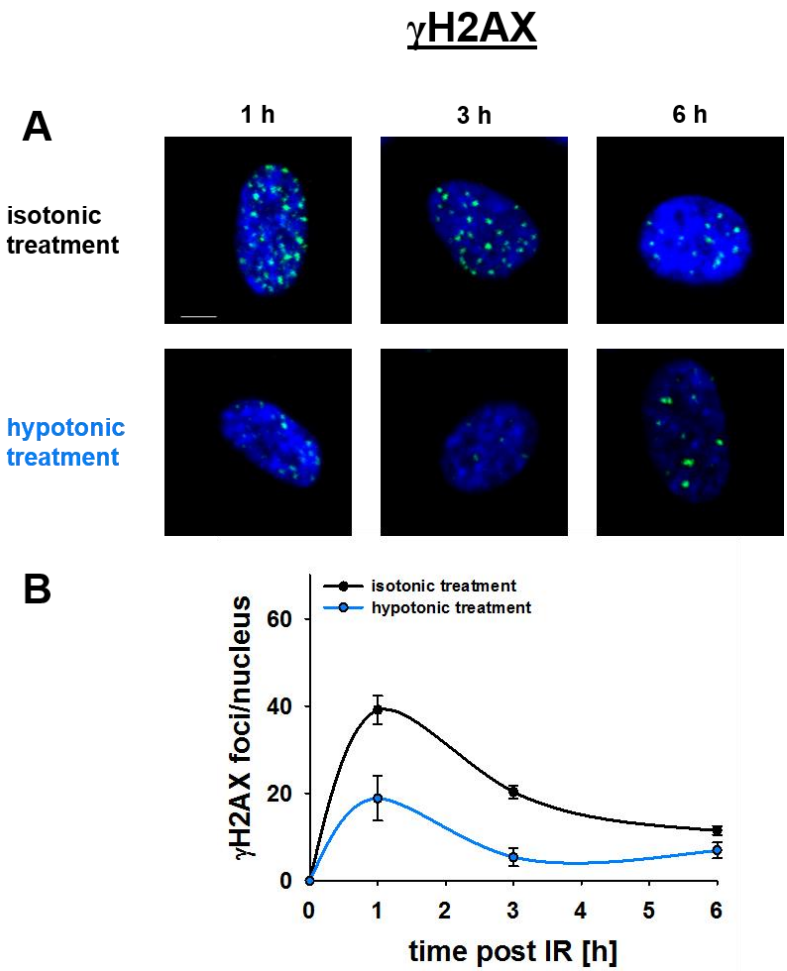

Figure 29 Formation of γH2AX foci after incubation in hypotonic medium.
(A) Representative images of γH2AX foci in RPE-1 cells after 2 Gy of IR at different times of incubation in isotonic or hypotonic medium. Scale bar: 5 μm (B) Formation of γH2AX foci in cells maintained in isotonic medium (black plot) or in hypotonic medium (blue plot) following 2 Gy of IR. Data shown represent means ± SE calculated from six (isotonic) and five (hypotonic) independent experiments.

A lower number of DSBs actually induced, as an explanation for the decreased number of γH2AX foci can be excluded, as irradiation is performed under isotonic conditions and treatment starts post-irradiation. Thus, global chromatin relaxation seems to inhibit the phosphorylation of H2AX.

As mentioned above, ATM is the main kinase for the phosphorylation of H2AX. So we investigate the number of pATM foci (active form of ATM; phosphorylated on serine1981) in 75 mM NaCl. When cells are treated in hypotonic medium, less pATM foci are counted in comparison to control cells (see Figure 30 B).

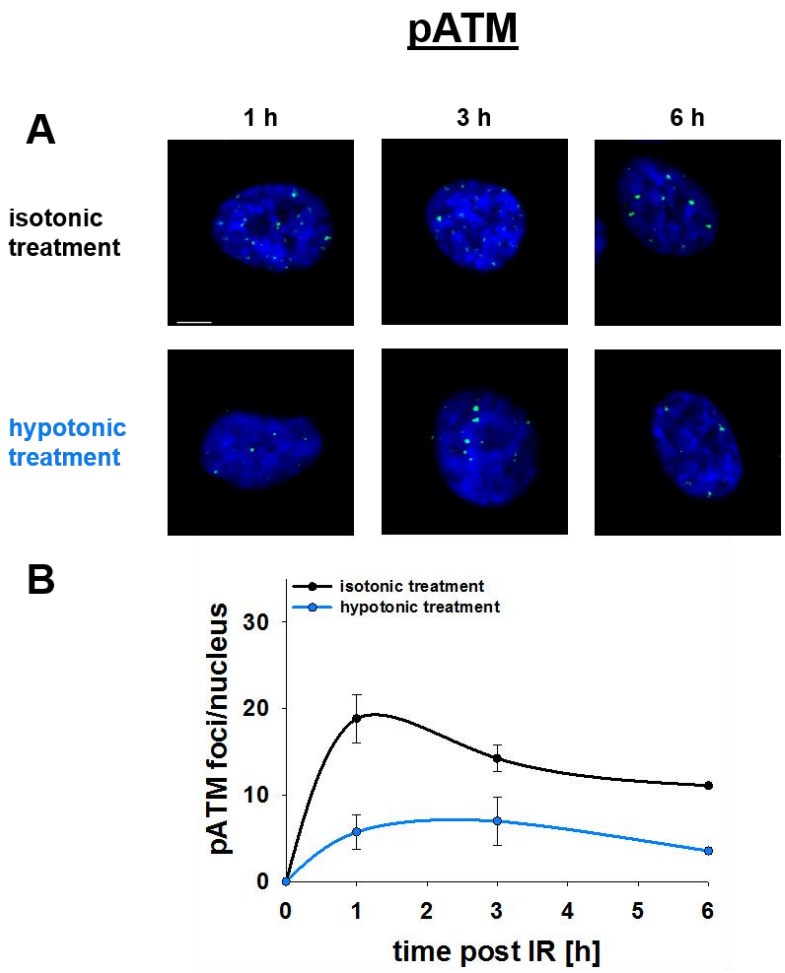

Figure 30 Formation of pATM foci under hypotonic conditions.
(A) Representative images of pATM foci in RPE-1 cells after 2 Gy of IR at different times of incubation in isotonic or hypotonic medium. Scale bar: 5 μm (B) Formation of pATM foci in isotonically (black plot) or hypotonically (blue plot) treated cells following 2 Gy of IR. Data represent means and SE from five independent experiments (for 1 and 3 h time points).

These results are in line with the impaired γH2AX foci formation under hypotonic condition and strengthens the hypothesis of an upstream suppression of DNA damage signaling due to global chromatin relaxation. As the MRN complex is one of the first responders to DSBs, it would be interesting to investigate the formation of Mre11 foci under hypotonic conditions.

Downstream of ATM, the mediator protein 53BP1 gets activated upon DSB induction. This protein, in interplay with BRCA1, is thought to play a role in repair pathway choice favoring cNHEJ by inhibiting end resection. It was shown that 53BP1 is more likely to bind to heterochromatin than to euchromatin upon DNA damage induction (Demond 2016). We investigate, therefore, 53BP1 foci formation in cells treated in chromatin relaxing medium after IR.

When cells are incubated in 75 mM NaCl after IR, the number of 53BP1 is strongly decreased as compared to controls (see Figure 31 B).

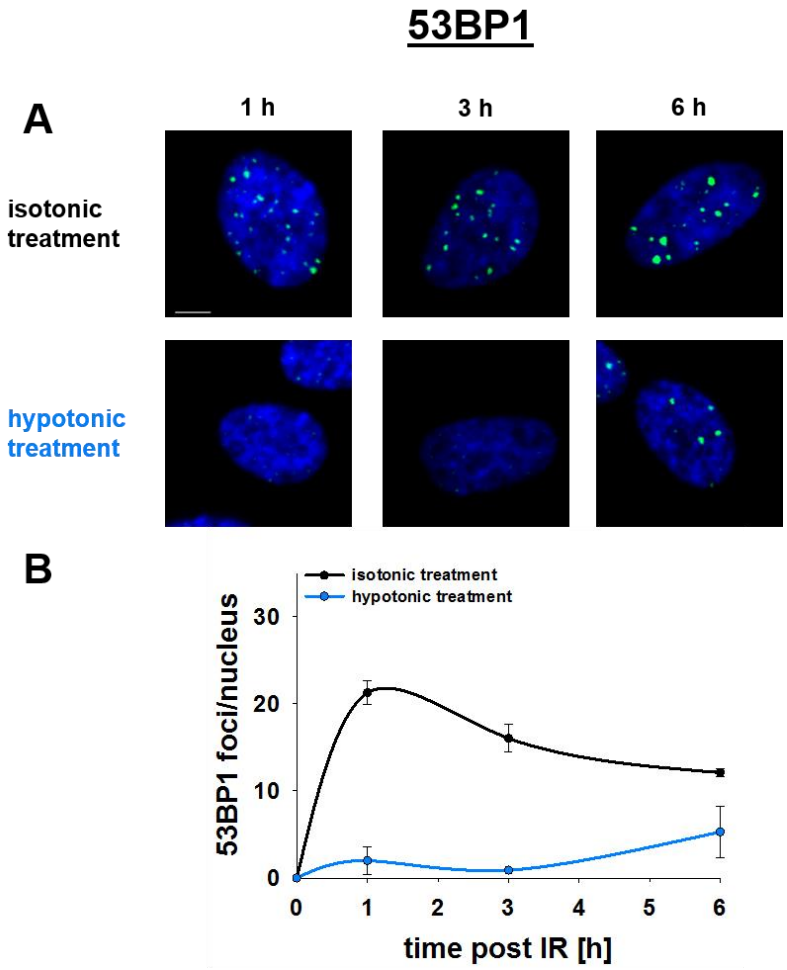

Figure 31 Formation of 53BP1 foci after treatment in hypotonic medium.
(A) Representative images of 53BP1 foci in RPE-1 cells after 2 Gy of IR at different times of incubation in isotonic or hypotonic medium. Scale bar: 5 μm (B) Formation of 53BP1 foci in isotonically (black plot) or hypotonically (blue plot) treated cells following 2 Gy of IR. Data shown represent means ± SE calculated from three independent experiments.

Considering that upstream signaling, like pATM foci formation (see Figure 30), is suppressed and that 53BP1 prefers HC regions, it is likely that 53BP1 foci formation is inhibited when chromatin is decondensed, similar to γH2AX and pATM inhibition. However, ATM is activated upon changes in chromatin themselves, also in the absence of DNA damage (Bakkenist and Kastan 2003), which makes the suppression of pATM foci seen here even more surprising.

7.2.5) Hypotonic treatment disturbs G2-checkpoint machinery

From the previous results it is evident that the initial DDR signaling is severely suppressed when chromatin is globally relaxed by hypotonic treatment. Beside the repair of DSBs another endpoint of DDR signaling is the activation of cell cycle checkpoints to prevent interference of damaged DNA with DNA replication or mitosis. Especially the G2-checkpoint is known as the DNA damage checkpoint and prevents the progression of damaged cells into mitosis, which would endanger genomic integrity. As ATM activation, which is inhibited under hypotonic conditions (see Figure 30), plays beside ATR activation a central role in G2-checkpoint response, we investigate how global chromatin relaxation influences the activation of the DNA damage checkpoint.

Thus, the MI of cells treated with medium globally relaxing chromatin is investigated after IR. When cells are treated in isotonic medium after exposure to 2 Gy a clear G2-checkpoint activation can be observed as the MI decreases to 0 % at 1 h after IR and recovers to 100 % at 6 h after irradiation (see Figure 32 A). When chromatin is globally relaxed after 2 Gy of IR the MI decreases to 0 % after 1 h like in controls (see Figure 32 A). However, in contrast to isotonically treated cells the MI does not recover within 6 h after IR but remains very low. At first glance this could show that the G2-checkpoint under hypotonic conditions is strengthened.

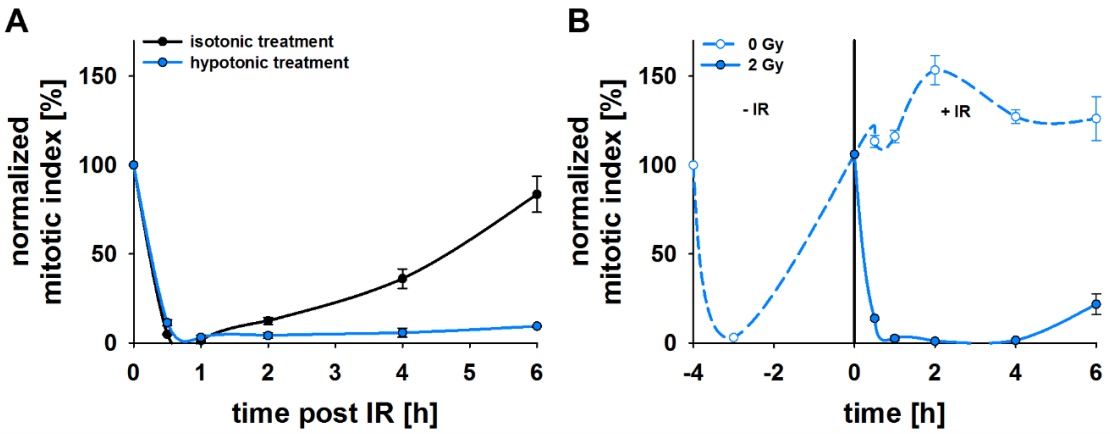

Figure 32 MI of RPE-1 cells after 2 Gy of IR and subsequent isotonic or hypotonic treatment.
(A) MI (normalized to 0 h) of RPE-1 cells under isotonic (black plot) or hypotonic conditions (blue plot) after 2 Gy irradiation. (B) MI (normalized to -4 h) of RPE-1 cells that are treated in hypotonic medium starting 4 h prior irradiation with 0 and 2 Gy (dashed and solid line, respectively). Data in this figure represent the means and SE calculated from three (A) and two (B) independent experiments.

Concerning the previous results of MI of cells with globally relaxed chromatin without IR (see Figure 27 A), we wonder whether the G2-checkpoint response seen after 2 Gy of IR is a real checkpoint response, or whether it reflects the above mentioned inhibition in the progression of unirradiated but hypotonically treated cells to mitosis. To avoid this complication in the design of the experiment and separate between effects of hypotonic medium on cell cycle versus the DNA damage checkpoint, cells are first treated with hypotonic medium for 4 h (time at which MI recovers, see Figure 27 A) and then irradiated with 2 Gy. Under these conditions, after IR, the MI decreases to 0 % which shows that the activation of the G2-checkpoint response remains intact (see Figure 32 B). In contrast to controls, hypotonically treated cells start progressing to mitosis the earliest 4 h after IR and recovery is incomplete even at 6 h after IR.

Thus, global chromatin relaxation delays the recovery from the G2-checkpoint (see Figure 32). In cells synchronized in G2-phase, using combined incubation with the CDK4/6 inhibitor PD0332991 and thymidine (see Figure 26 A), treatment in 75 mM NaCl, with or without irradiation, delays progression from mitosis to G1-phase (see Figure 33).

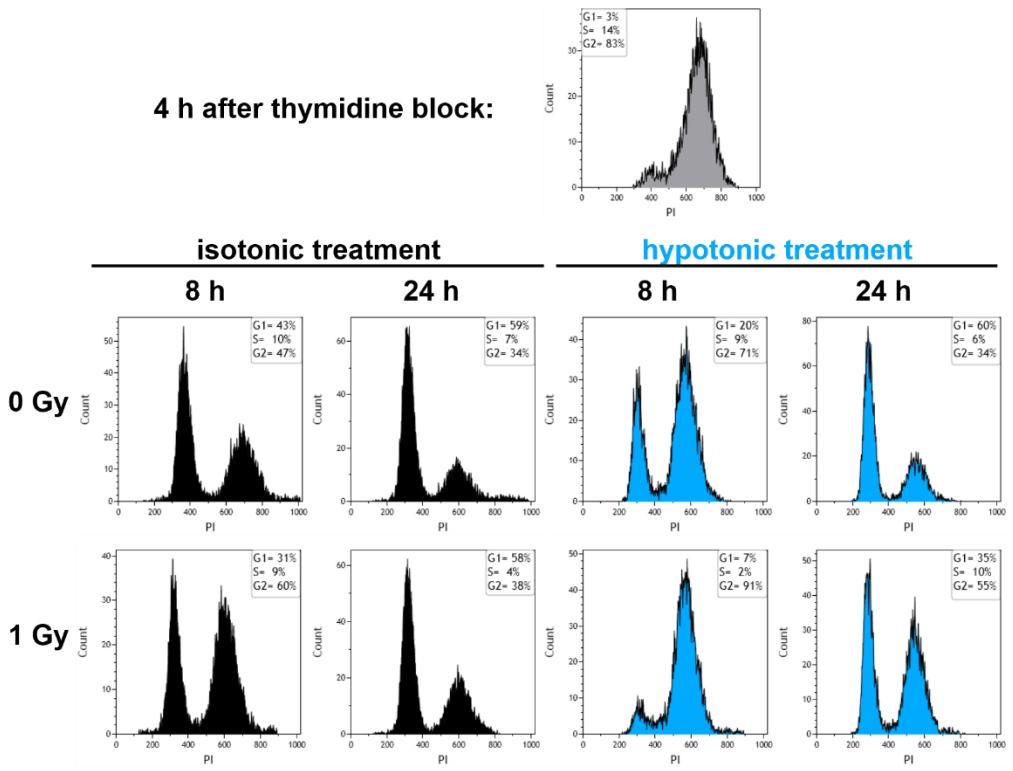

Figure 33 Cell cycle distribution of synchronized RPE-1 cells after treatment in hypotonic medium.
PI histograms measured by FC showing cell cycle distribution of RPE-1 cells at 4 h after release of thymidine block (see Figure 26) and subsequent treatment with isotonic or hypotonic medium after IR.

In unirradiated samples only 20 % of cells are in G1-phase after 8 h of hypotonic treatment as compared to 47 % in the controls (see Figure 33). After 24 h of incubation in hypotonic medium the cell cycle distribution is comparable to controls. When cells are exposed to 1 Gy of IR they progress from mitosis into G1-phase but in a delayed manner in comparison to control samples. Thus, 8 h after 1 Gy the majority of cells (> 90 %) are still in G2-phase. Even after 24 h, half of the cell population is still in G2-phase, while in controls only 38 % remain in G2.

These findings suggest that chromatin can condense for mitosis even under conditions of global chromatin relaxation (which is also shown by analyzing metaphases cytogenetically, see Figure 22). Yet, cells need time to adapt to this condition and overcome its effects causing the observed delay in cell cycle progression.

In experiments concerning DDR signaling we observe a reduction in γH2AX, pATM and 53BP1 foci under chromatin relaxing conditions (see Figure 29, Figure 30 and Figure 31), and consequently we also expect to find a weakened G2-checkpoint, so

the previous findings of a strengthened response are surprising. Thus, we use PIKK inhibitors in combination with hypotonic treatment to elucidate how the G2-checkpoint is regulated under this condition.

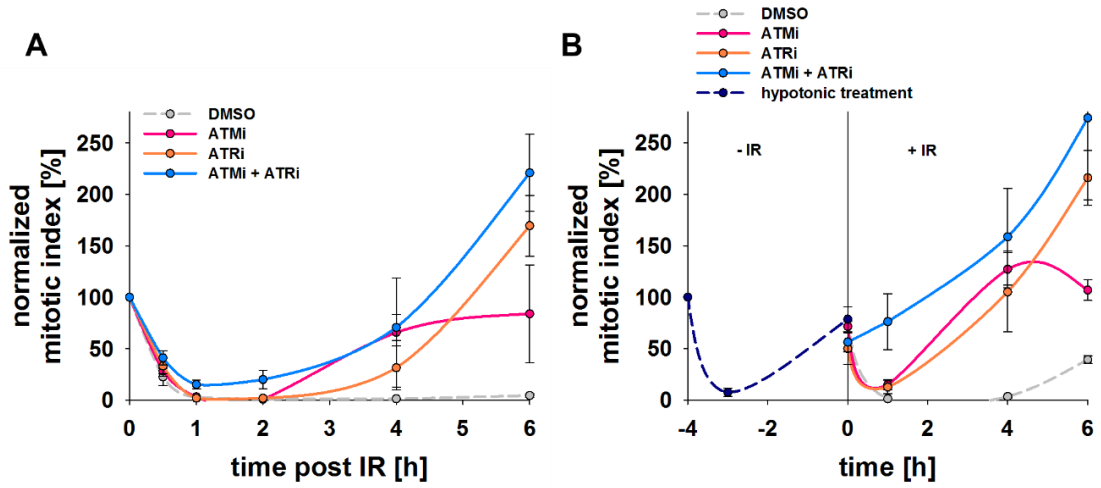

Figure 34 MI of RPE-1 cells under hypotonic conditions and treatment with PIKK inhibitors.
(A) MI (normalized to 0 h) of RPE-1 cells under hypotonic condition and after treatment with DMSO (grey dashed curve), 10 µM KU55933 (ATMi, pink curve), 5 µM VE-821 (ATRi, orange curve) or combination of both for 1 h before IR with 2 Gy and applying hypotonic conditions. Graph shows means ± SE of three independent experiments. (B) MI (normalized to -4 h) of RPE-1 cells that are pretreated in hypotonic medium for 3.5 h before starting incubation with DMSO (grey dashed line), 10 µM KU55933 (ATMi, pink curve), 5 µM VE-821 (ATRi, orange curve) or combination of both for 30 min before IR with 2 Gy. Results show mean values and SE calculated from four independent experiments.

When cells are irradiated with 2 Gy, inhibition of ATM or ATR abolishes the activation of G2-checkpoint. This is not the case when the cells are treated with hypotonic medium (see Figure 34 A). However, the strong checkpoint response of cells with globally relaxed chromatin (still 0 % after 6 h, DMSO treatment, see Figure 34 A) is attenuated at later time points when ATM and/or ATR are inhibited, represented by an increase in MI starting at 2 h after IR.

Considering the initial decrease of MI as a result of the hypotonic treatment without IR, an abrogation of G2-checkpoint by PIKK inhibition could be masked. Therefore, we pretreat cells for 4 h with hypotonic medium to allow adaptation and irradiate them then in the presence of ATM and/or ATR inhibitors. Inhibition of ATM or ATR alone cannot abolish the G2-checkpoint response in cells adapted to hypotonic conditions (see Figure 34 B), but in combination there is no drop in MI seen after IR. ATM and ATR can replace each other in activating the checkpoint response but in case of inhibition of both kinases the G2-checkpoint is not operating anymore. This

is also known from cells that are not treated with hypotonic medium, so that we can conclude that the G2-checkpoint machinery can function properly when cells are adapted to the situation of globally relaxed chromatin.

We wonder if this adaptation may also influence the formation of IRIF. Therefore, cells are pretreated with hypotonic medium for 4 h before IR and kinetics of γH2AX and 53BP1 foci are measured (see Figure 35).

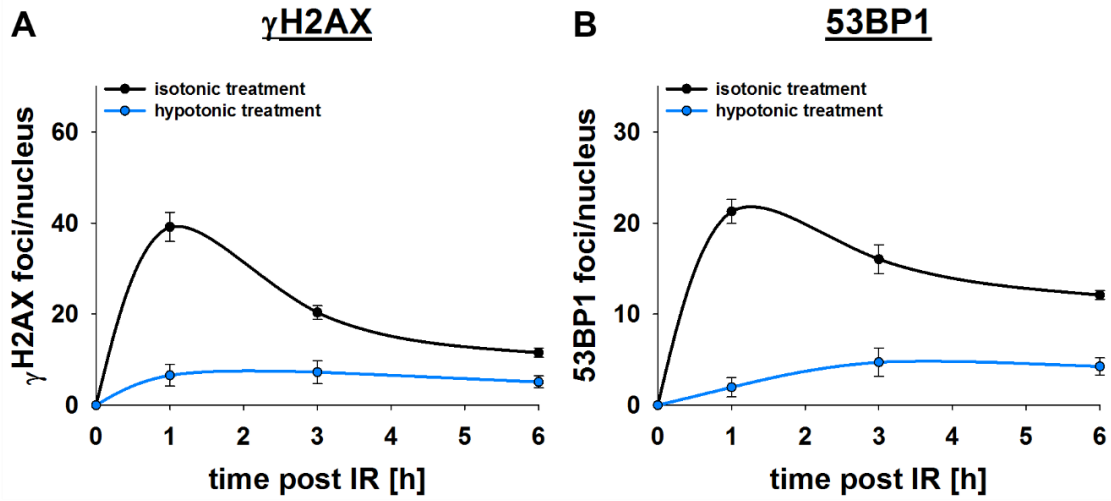

Figure 35 Formation of γH2AX and 53BP1 foci after IR in cells adapted to hypotonic medium.
Formation of γH2AX (A) and 53BP1 (B) foci in isotonically (black plot) or hypotonically (blue plot) treated cells following 2 Gy of IR. Hypotonic pretreatment starts 4 h before irradiation. Controls are treated isotonically and data is the same like in Figure 29 and Figure 31. Data for hypotonic treatment show means and SE for three (A) and five (B) independent experiments.

In contrast to MI measurements, there is no adaptation of IRIF formation after 4 h treatment in chromatin relaxing medium. 53BP1 and γH2AX foci numbers are decreased dramatically at 1 and 3 h after IR. Especially the number of γH2AX foci at 1 h time point decreases even more when compared to normally treated cells (no pretreatment) that develope around 18 foci at this time point (see Figure 29 A). However, at 6 h after IR γH2AX foci numbers converge to control numbers (see Figure 29 and Figure 31). This result confirms the suppression of DDR signaling after chromatin relaxation and shows that the recovery of G2-checkpoint response is uncoupled from DDR signaling suppression under hypotonic conditions.

7.2.6) Global chromatin relaxation by hypotonic treatment shifts DSB repair from main repair pathways to SSA

Previous results show massive interference of global chromatin relaxation with DDR signaling and DNA damage checkpoint activation. This raises the question: what happens to DSB repair under conditions of chromatin relaxation?

In order to investigate the influence of global chromatin relaxation on the ability of cells to rejoin DSBs, PFGE experiments with exponentially growing RPE-1 cells are performed. As chromatin is relaxed post-irradiation, the induction of DSBs is not affected by tonicity changes, and increases as expected linearly with increasing radiation dose (see Figure 36 A). The kinetics of DSB repair have two components: the majority of breaks are repaired within the first 30 min after IR (fast component), while a few DSBs appear to be repaired with significantly slower kinetics (slow component).

The fast component of DSB repair cannot be calculated for the shown experiments as there are no time points taken between 0 h and 30 min. Nevertheless, the number of unrepaired breaks is double as high in cells with globally relaxed chromatin as in controls (see Figure 36 B). The effect of chromatin relaxation is more pronounced on the slow component of repair. Thus, half-time constants in hypotonically treated cells increases by 80 % in comparison to controls and the fraction of DSBs that get repaired by the slow component is elevated as well.

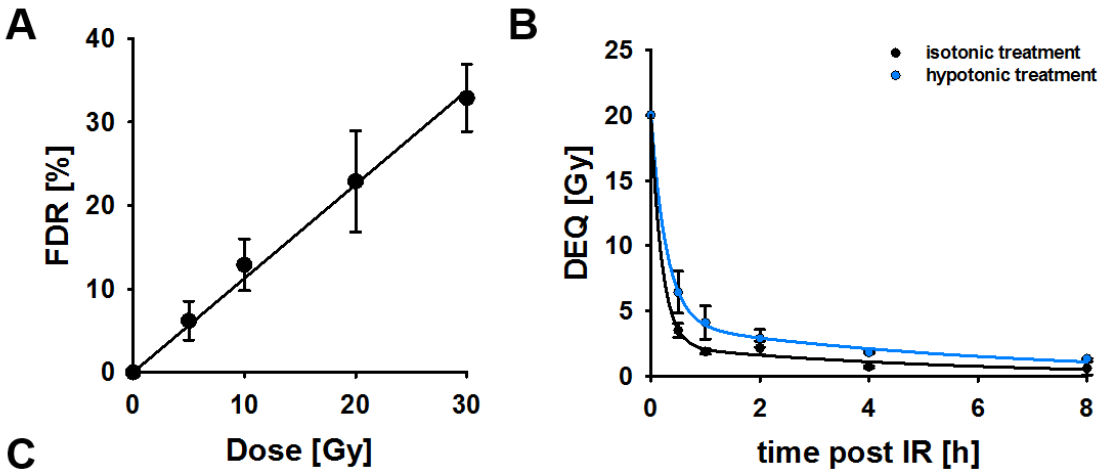

	plot equation
isotonic treatment	$f(x) = 20e^{-3.4721x} + 2.4935e^{-0.2165x}$
hypotonic treatment	$f(x) = 20e^{-2.2668x} + 4.3627e^{-0.1723x}$

	$t_{50,slow}$	fraction of DSBs repaired by slow component
isotonic treatment	192 min	11 %
hypotonic treatment	241 min	18 %

Figure 36 Global chromatin relaxation impairs DSB repair as measured by PFGE. (A) Dose response for DSB induction in RPE-1 cells irradiated under isotonic conditions. (B) Chromatin relaxation by hypotonic treatment (blue line) compromises DSB repair. (C) Half-time constants for the slow component ($t_{50,slow}$), as well as the fraction of DSBs repaired by this component are calculated according to (Metzger and Iliakis 1991). Data shown here represent means and SD from eight determinations in two experiments.

However, the effects of global chromatin relaxation on the repair of DSBs is minor compared to controls, which is surprising concerning the massive perturbations seen on DDR. It was shown that the repair of DSBs as measured by PFGE mainly reflects the function of performed cNHEJ, as HRR is inhibited at high IR doses (Wang et al. 2001). We conclude that DSB repair by cNHEJ is only slightly affected by hypotonic treatment. It should be pointed out that experiments analyzing the effects on DDR are performed after low dose irradiation (1 and 2 Gy), whereas PFGE experiments require high IR doses (20 Gy). As cell response to IR varies between low and high doses, direct comparison of PFGE results with those on DDR signaling is not appropriate. The results allow however the conclusion that when cNHEJ is the predominant repair pathway, the effects of chromatin relaxation of DSB processing is small.

In the literature it is reported that chromatin relaxation can improve repair of DSBs by altEJ in cells that are grown into plateau-phase of growth (Moscariello and Iliakis 2013). In contrast, in exponentially growing cells incubation in medium containing 75 mM NaCl compromises altEJ in comparison to controls. In this study Lig4$^{-/-}$ mouse embryonic fibroblast (MEF) cells are incubated starting 24 h before IR. In this case, chromatin condensation status is already changed before damage is induced and, as we know now, cells already adapted to conditions of hypotonic medium (see Figure 19 and Figure 20). Thus, we perform PFGE experiments in combination with NU7441 (a specific DNA-PK inhibitor) in order to suppress cNHEJ and analyze the effects of chromatin relaxation induced subsequently to IR on altEJ in exponentially growing RPE-1 cells.

A

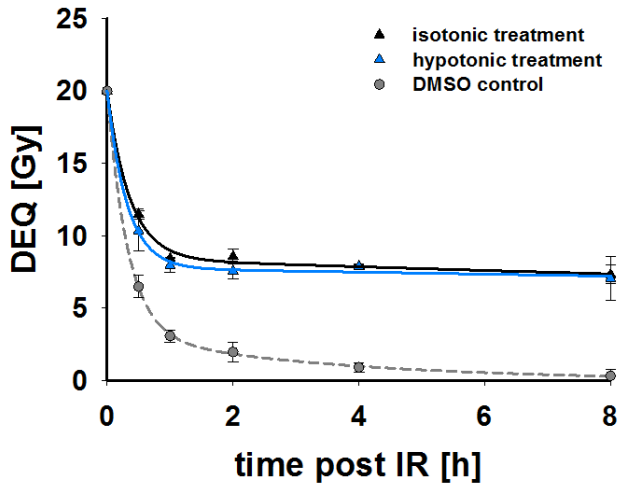

B

	plot equation
isotonic treatment	$f(x) = 20e^{-1.108x} + 8.7245e^{-0.0224x}$
hypotonic treatment	$f(x) = 20e^{-1.3191x} + 8.0334e^{-0.0147x}$

	$t_{50,slow}$	fraction of DSBs repaired by slow component
isotonic treatment	31 h	30 %
hypotonic treatment	47 h	29 %

Figure 37 altEJ in RPE-1 cells remains unaffected by global chromatin relaxation.
(A) Cells are treated with DNA-PKi (5 µM NU7441) starting 1 h before IR to specifically inhibit cNHEJ (except for DMSO control, grey, dashed line). After IR, cells are treated either with isotonic (black line) or hypotonic (blue line) medium. (B) Half-time constants for the slow component ($t_{50,slow}$) of end joining as well as the fraction of DSBs processed by the slow component calculated according to (Metzger and Iliakis 1991). Data shown represent means and SE from eight determinations in two experiments.

In comparison to cNHEJ proficient controls (DMSO control) repair performed by altEJ is compromised (see Figure 37). However, chromatin relaxation under conditions of DNA-PK inhibition minimally increases the fraction of DSBs repaired after 30 min in comparison to isotonically treated cells. In contrast, half-time of the slow component is slightly increased. The findings of Moscariello and Iliakis, 2013 cannot be reproduced here, which may be due to the different protocols used. Taken together the repair by altEJ is not significantly influenced when chromatin gets globally relaxed.

To study further mechanisms of DSB repair, especially after low IR doses, we measure IRIF of proteins involved in HRR under conditions of globally relaxed chromatin. As mentioned above PFGE using high IR doses precludes analysis of HRR, as it saturates above 4 Gy (unpublished data).

An important step of HRR (see Figure 7) is DNA end resection and it is investigated here by measuring RPA70 staining by FC. In contrast to evaluation of IRIF numbers, measurement of RPA70 by FC has several advantages. Using high doses is limited when foci shall be counted, but by FC the mean intensity of immunostained RPA70 is possible. Analysis of cell cycle distribution by combined PI and EdU staining facilitates quantification of only G2/M-phase cells and exclusion of late-S cells.

When chromatin structure is relaxed after IR by incubation in medium with 75 mM NaCl, the levels of RPA70 intensity do not change in comparison to control levels (see Figure 38 A). It seems that end resection remains unaffected under conditions of chromatin relaxation, which further supports the previous finding that DSB repair by altEJ remains unchanged (see Figure 37) as this repair benefits from resection.

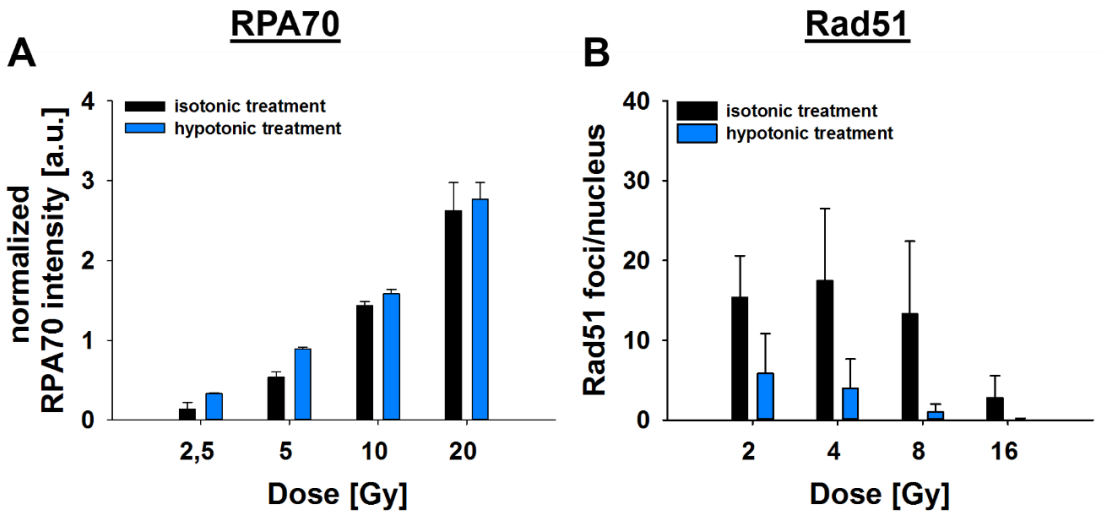

Figure 38 DNA end resection and HRR in globally relaxed chromatin.
(A) Arithmetic mean values of AF488 intensity of RPA70 measured by FC and gated for G2-phase at 3 h post IR are normalized to the non-irradiated control values and plotted against IR dose. Cells are treated in isotonic (black bars) or hypotonic medium (blue bars). Means and SE calculated from three experiments have been plotted. (B) Formation of Rad51 foci in isotonically (black bars) or hypotonically (blue bars) treated S/G2-phase cells at 3 h after different doses of IR. Data shown here represent means and SD of two independent experiments.

As DNA end resection is needed for HRR, but can also prepare DSBs for repair by altEJ, the formation of Rad51 foci is investigated to measure ongoing HRR.

Global chromatin relaxation decreases the number of Rad51 foci after IR in comparison to control (see Figure 38 B).

Upon DSB induction the resection of DNA ends is still functional when chromatin is globally relaxed but obviously those breaks are not repaired by HRR as the formation of Rad51 is decreased. Resected breaks do not necessarily need to be repaired by HRR, but can also be shunted to altEJ or SSA, which implies a repair pathway switch under hypotonic conditions. This is in line with PFGE results that show no effects of hypotonic treatment on altEJ (see Figure 37).

Another way to examine the efficiency of the different DSB repair pathways under conditions of global chromatin relaxation and to uncover a possible pathway switch, is to use U2OS reporter assay cell lines.

These cell lines have integrated reporter constructs which are specifically designed to measure the activity of the corresponding repair pathway upon DSB induction by the endonuclease I-SceI. When cells repair the I-SceI induced DSB by the pathway integrated in the design of the reporter, GFP is expressed and this expression can

be measured by FC. As we wish to investigate DSB repair in these cell lines after treatment with hypotonic medium, we first have to demonstrate that the GFP protein is expressed and folds correctly under hypotonic conditions. Therefore, exponentially growing U2OS 282C DRGFP, U2OS 279A EJ2GFP, U2OS 280A EJ5GFP and U2OS 283C SAGFP cells are transfected with the pEGFP-N1 plasmid (as positive control for GFP expression) by electroporation and incubated in isotonic or hypotonic medium at 2.5 h after transfection. Cells are collected and pEGFP-N1 expression is measured by FC 24 h later.

In all cell lines the cell viability after isotonic or hypotonic treatment is high (~ 70 - 90 %) and almost all viable cells express GFP protein (> 90 %) (see Figure 39).

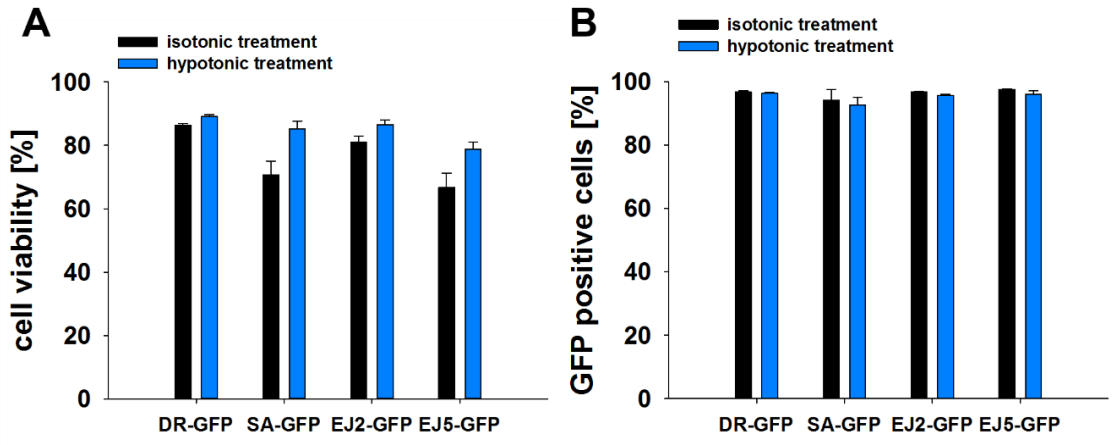

Figure 39 Cell viability and GFP expression in U2OS reporter cell lines.
(A) Cell viability of U2OS DR-GFP, SA-GFP, EJ2-GFP and EJ5-GFP cells after transfection with pEGFP-N1 plasmid by nucleofection and incubation in isotonic (black bars) or hypotonic (blue bars) medium for 24 h at 2.5 h after transfection. (B) Percentage of cells expressing GFP after transfection with the pEGFP-N1 plasmid by nucleofection and incubation in isotonic (black bars) or hypotonic (blue bars) medium for 24 h at 2.5 h after transfection. Data in this figure represent the means and SD/SE calculated from two (SA-GFP) and three (DR-GFP, EJ2-GFP, EJ5-GFP) independent experiments.

This experiment shows that GFP expression is not affected by low tonicity and that the reporter assay results can be interpreted without caveats.

In order to investigate the efficiency of HRR, U2OS 282C cells are used. These cells possess an integrated construct consisting of two modified *GFP* gene sequences, which are oriented as direct repeats; it is therefore named DR-GFP (see Figure 40 A). The *GFP* sequence is disrupted by the *Sce* sequence and a premature stop codon. In addition, there is an inactive copy of *GFP* gene (*iGFP*) harboring a 5' and 3' truncated sequences. Expression of a functional GFP protein in this configuration

is impossible. In order to introduce a DSB within the *SceGFP* sequence U2OS 282C cells are transfected with an I-*Sce*I expression vector. I-*Sce*I is introducing by its endonuclease activity a DSB at the I-*Sce*I site at the *SceGFP* site. When cells repair this break by HRR using the *iGFP* locus as a homologous sequence, the I-*Sce*I site as well as the premature stop codon are lost and a functional *GFP* gene is generated. These cells can be detected by the GFP fluorescence signal measured by FC. In order to investigate the effect of global chromatin relaxation on HRR, cells are incubated in 75 mM NaCl containing medium at 2.5 h after I-*Sce*I transfection. After 24 h the expression of GFP protein is analyzed by FC (see Figure 40 B and C).

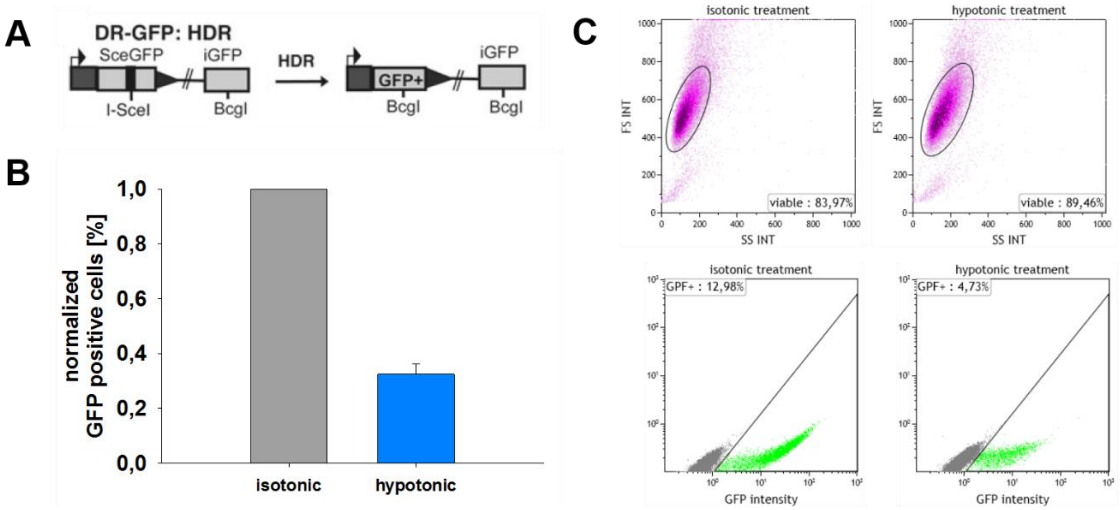

Figure 40 Effects of global chromatin relaxation on HRR as measured by the U2OS DR-GFP reporter assay.
(A) Schematic drawing of the DR-GFP construct (Moscariello et al. 2015). (B) Normalized results of GFP intensity of U2OS DR-GFP reporter measured by FC 24 h after transfection with an I-*Sce*I expressing plasmid and treatment with isotonic or hypotonic medium. Graph shows mean values and SD from two independent experiments. (C) Histograms of cell viability (upper panel) and GFP intensity (lower panel) of U2OS DR-GFP cells after transfection with I-*Sce*I expressing plasmid and treatment in isotonic or hypotonic medium.

Under control conditions 12 % of viable cells express GFP, representing successful repair by HRR. Only a third of repair events by HRR can be detected when chromatin is relaxed. These results are in line with the observation of decreased numbers of Rad51 foci (see Figure 38 B) and consequently decreased HRR efficiency.

To study DSB repair by NHEJ, two different cell lines harboring genome-integrated reporter constructs are used. U2OS EJ5-GFP cells have incorporated a reporter construct measuring NHEJ events that are accompanied by extensive deletions. In this construct a full length *GFP* open reading frame is segregated from its promoter

by a *puromycin* gene (*puro*), which is flanked by two I-*Sce*I cutting sites. Here, two DSBs are induced by I-*Sce*I transfection. The GFP signal can be detected when the *puro* gene is lost and the two distal ends are rejoined (see Figure 41 A).

U2OS EJ2-GFP cells serve to detect repair by microhomology dependent altEJ. In this construct the *GFP* gene is fused to an N-terminal tag but separated by an I-*Sce*I site and a stop codon. These sites are flanked by 8 nt of microhomology. The *GFP* sequence is restored when the cells repair the I-*Sce*I mediated DSB by microhomology dependent altEJ (see Figure 41 B).

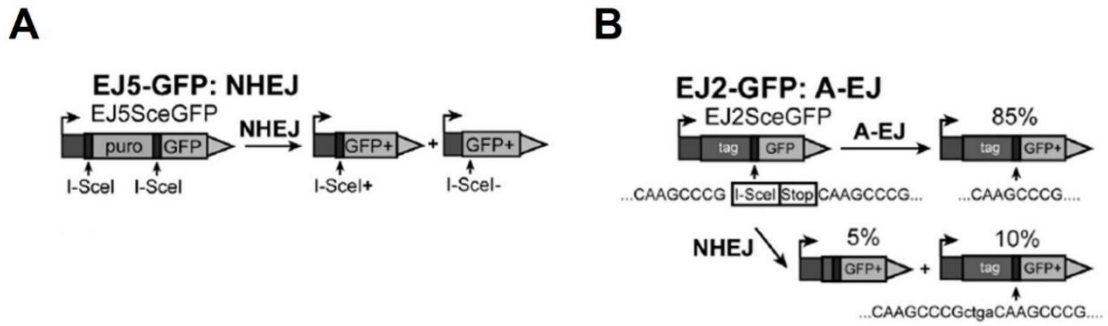

Figure 41 Schematic drawn of EJ5-GFP (A) and EJ2-GFP (B) (Moscariello et al. 2015). See text for more detail.

When U2OS EJ5-GFP cells are incubated in hypotonic medium 2.5 h after transfection of the I-*Sce*I expressing plasmid only 50 % of GFP signal can be detected (normalized to control) (see Figure 42 A) which shows that NHEJ is significantly affected by global chromatin relaxation.

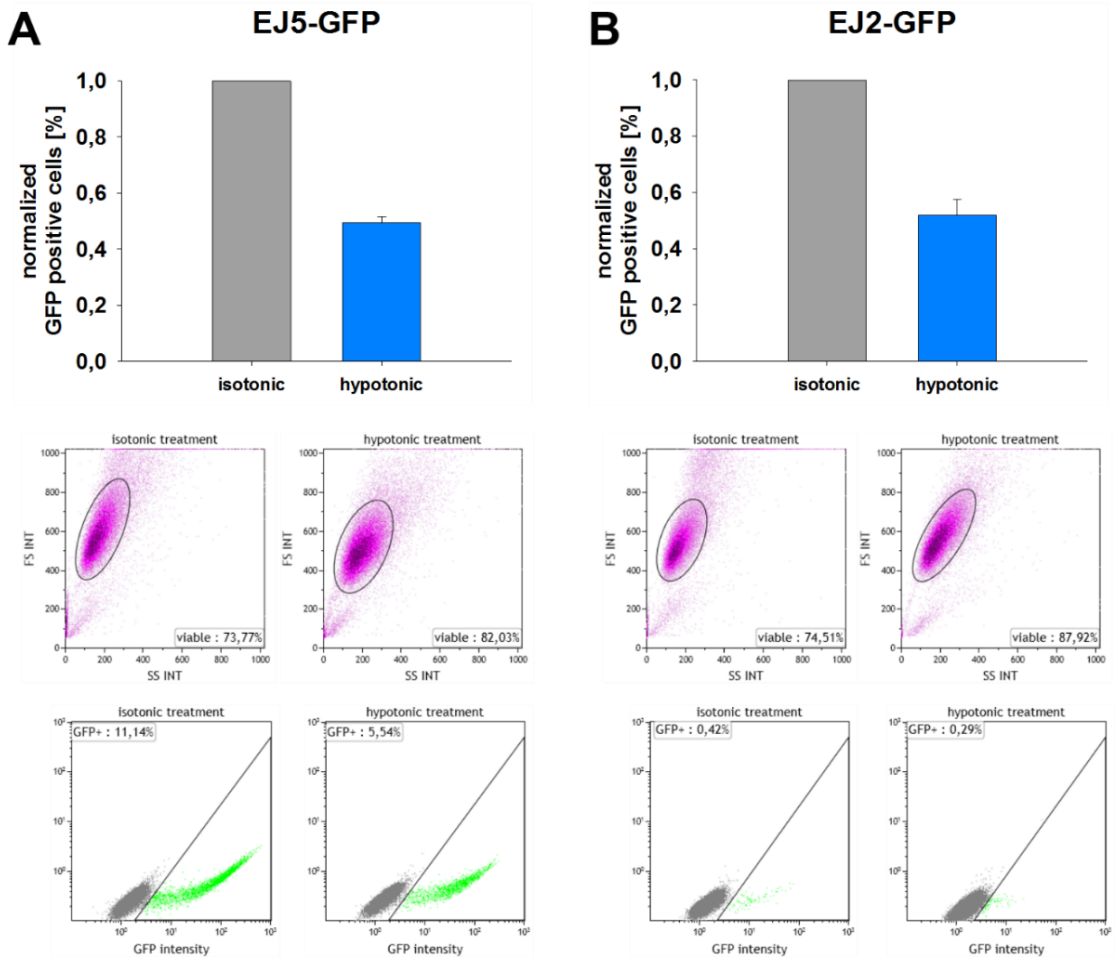

Figure 42 Effects of global chromatin relaxation on end joining events measured using the U2OS EJ5-GFP (A) and U2OS EJ2-GFP (B) reporter cell lines.
(A) Normalized GFP intensity of U2OS EJ5-GFP cells measured by FC 24 h after transfection with I-*Sce*I expressing plasmid and treatment in isotonic or hypotonic medium. Graph shows means ± SD calculated from two independent experiments. Histograms of cell viability (upper panel) and GFP intensity (lower panel) of U2OS EJ5-GFP cells after transfection with the I-*Sce*I expressing plasmid and treatment in isotonic or hypotonic medium. (B) Same like in A, but here the results of U2OS EJ2-GFP reporter assay are shown. Data for EJ2-GFP represent mean and SD from two independent experiments.

Also, incubation in hypotonic medium reduces the expression of GFP in the U2OS EJ2-GFP cell line by 50 % and thereby the repair by microhomology dependent altEJ (see Figure 41 B). Thus this repair pathway is similarly affected by global chromatin relaxation as cNHEJ. The results obtained by U2OS EJ5-GFP as well as by U2OS EJ2-GFP do not fit to previous PFGE experiments showing only very small effects on DSB repair by cNHEJ and altEJ. However, repair of enzymatically induced DSBs may not be representative of DSBs induced by IR. Enzymes usually create clean ends that are easy to repair while IR induces additional damages around the breaks that need further processing (see introduction).

However, a previous assumed pathway switch of resected DNA ends from HRR to altEJ cannot be detected here. But resected breaks are also needed for repair by SSA and so we investigate a possible repair pathway switch from HRR to SSA by using U2OS SA-GFP cells.

The reporter construct in the U2OS SA-GFP cell line contains a 5' *GFP* fragment which is separated from a 3' *GFP* fragment by 2.7 kb containing I-*Sce*I recognition site (see Figure 43 A). The induced DSB can be bridged during SSA by 266 nt of common sequence (Gunn and Stark 2012).

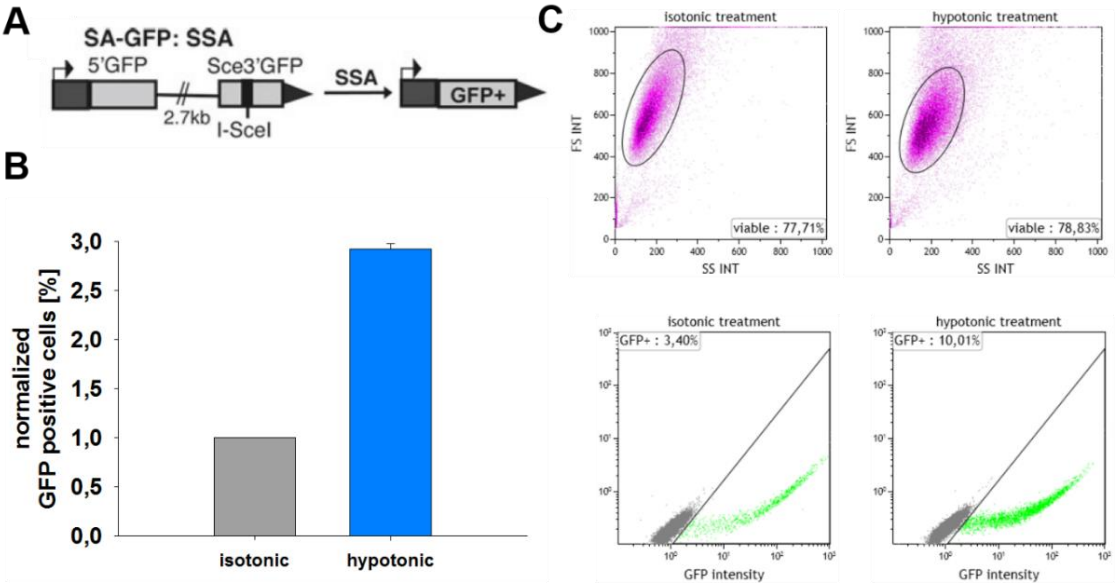

Figure 43 Effects of global chromatin relaxation on SSA repair measured using the U2OS SA-GFP reporter cell line.
(A) Schematic drawing of the SA-GFP construct (Gunn and Stark 2012). (B) Normalized results of GFP intensity in U2OS SA-GFP cells measured by FC 24 h after transfection with the I-*Sce*I expressing plasmid and treatment in isotonic or hypotonic medium. Means and SD are calculated from two independent experiments. (C) Histograms of cell viability (upper panel) and GFP intensity (lower panel) of U2OS SA-GFP cells after transfection with the I-*Sce*I expressing plasmid and treatment in isotonic or hypotonic medium.

When cells are incubated in hypotonic medium repair by SSA is three times increased in comparison to controls (see Figure 43 B). Indeed, SSA is known to function as back up to HRR which may be seen here.

Taken together, the results presented here show an inhibition of the main repair pathways cNHEJ and HRR when chromatin is globally relaxed by hypotonic treatment. Also the repair efficiency of the backup pathway altEJ is decreased under this condition, while resection is still functional. The indicated repair pathway switch is given from resected breaks undergoing SSA as this repair pathway shows a much

higher contribution as measured by reporter assays. However, this repair pathway is highly mutagenic, so that in the next section clonogenic assays are performed to evaluate cell radiosensitivity to killing under conditions of globally relaxed chromatin.

7.2.7) Radiosensitivity to killing is minimally affected by global chromatin relaxation

When the cells are continuously incubated in medium containing 75 mM NaCl for 11 days for colony formation, plating efficiency (PE) decreases to 0 % (see Figure 44 A). Thus, the protocol for clonogenic survival assays is adapted accordingly and cells are treated with hypotonic medium for 6, 9, 16 and 24 h after IR before plating in normal cell culture medium.

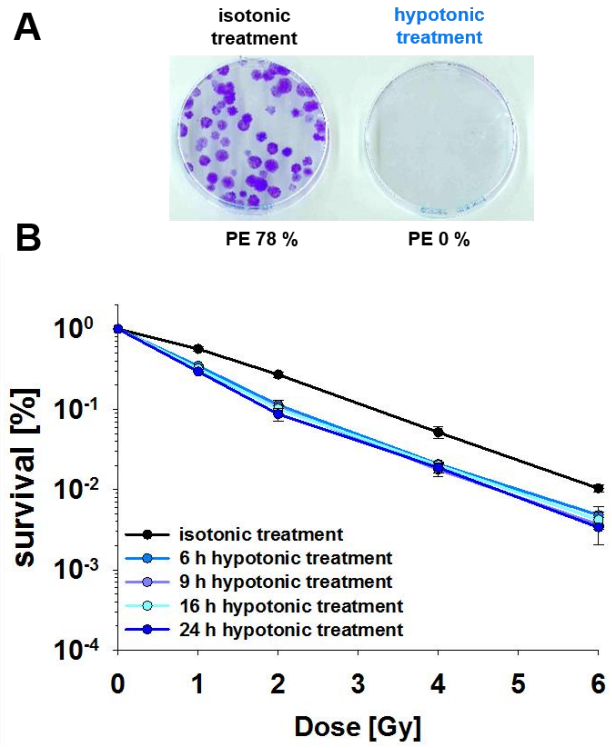

Figure 44 Clonogenic survival of RPE-1 cells when chromatin is globally relaxed. (A) PE of cells continuously treated with isotonic or hypotonic medium for colony formation. Colonies are counted after 11 days of growth. (B) Cells are treated with isotonic (black line) or hypotonic (blue lines) medium for 6, 9, 16 or 24 h immediately after IR before plating in isotonic medium for colony formation. Survival does not differ under the different isotonic treatment conditions (see supplementary Figure 73) so that here a representative curve is shown. Data shown represent means ± SD from four determinations in two experiments.

After 11 days of growth colonies are counted and the results (see Figure 44 B) reveal a modest sensitization to IR by global chromatin relaxation, independently of treatment time.

As the effects of global chromatin relaxation achieved on cell radiosensitization to killing are not as severe as the previously discussed results on DDR, G2-checkpoint and DSB repair at low IR doses, we wish to investigate the role of reversion of chromatin state on the final outcome. We point out that in clonogenic survival assays, cells are returned to normal growth conditions after hypotonic treatment for colony formation. Therefore, in the following section we investigate whether the above detected effects of global chromatin relaxation are reversible.

7.2.8) Effects of globally relaxed chromatin on DDR signaling and cell proliferation are fully reversible

Indeed, there are reports in the literature of recovery of γH2AX foci when cells are returned to isotonic conditions after 1 h of treatment, and that the number of foci converge to those of untreated control cells (Reitsema et al. 2004). Thus, we test such recovery after 1 h of incubation in hypotonic medium.

The inhibitory effects of globally relaxed chromatin on the formation of γH2AX, pATM and 53BP1 foci are completely reversed and foci numbers recover to the levels of the isotonically treated controls (see Figure 45 A). As the induction of DSBs is the same in all samples, owing to the experimental protocol used, we can assume that also the number of breaks is the same in all samples.

Global relaxation of chromatin interferes with the phosphorylation of H2AX but recovers when the osmotic pressure becomes normal again.

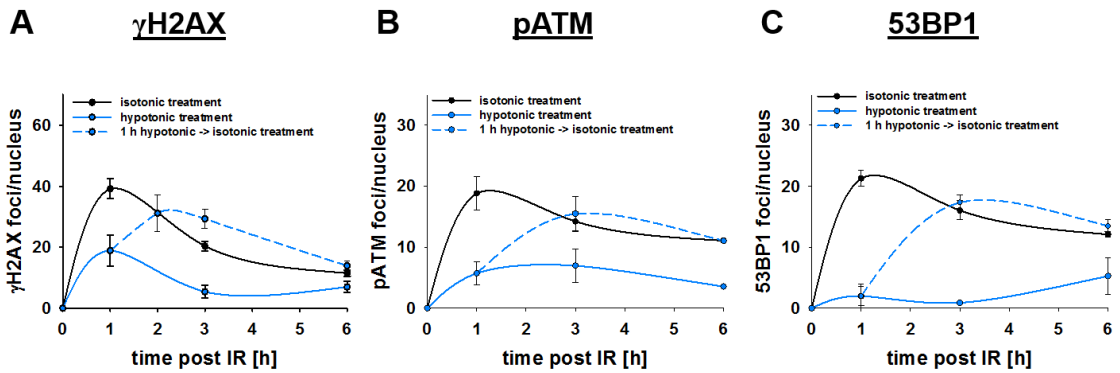

Figure 45 Recovery of IRIF of γH2AX (A), pATM (B) and 53BP1 (C) after short incubation in hypotonic medium.
Cells are either continuously incubated in isotonic (black plot) or hypotonic (blue, solid plot) medium or treated in hypotonic medium for 1 h (blue, dashed plot) before returning to isotonic conditions. Data for continuous treatments are the same as in Figure 29, Figure 30 and Figure 31. For reversible treatments means and SD of two (A and B) and one (C) independent experiments are plotted.

Also, reduced formation of IR induced pATM and 53BP1 foci in relaxed chromatin completely recovers when cells are returned to isotonic medium (see Figure 45 B and C). Thus, although the formation of γH2AX and the recruitment of pATM and 53BP1 to sites of DSBs are dramatically reduced upon global chromatin relaxation, this effect can be quickly reversed.

As these effects are likely to arise from a normalization of chromatin condensation status we investigate how the CCP and also the appearance of metaphase chromosomes change when control conditions are applied after 1 h of hypotonic treatment.

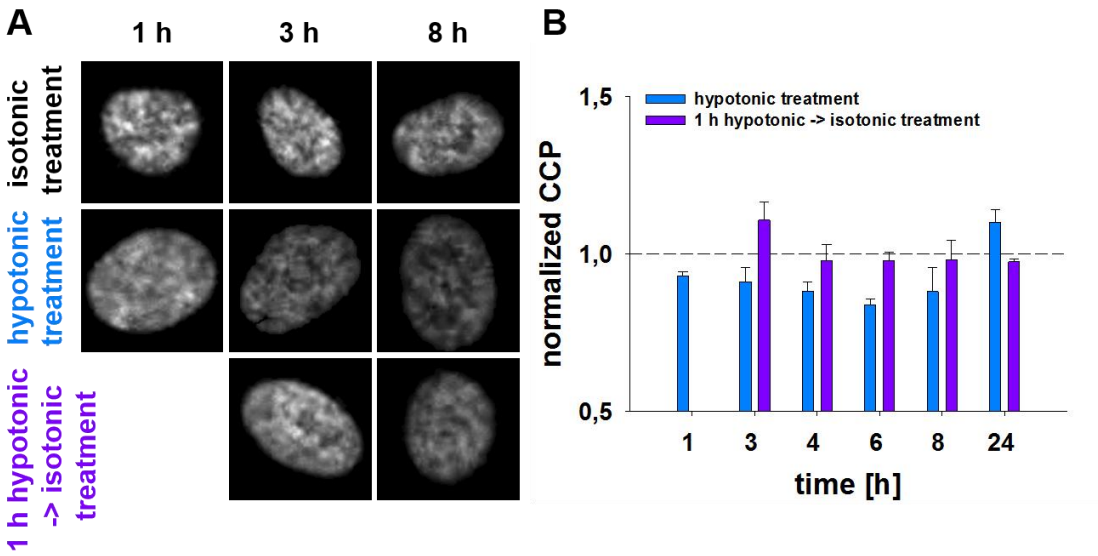

Figure 46 CCP of RPE-1 cells after either continuous treatment in hypotonic medium or 1 h treatment followed by return to normal conditions.
(A) Representative images taken by CLSM of DAPI stained RPE-1 nuclei at different times of treatment in isotonic or hypotonic media (continuously) or hypotonic medium for 1 h before changing to isotonic medium. (B) Graph shows mean CCP values of continuously hypotonically treated (blue bars) and 1 h hypotonically treated (violet bars) cells. Values are normalized to isotonic control values (represented by black dashed line). Graph shows means ± SD from two independent experiments.

Chromatin gets globally relaxed after a 1 h incubation in 75 mM of NaCl (represented by CCP values below 1), but the effect can be reversed just as promptly and efficiently (see Figure 46). This shows that global chromatin relaxation by hypotonic treatment is only transient and reversible.

The same conclusions can be drawn investigating the metaphase chromosomes in cells treated with hypotonic medium for 1 h and then incubated in normal medium again.

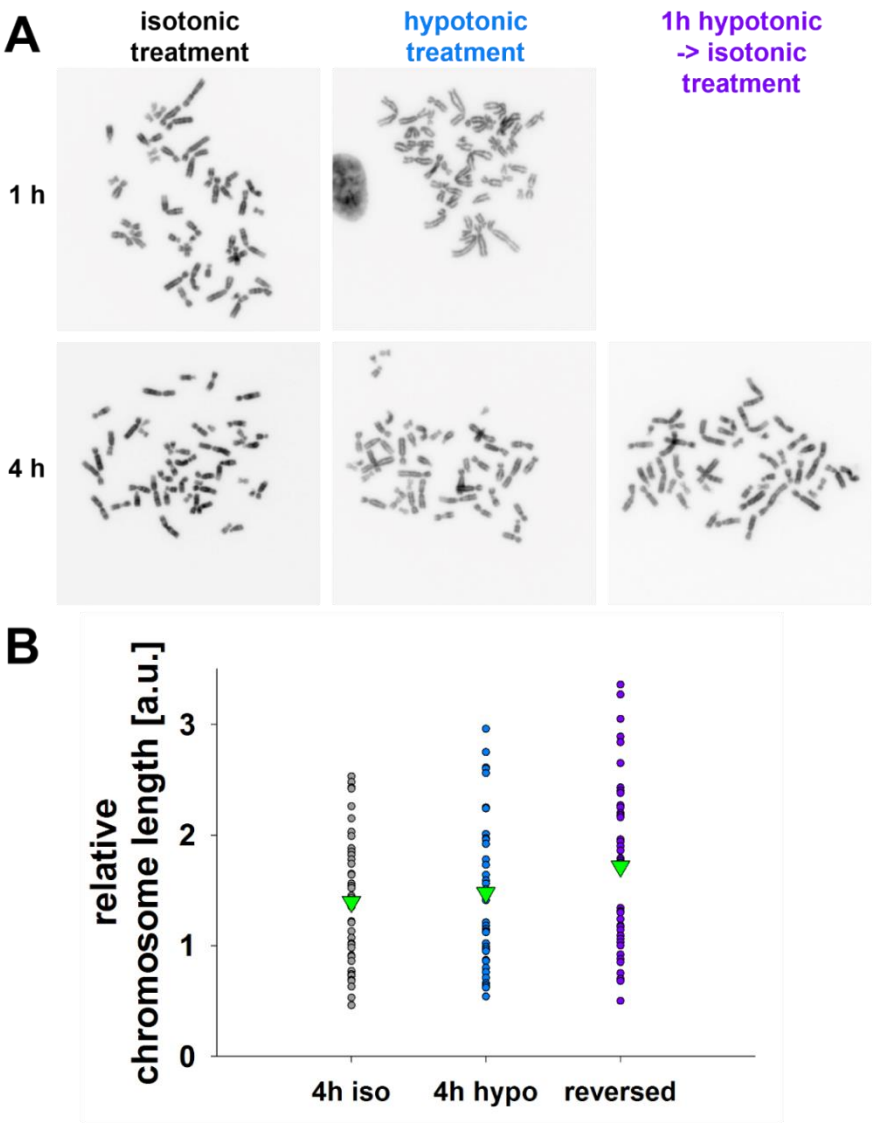

Figure 47 Representative images and length quantification of metaphases formed in hypotonically treated cells.
(A) Cells are incubated either in isotonic or hypotonic medium continuously or in hypotonic medium for 1 h and then in isotonic medium before a 30 min treatment with colcemid. DNA is stained with DAPI and is shown in inverted greyscale. The scale is the same in all images. (B) Quantification of chromosome length of metaphases shown in (A). X-axis is showing treatment times and green triangles represent means.

However, the length of chromosomes even increases when cells are reversed to isotonic conditions (see Figure 47 B), but the larger separation of sister chromatids observed in metaphase chromosomes after chromatin relaxation cannot be seen (see Figure 47 A). This shows a reversion of the hypotonic effects on the chromosomes at least in terms of sister chromatid separation.

Previous experiments show a delay in cell cycle progression when chromatin is globally relaxed preventing cells from entering mitosis. Cells synchronized in G2-

phase and then treated with hypotonic medium start to progress through mitosis and to G1-phase not before 8 h after starting the treatment (see Figure 26). Thus, we investigate the cell cycle distribution of G2-synchronized cells when hypotonic treatment lasts only 1 or 4 h and cells are then incubated in normal cell culture medium (see Figure 48).

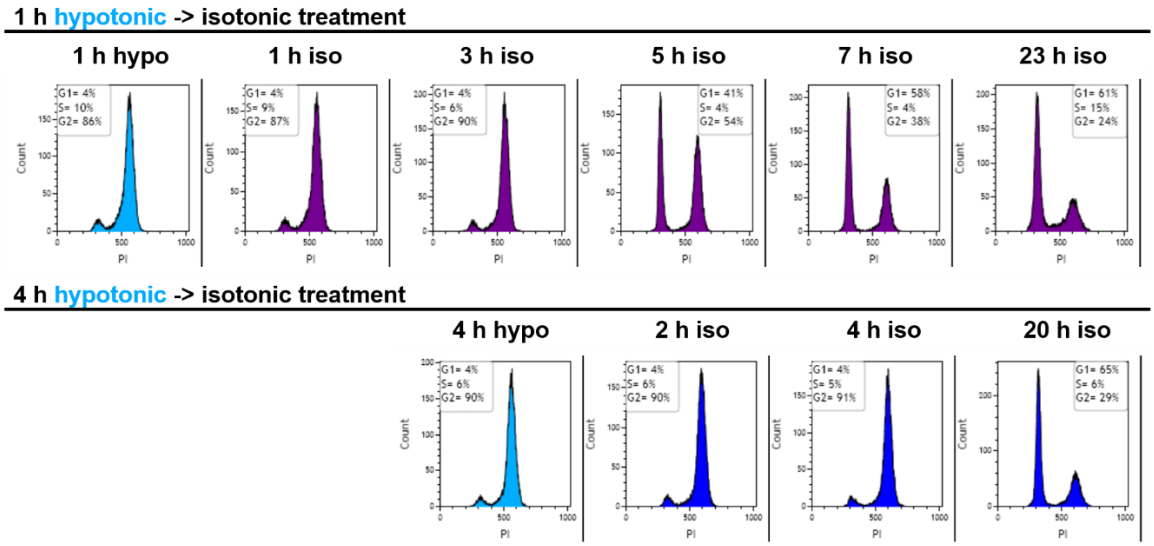

Figure 48 Cell cycle distribution of synchronous RPE-1 cells at different times after 1 or 4 h pretreatment in hypotonic medium.
Treatment of RPE-1 cells in hypotonic medium starts at 4 h after release of thymidine block when most cells accumulate in G2-phase (see Figure 26 A). After 1 h (upper panel) and 4 h (low panel) of pretreatment in hypotonic medium, cells are incubated in normal cell culture medium and cell cycle distribution is measured by PI staining and FC as a function of time.

When cells are pretreated with hypotonic medium for 1 h and then incubated in normal cell culture medium, cells start to divide and progress to G1-phase 4 h later (41 % in G1-phase, see Figure 48, upper panel, 5 h iso). Cell populations in which chromatin is globally relaxed for 4 h do not divide so quickly (4 h iso). It seems that cells need longer to resume cell cycle progression depending on the duration of treatment in hypotonic medium. However, at the final point of observation (23 h and 20 h, respectively), both cell populations show a similar cell cycle distribution. Again, we observe only a few cells in S-phase, which might be due to stress experienced during the synchronization procedure.

The results discussed above, clearly show that the effect of global chromatin relaxation is reversible. This might explain the reduced effects of long term treatments that include or require transfer of cells to normal growth conditions.

7.3) Global chromatin condensation induced by hypertonic treatment affects DDR signaling and DSB repair

Several studies report that local chromatin relaxation upon DNA damage induction facilitates repair by enabling the access of signaling and repair proteins to the damage sites. However, there are also reports of chromatin condensation in response to DNA damage induction. Global chromatin condensation may actually provide protective functions from DNA damage (Hamilton, Hayward, and Gilbert 2011). To further elucidate the impact of global chromatin condensation on DDR signaling and DSB repair, we utilize treatment in hypertonic medium (containing 300 mM NaCl).

7.3.1) Increase in extracellular NaCl concentration globally condenses chromatin

Measurements performed using a Beckmann Coulter Counter reveal rapid changes in cell diameter and cell volume upon incubation in hypertonic medium (Figure 49).

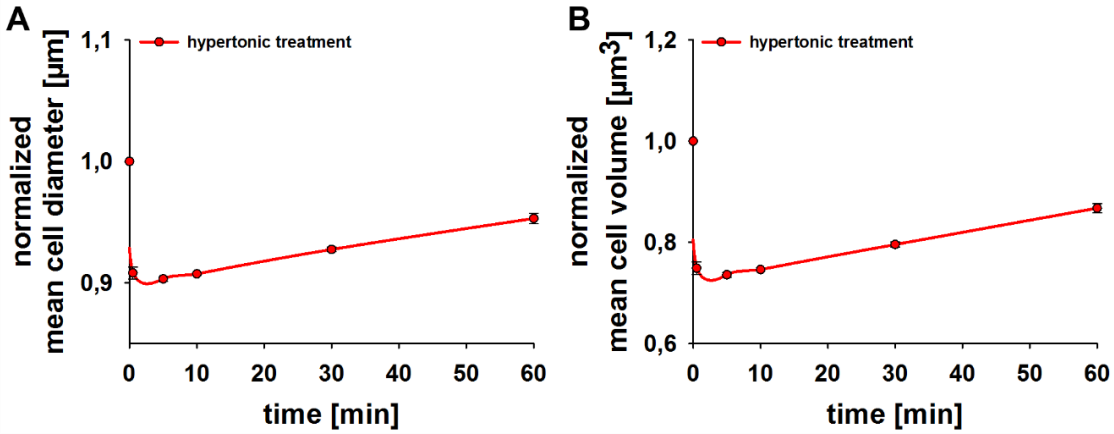

Figure 49 Influence of 300 mM NaCl on RPE-1 cell diameter and cell volume.
Mean cell diameter (A) and mean cell volume (B) of hypertonically treated RPE-1 cells at different times as measured in a Beckmann Coulter Counter. Values are normalized to initial diameter and volume (at 0 h), respectively. Graphs show means and SE calculated from four independent experiments.

Cells incubated in hypertonic medium are exposed to high osmotic pressure. By moving out inorganic ions and water, the cell volume decreases. As cells rapidly activate RVD processes the cell volume is normalizing after 1 h of treatment (see Figure 49 B).

In order to demonstrate that treatment with hypertonic medium induces a change of chromatin condensation level, DAPI stained nuclei are imaged after incubation in medium containing 300 mM NaCl by CLSM (see Figure 50 A).

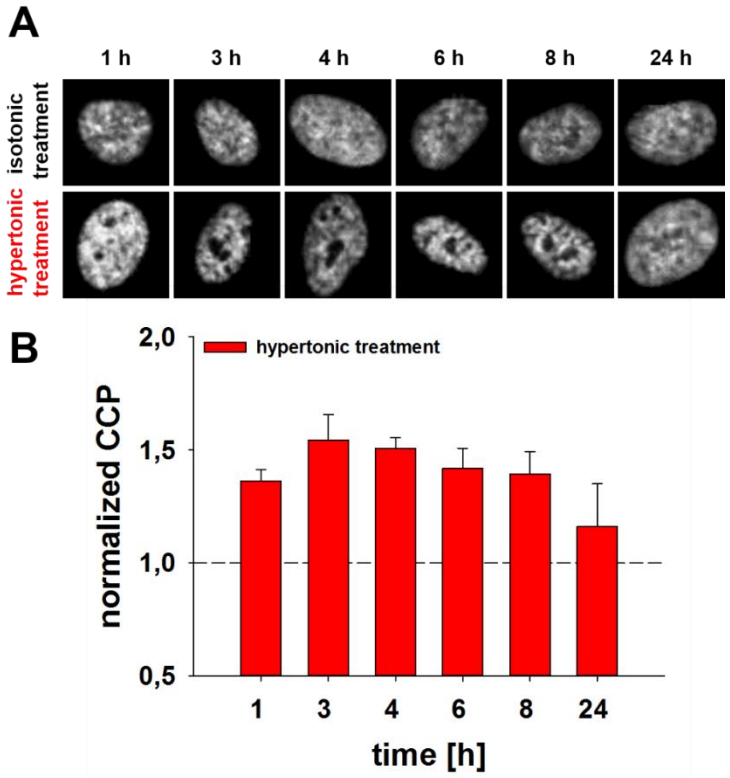

Figure 50 CCP of RPE-1 cells treated in hypertonic medium.
(A) Images taken by CLSM of DAPI stained RPE-1 nuclei after different times of treatment with isotonic or hypertonic medium. (B) Mean CCP of RPE-1 cells treated with hypertonic medium for different times. Values are normalized to isotonic control values (represented by black dashed line) at each time point. Mean CCPs and SD are calculated from two independent experiments.

The CCP is calculated (see 6.2.8.2) for each condition and normalized to controls. Indeed, hypertonic medium is globally condensing chromatin represented by an increase in CCP. With increasing treatment time global chromatin condensation becomes more pronounced. While volume regulation occurs within short time (see Figure 49 B), the condensation of chromatin is still increased after 8 h as the ionic strength inside the cells need longer times to normalize. However, after 24 h of incubation in hypertonic medium, the CCP reaches control levels, suggesting an adaptation to the hypertonic environment.

For further investigation global chromatin condensation is analyzed in cells accumulated at metaphase using the mitotic spindle inhibitor colcemid. Notably, to

exclude changes in chromatin condensation based on different treatment times with colcemid all samples are incubated only for 30 min with this agent.

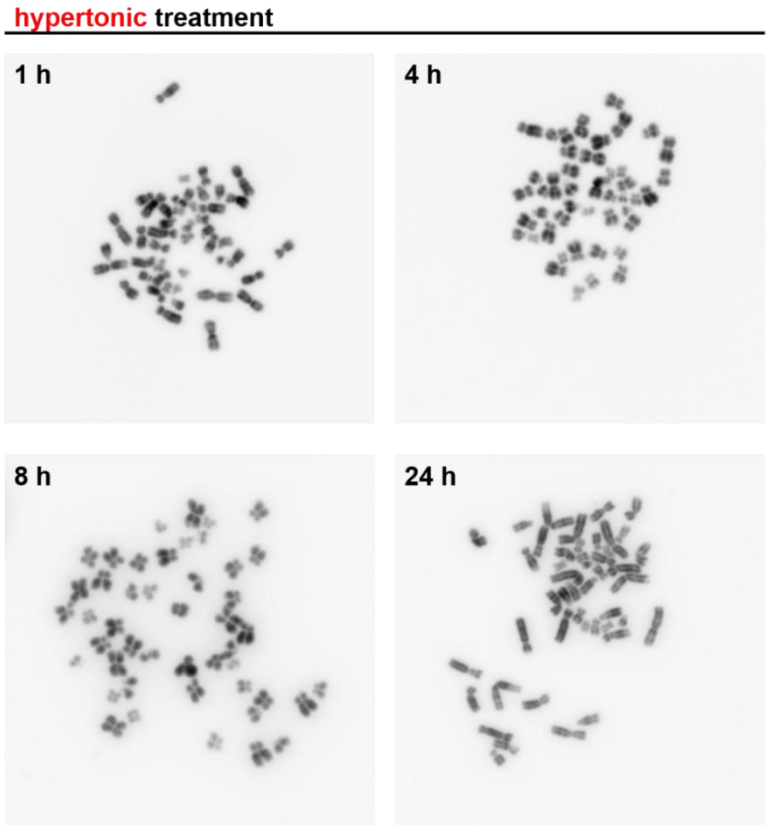

Figure 51 Representative images of metaphases formed in hypertonically treated cells. Cells are incubated in hypertonic medium for different times as indicated, before a 30 min treatment with colcemid. DNA is stained by DAPI and is shown in inverted greyscale. The scale is the same in all images.

CCP measurements already reveal a chromatin condensation upon treatment in hypertonic medium (see Figure 50), which is further confirmed by metaphase analysis as highly condensed chromosomes are found (see Figure 51). Especially, when chromatin is globally condensed by hypertonic treatment for longer periods of time (4 and 8 h) very short chromosomes can be observed. These images are reminiscent to those of metaphases after long colcemid treatments (Miura et al. 2012). Thus, strong chromatin condensation is induced by high concentration of NaCl. Length quantification confirms the observed shortening of chromosomes upon treatment with hypertonic medium (see Figure 52 B).

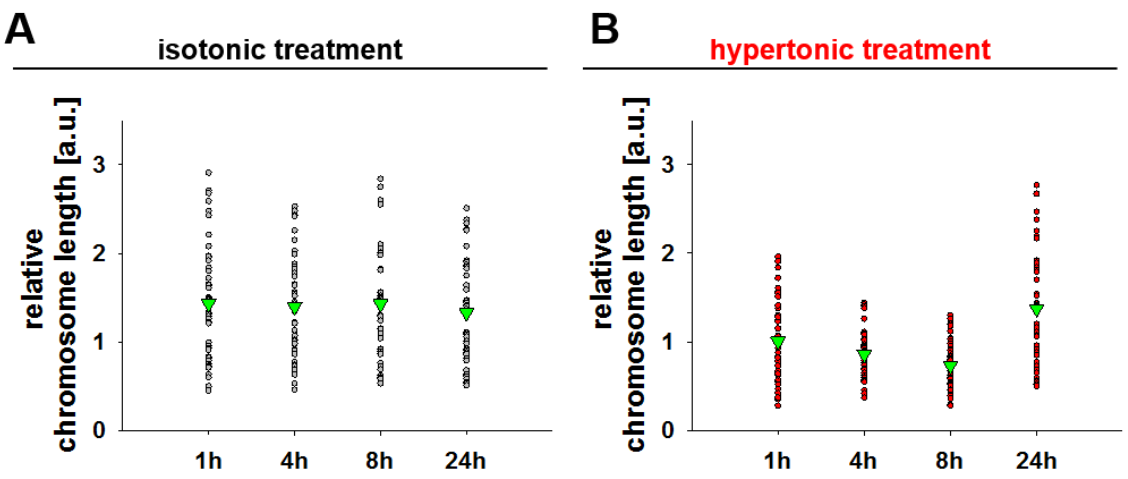

Figure 52 Chromosome length quantification in isotonically and hypertonically treated metaphases.
Lengths of chromosomes at metaphase measured by ruler tool in Adobe Photoshop CS5 from representative images of isotonically (A) and hypertonically (B) treated cells. Images are shown in Figure 21 and Figure 51 and are processed at the same scale. X-axis indicates treatment times and green triangles represent means.

However, after 24 h of incubation in hypertonic medium the cells adapt and the chromosomes appear nearly normal again and also their mean length increases (see Figure 51 and Figure 52), as also indicated by CCP measurement (see Figure 50).

In order to explore if the global chromatin condensation achieved by treatment with hypertonic medium is similar to the condensed facultative HC, we investigate levels of the HC marker H3K27me3 (see Figure 53).

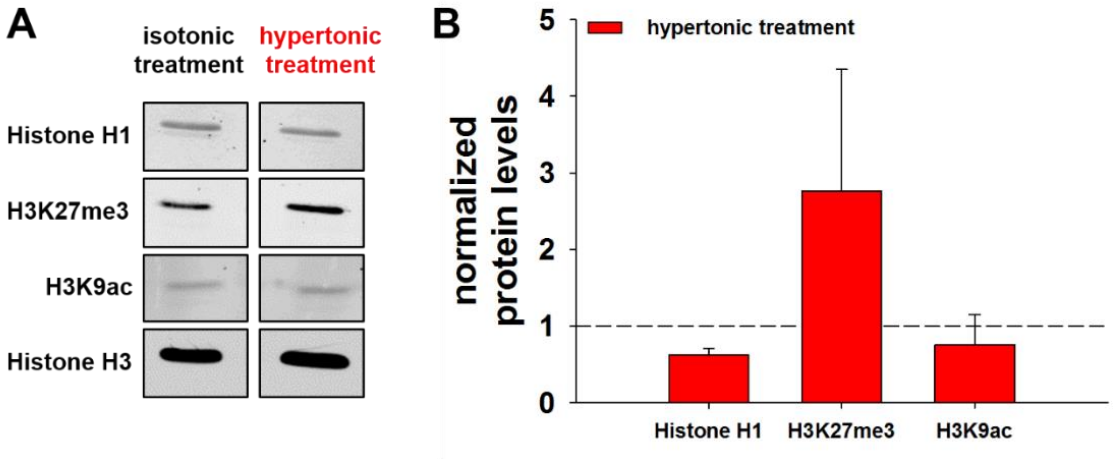

Figure 53 Changes in levels of linker histone H1 and HC/EC markers in globally condensed chromatin.
(A) WB analysis of histone H1, H3K27me3 and H3K9ac. RPE-1 cells are treated in isotonic (control) or hypertonic medium for 1 h before histone extraction. Histone H3 serves as loading control. (B) Levels of histone H1 and HC/EC markers are normalized to loading control and then normalized to isotonic samples (represented by black dashed line). Data represent means ± SD from two independent experiments.

Indeed, levels of HC marker H3K27me3 are increased three-fold in comparison to controls which further confirms the chromatin condensing character of hypertonic medium. Additionally, levels of EC marker H3K9ac decreases slightly when chromatin gets globally condensed. As high histone H1 levels are associated with chromatin compaction as well, it is surprising that we find a decrease in response to hypertonic treatment. Perhaps, the increased ionic strength within the nucleus disrupts partially the binding of H1 to linker DNA.

7.3.2) Global chromatin condensation inhibits cell growth

As changing salt concentration of the cell culture medium may not only influence chromatin architecture but also the overall condition of the cells, we analyze cell growth and cell cycle distribution to investigate whether cells continue proliferation. Therefore, cells are incubated in hypertonic medium and cell numbers and cell cycle distribution are analyzed by PI staining and FC measurement.

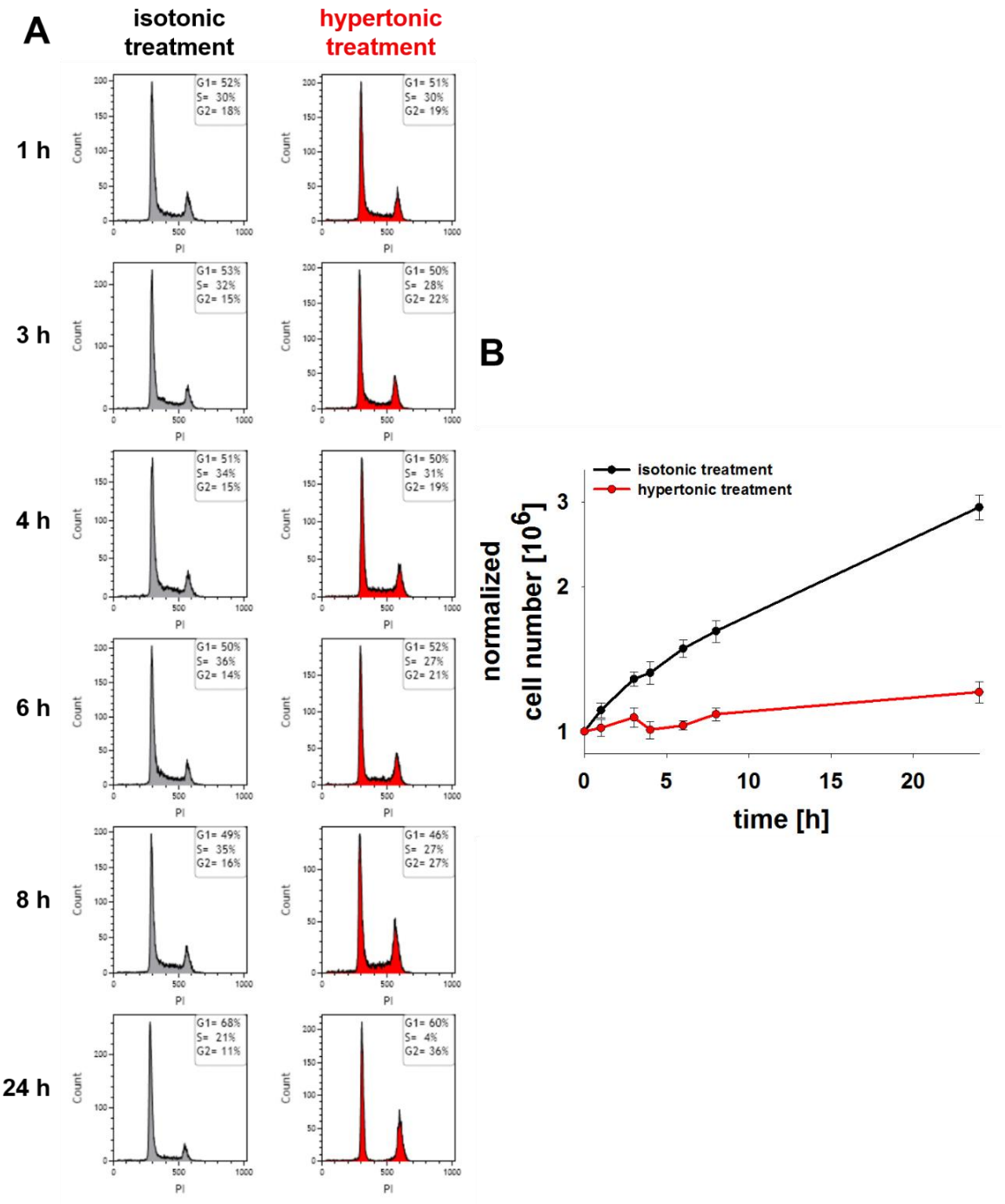

Figure 54 Cell number and cell cycle distribution of hypertonically treated RPE-1 cells. (A) Representative PI histograms measured by FC of RPE-1 cells treated with isotonic (grey histograms) or hypertonic medium (red histograms) for different times. (B) Number of RPE-1 cells after growing in isotonic (black line) or hypertonic (red line) medium. Values are normalized to starting point (0 h) and represent means and SE of three independent experiments.

Figure 54 B shows that incubation in hypertonic medium stops proliferation of RPE-1 cells. During 24 h treatment, the cell number does not markedly increase and only 4 % of cells remain in S-phase at endpoint of experiment, whereas the percentage

of G1-phase cells increases by 12 % and the number of G2-phase cells doubles (see Figure 54). This has been reported before and it was shown that this block is independent of Chk1, which is known to be acting in the DNA damage checkpoint response causing a G2-block upon damage induction (Burg, Ferraris, and Dmitrieva 2007). During DNA replication chromatin naturally relaxes which is antagonized by hypertonic treatment condensing chromatin; this explains the decrease of S-phase cells. On the other hand, during mitosis chromatin condensation is needed to facilitate proper distribution of chromosomes to the two daughter cells. However, global chromatin condensation induced by hypertonic treatment seems to stop this highly regulated process of cell division as well.

Especially, when cells are synchronized in G2-phase (see Figure 26 A), it is obvious that cells do not divide when chromatin is globally condensed (see Figure 55).

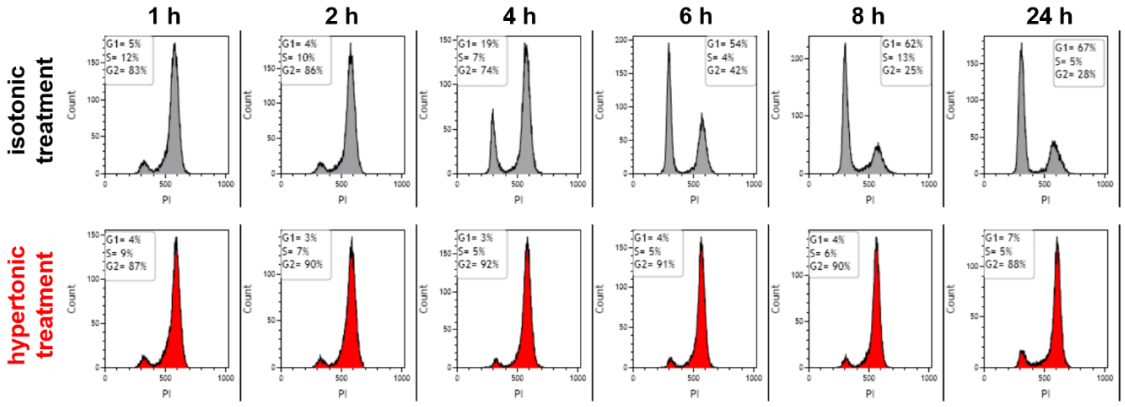

Figure 55 Progression through the cell cycle of cells synchronized in G2-phase and treated in chromatin condensing medium.
Cell cycle distribution of synchronized cells treated with isotonic (upper panel) or hypertonic (lower panel) medium for different times starting at 4 h after thymidine block release (see Figure 26 A).

Even after 24 h, cells remain in G2-phase suggesting suppression of cell progression to mitosis (see Figure 55).

Another approach to investigate cell proliferation is the examination of the MI of RPE-1 cells incubated in hypertonic medium as a function of incubation time. In asynchronous cells no significant change in MI is observed after treatment in hypertonic medium (see Figure 56 A). This result gives the impression that cells proliferate normally, which we know is not the case given the results presented above. One possible explanation for this constant MI can be that cells in M-phase

remain in mitosis during the treatment. The observations of highly condensed metaphase chromosomes underpin this postulate.

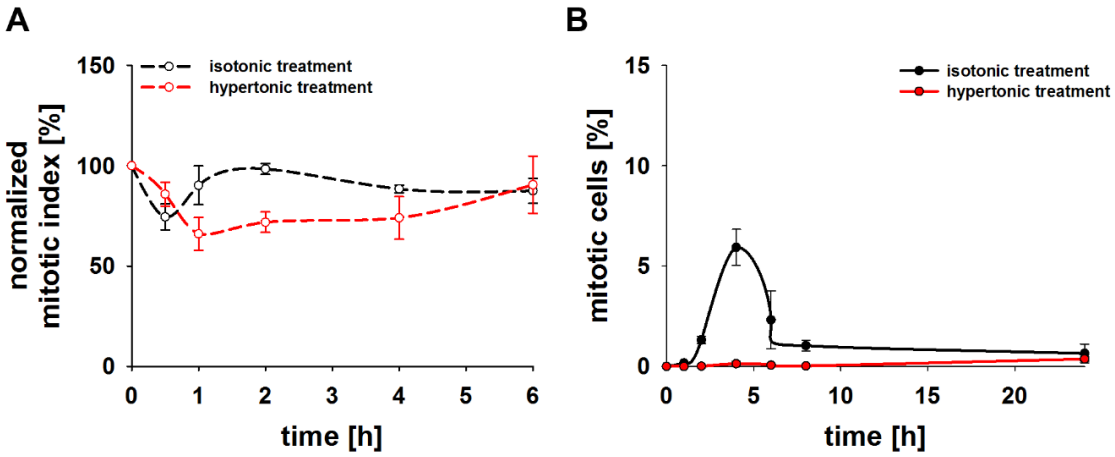

Figure 56 Proportion of mitotic cells under chromatin condensing conditions.
(A) MI is measured by FC and H3pS10 staining. Percentages are normalized to 0 h control. Asynchronous cells are treated with isotonic (black line) or hypertonic medium (red line) and fixed at different times thereafter. Data represent mean values and SE calculated from three (isotonic) or five (hypertonic) independent experiments. (B) Cells are synchronized in G2-phase as described in Figure 26 A. At 4 h after release of thymidine block cells are incubated in isotonic (black line) or hypertonic (red line) medium (marks starting point: 0 h). Graph shows percentage of cells in mitosis as determined by FC and H3pS10 staining at different times thereafter. Data represent means and SD from two independent experiments.

Additional confirmation that cells do not enter M-phase is given by following the progression of synchronized cells from G2-phase into mitosis when chromatin is globally condensed (see Figure 56 B).

7.3.3) DNA damage checkpoint is masked after hypertonic treatment

The above results clearly show a proliferation arrest and blocks in G1-, G2- and M-phase after incubation of cells in hypertonic medium. It is known that the PIKK ATM is activated by changes in chromatin conformation activating an entire signaling cascade able to stop cell proliferation (see introduction). Therefore, we are interested how global chromatin condensation achieved by incubation in medium containing 300 mM NaCl is affecting the activation of the G2-checkpoint, in which both, ATM and ATR, are playing a role, after DNA damage induction by IR.

While control cells (treated in isotonic medium after exposure to 2 Gy) show a typical G2-checkpoint activation as the MI decreases to 0 % at 1 h after IR and recovers to 100 % at 6 h after IR (see Figure 57 A), the MI of RPE-1 cells treated in hypertonic medium shows only small decreases (25 %) as a function of time after IR (see Figure

57 A). Considering only this result, we could assume that there is no or only very weak G2-checkpoint activation upon DNA damage induction. But as previous results already show that cells do not proliferate and are blocked in G1-, G2- and M-phase, the constant MI after 2 Gy of IR in hypertonically treated cells may only represent the mitotic cells from the beginning of the experiment that are blocked in M-phase due to the treatment.

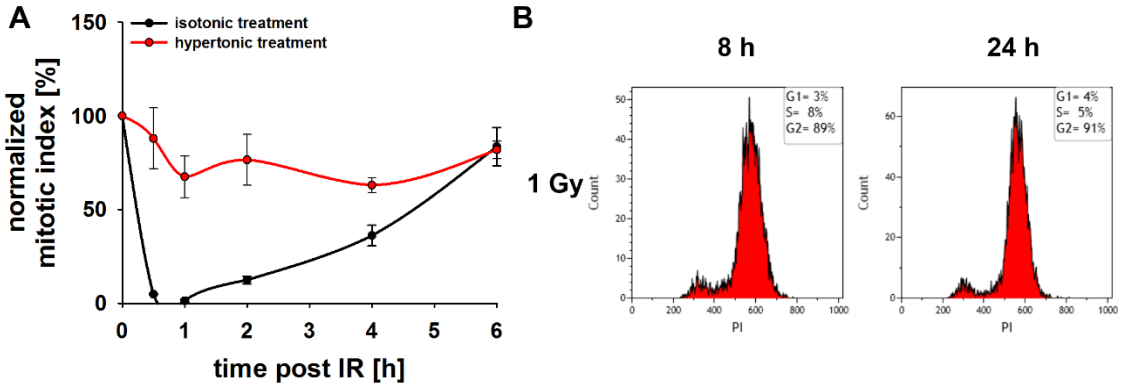

Figure 57 Investigation of G2-checkpoint under hypertonic conditions.
(A) MI (normalized to 0 h) of RPE-1 cells under isotonic or hypertonic conditions (black and red plots, respectively) after 2 Gy of IR. Data in this figure represent the means and SE calculated from three independent experiments. (B) PI histograms measured by FC in cells synchronized in G2-phase (see Figure 26 A), irradiated with 1 Gy and subsequently treated in hypertonic medium for 8 and 24 h.

In contrast, investigating the cell cycle distribution of synchronized cells treated with hypertonic medium after IR with 1 Gy underline that cells do not progress from G2-phase even after 24 h, meaning cells are blocked in G2-phase and cannot overcome this block (see Figure 57 B).

These contrary results let us assume that a G2-checkpoint activation under conditions of global chromatin condensation achieved by hypertonic treatment is not possible to be observed after IR (see Figure 57 A) and that a block in G2-phase even after long treatment times (see Figure 57 B) may not be due to G2-checkpoint activation (Burg, Ferraris, and Dmitrieva 2007), but is related to cell cycle effects due to the hypertonic treatment (see section before).

7.3.4) DSB repair and signaling are disturbed upon global chromatin condensation

DSBs induce structural changes in chromatin that activate the MRN complex, which in turn recruits ATM to break sites that phosphorylates H2AX.

In order to investigate DSB repair kinetics under conditions of globally condensed chromatin, we examine the formation and resolution of γH2AX foci after treatment in hypertonic medium. Under control conditions approx. 40 γH2AX foci form per nucleus at 1 h post 2 Gy of IR and more than 50 % are resolved after 6 h (see Figure 58 B).

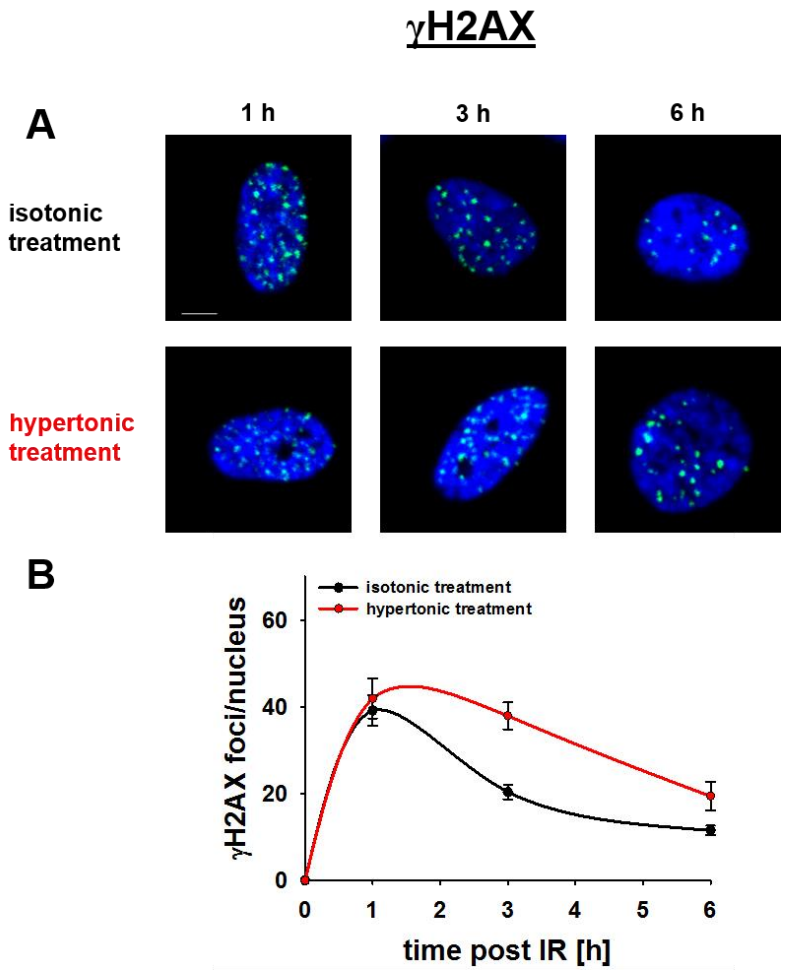

Figure 58 Formation of γH2AX foci when chromatin is globally condensed.
(A) Representative images of γH2AX foci in RPE-1 cells after 2 Gy of IR after different times of incubation in isotonic or hypertonic medium. Scale bar: 5 μm (B) Formation of γH2AX foci in cells maintained in isotonic medium (black plot) or in hypertonic medium (red plot) following 2 Gy of IR. Data represent means ± SE from six (isotonic) and five (hypertonic) independent experiments.

In cells with globally condensed chromatin the maximal number of γH2AX foci is similar to that of control cells (see Figure 58 B). Thus global chromatin condensation is not affecting the initial evolution of DDR. Processing of DSBs, on the other hand, as measured by the resolution of γH2AX foci is impaired. Additionally, at late time points (6 h) γH2AX foci appear larger in samples treated in hypertonic medium. This observation confirms earlier reports of enhanced phosphorylation of H2AX when

chromatin is globally condensed by hypertonic treatment, marking an inhibited DSB repair (Reitsema et al. 2005).

The phosphorylation of H2AX is mainly performed by ATM, so we wish to investigate if ATM is hyperactivated and thereby responsible for the higher numbers of γH2AX foci under hypertonic conditions. Indeed, when chromatin is globally condensed after IR, more pATM foci are counted in comparison to the controls (see Figure 59 B).

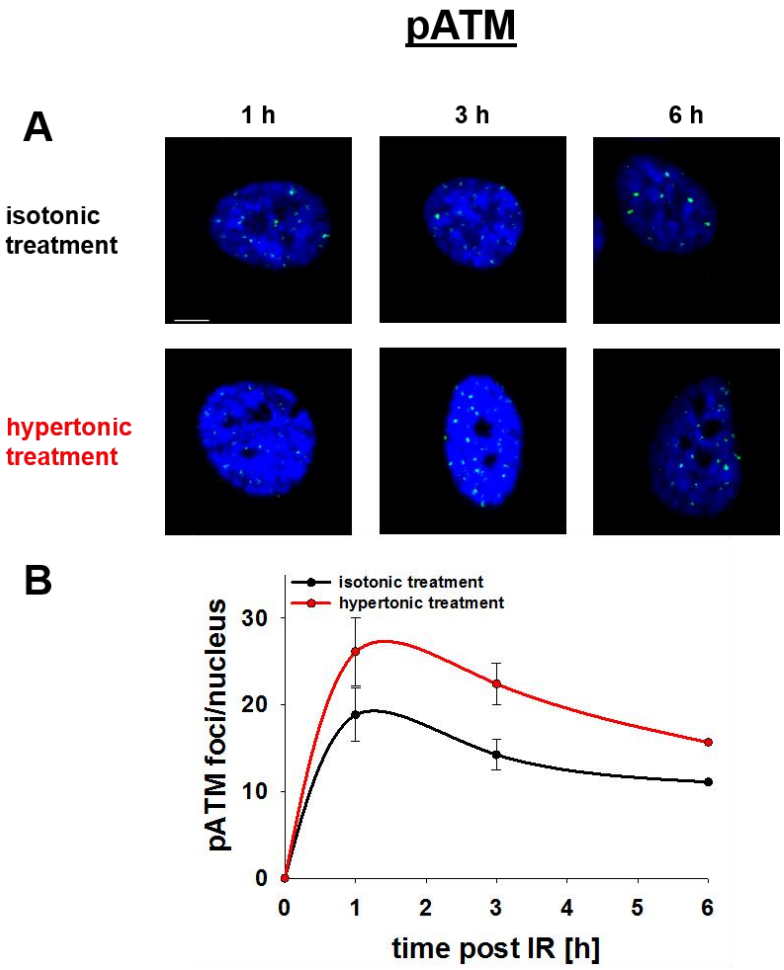

Figure 59 Formation of pATM foci under hypertonic conditions.
(A) Representative images of pATM foci in RPE-1 cells after 2 Gy of IR at different times of incubation in isotonic or hypertonic medium. Scale bar: 5 μm (B) Formation of pATM foci in isotonically (black plot) or hypertonically (red plot) treated cells following 2 Gy of IR. Data shown here represent means ± SE from five independent experiments (for 1 and 3 h time points).

These results are in line with the elevated γH2AX foci formation under these conditions. It would be interesting to investigate if upstream ATM signaling (e.g.

MRN complex) is also increased; this could be done by quantifying Mre11 foci formation.

Further downstream signaling, by means of 53BP1 foci formation, is also investigated under conditions of globally condensed chromatin.

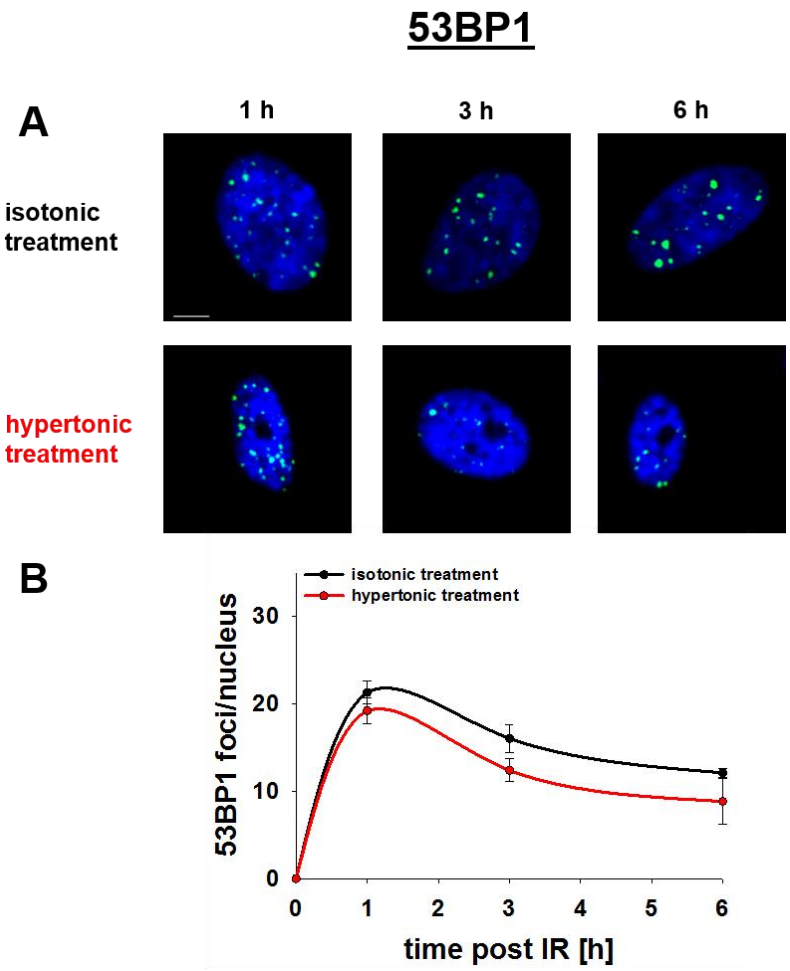

Figure 60 Formation of 53BP1 foci after treatment in hypertonic medium.
(A) Representative images of 53BP1 foci formation in RPE-1 cells after 2 Gy of IR at different times of incubation in isotonic or hypertonic medium. Scale bar: 5 μm (B) Formation of 53BP1 foci in isotonically (black plot) or hypertonically (red plot) treated cells following 2 Gy of IR. Data shown represent means and SE from three independent experiments.

When cells are incubated in hypertonic medium after IR, the number of 53BP1 foci is slightly reduced (see Figure 60 B). Considering the elevated number of pATM foci forming under these conditions, it is unexpected that 53BP1 foci number does not increase when chromatin is globally condensed. Further it is reported that 53BP1 favors HC regions (Demond 2016), which would also lead to the expectation of elevated 53BP1 foci numbers. However, the recruitment of 53BP1 to breaks is not only dependent on phosphorylation mediated by ATM but also on ubiquitylation

performed by RNF8 and RNF168. Further investigation of these proteins when chromatin is globally condensed may help to understand this unexpected response of 53BP1 foci formation. Perhaps global chromatin condensation hides histone PTMs 53BP1 is binding to and thereby disturbs its recruitment. However, effect of global chromatin condensation on 53BP1 foci formation is very small.

The experiments above help to understand DSB repair signaling in globally condensed chromatin. As DDR signaling is at least partially disturbed, we are interested in how these changes may influence DSB repair. A direct way to investigate the ability of cells to repair DSBs is PFGE. Therefore, experiments with exponentially growing RPE-1 cells are performed when chromatin is globally condensed by incubation in medium containing 300 mM NaCl.

Global chromatin condensation slows down the initial repair of DSBs after irradiation as the number of repaired DSBs after 30 min is increased two-fold in comparison to controls (see Figure 61). This effect of tonicity is not that pronounced on the slow component of DSB repair. Here the half-time constant is increased by ~30 %. However, almost one quarter of DSBs gets repaired by the slow component in cells with globally condensed chromatin.

A

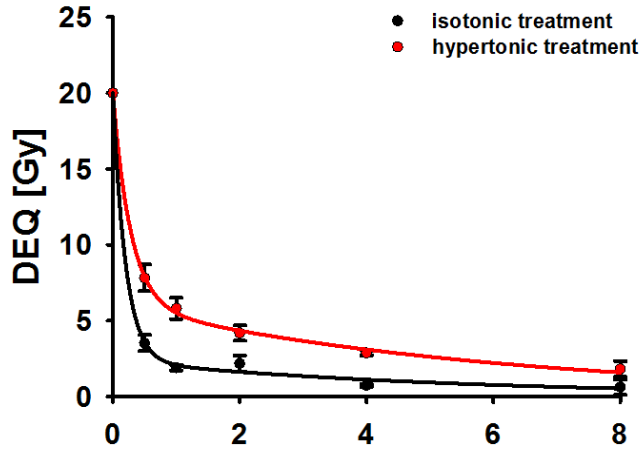

B

	plot equation
isotonic treatment	$f(x) = 20e^{-3.4721x} + 2.4935e^{-0.2165x}$
hypertonic treatment	$f(x) = 20e^{-1.8789x} + 6.2929e^{-0.1704x}$

	$t_{50,slow}$	fraction of DSBs repaired by slow component
isotonic treatment	192 min	11 %
hypertonic treatment	244 min	24 %

Figure 61 Chromatin condensation impairs DSB repair as measured by PFGE.
(A) Chromatin condensation by hypertonic treatment (red line) compromises DSB repair in comparison to untreated controls (black line). (B) Half-time constants ($t_{50,slow}$) and the fraction of DSBs repaired by slow component are calculated according to (Metzger and Iliakis 1991). Data shown here represent means and SD from eight determinations in two experiments.

PFGE experiments performed at high doses measuring DSB repair mainly reflects the activity of cNHEJ. In order to further investigate DSB repair by altEJ we perform PFGE when DNA-PK is inhibited.

A

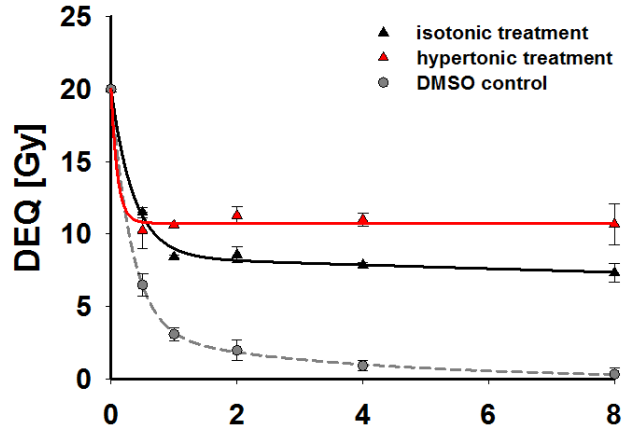

B

	plot equation
isotonic treatment	$f(x) = 20e^{-1.108x} + 8.7245e^{-0.0224x}$
hypertonic treatment	$f(x) = 20e^{-1.3375x} + 10.9791e^{-0.0024x}$

	$t_{50,slow}$	fraction of DSBs repaired by slow component
isotonic treatment	31 h	30 %
hypertonic treatment	289 h	35 %

Figure 62 altEJ in RPE-1 cells gets compromised upon global chromatin condensation. (A) Cells are treated with DNA-PKi (5 µM NU7441) starting 1 h before IR to specifically inhibit cNHEJ (except for DMSO control, grey, dashed line). After IR cells are treated either in isotonic (black line) or hypertonic (red line) medium. (B) Half-times ($t_{50,slow}$) and the fraction of DSBs repaired by slow component are calculated according to (Metzger and Iliakis 1991). Data shown here represent means and SD from eight determinations in two experiments.

The results show that the initial repair by altEJ is not influenced when chromatin is globally condensed in comparison to controls (DEQ at 30 min, see Figure 62). However, the slow component is clearly compromised with half-time constants increasing from 31 h (control) up to 289 h (hypertonically treated cells). This experiment shows that altEJ does not benefit from chromatin condensation. A possible explanation for this effect may be the partial dependency of altEJ on DNA end resection that needs relaxed chromatin to function properly. However, mechanisms of altEJ are not completely elucidated and not necessarily dependent on resection.

To elucidate functionality of DNA end resection, and also other mechanisms of DSB repair, in globally condensed chromatin, we measure intensity levels of bound RPA70 and IRIF of the recombinase Rad51 involved in HRR. As already mentioned

PFGE using high IR doses precludes analysis of HRR due to a saturation above 4 Gy (unpublished data).

DNA end resection is not only needed for parts of altEJ repair but is also an indispensable preparative step of HRR (see Figure 7). Thus, we start our investigations of this repair pathway with measurements of RPA70 intensity by FC. After induction of global chromatin condensation RPA70 intensity is abolished at low IR doses; a pronounced reduction is observed at high IR doses (see Figure 63 A).

This finding promotes the above mentioned impairment of altEJ. Further, in previous work from our lab it is shown that DSBs positioned in condensed chromatin favor the binding of 53BP1 (Demond 2016), which is inhibiting DNA end resection and may explain the reduced levels of RPA70.

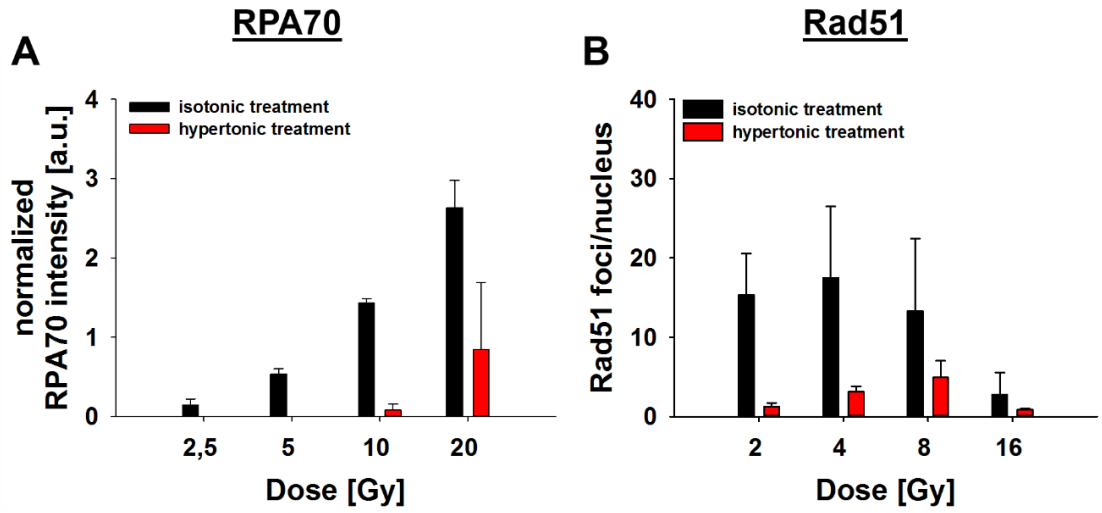

Figure 63 Effects of global chromatin condensation on DNA end resection and Rad51 foci formation in RPE-1 cells.
(A) Arithmetic means of AF488 intensity of RPA70 measured by FC and gated for G2-phase at 3 h post IR are normalized to the non-irradiated controls and plotted against IR dose. Cells are treated in isotonic (black bars) or hypertonic medium (red bars). The mean values ± SD and SE of two (hypertonic) and three (isotonic) experiments, respectively, are shown. (B) Formation of Rad51 foci in isotonically (black bars) or hypertonically (red bars) treated S/G2-phase cells at 3 h after different doses of IR. Data shown here represent means and SD of two independent experiments.

Our assumption that HRR, measured by the formation of Rad51 foci, will be disrupted as DNA end resection is inhibited by hypertonic treatment can be confirmed (see Figure 63 B). In addition, during HRR chromatin needs to get opened to facilitate proper homology search on the sister chromatid, which is most properly inhibited by the high condensation status of chromatin after hypertonic treatment.

In order to confirm the above results on DSB repair under conditions of global chromatin condensation, we utilize the U2OS reporter cell lines (see 7.2.6) to analyze events on different repair pathways.

In order to verify cell viability and proper GFP expression levels initial tests are performed in all cell lines under isotonic and hypertonic conditions (see Figure 64).

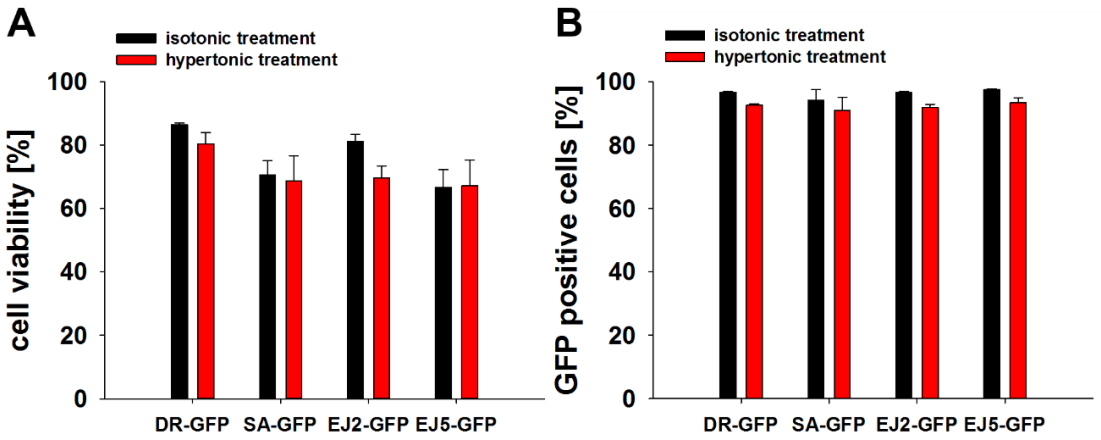

Figure 64 Cell viability and GFP expression in U2OS reporter cell lines.
(A) Cell viability of U2OS DR-GFP, SA-GFP, EJ2-GFP and EJ5-GFP cells after transfection with pEGFP-N1 plasmid by nucleofection and incubation in isotonic (black bars) or hypertonic (red bars) medium for 24 h, starting 2.5 h after transfection. (B) Percentage of cells expressing GFP protein after transfection with pEGFP-N1 plasmid by nucleofection and incubation in isotonic (black bars) or hypertonic (red bars) medium for 24 h starting 2.5 h after transfection. Data in this figure represent the means and SD/SE calculated from two (SA-GFP) and three (DR-GFP, EJ2-GFP, EJ5-GFP) independent experiments.

Both parameters show only minor decreases upon chromatin condensation, so that the following reporter assay results can be interpreted without caveats.

In order to investigate the efficiency of HRR, U2OS 282C cells are used. Cells are incubated in hypertonic medium at 2.5 h after I-*Sce*I transfection and GFP expression is analyzed by FC after 24 h (see Figure 65).

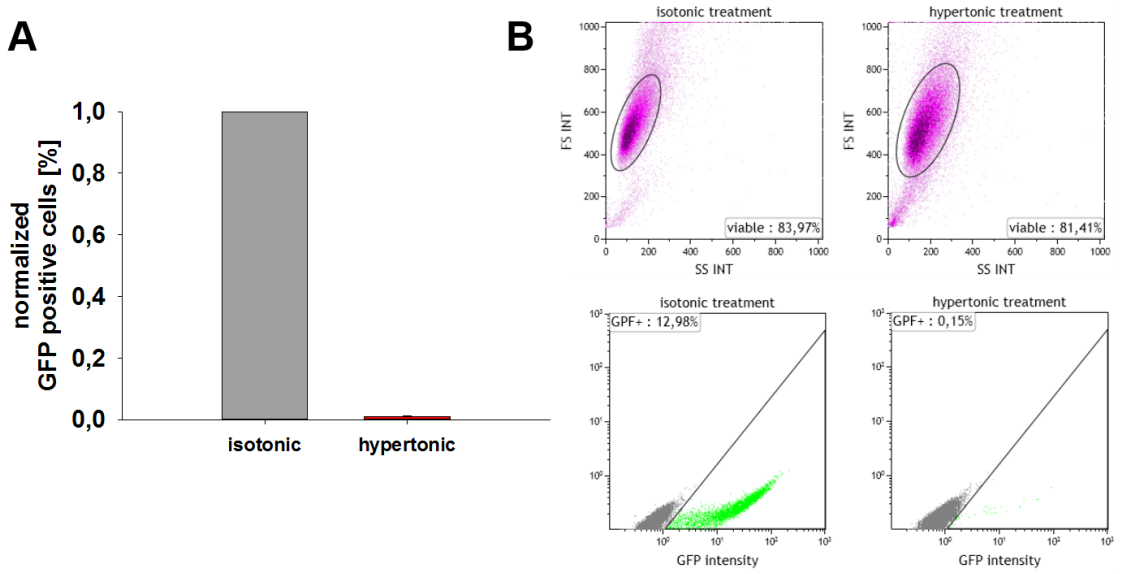

Figure 65 Effects of chromatin condensation on HRR.
(A) Normalized results of GFP intensity using the U2OS DR-GFP reporter cell line as measured by FC 24 h after transfection with an I-*Sce*I expressing plasmid and treatment in isotonic or hypertonic medium. Graph shows means and SD calculated from two independent experiments. (B) Histograms of cell viability (upper panel) and GFP intensity (lower panel) of U2OS DR-GFP cells after transfection with I-*Sce*I and treatment in isotonic or hypertonic medium.

Under control conditions 12 % of cells express GFP, as a result of successful repair of the induced DSB by HRR, but when chromatin is globally condensed almost no repair by HRR can be detected. These results are in line with the observation of decreased numbers of Rad51 foci and confirms that chromatin condensation inhibits HRR (see Figure 63 B).

End joining events are studied using the U2OS EJ5-GFP (NHEJ) and U2OS EJ2-GFP (microhomology dependent altEJ) reporter cell lines. Upon global chromatin condensation U2OS EJ5-GFP cells show only 50 % of GFP signal in comparison to controls (see Figure 66 A) which indicates modest effects on NHEJ.

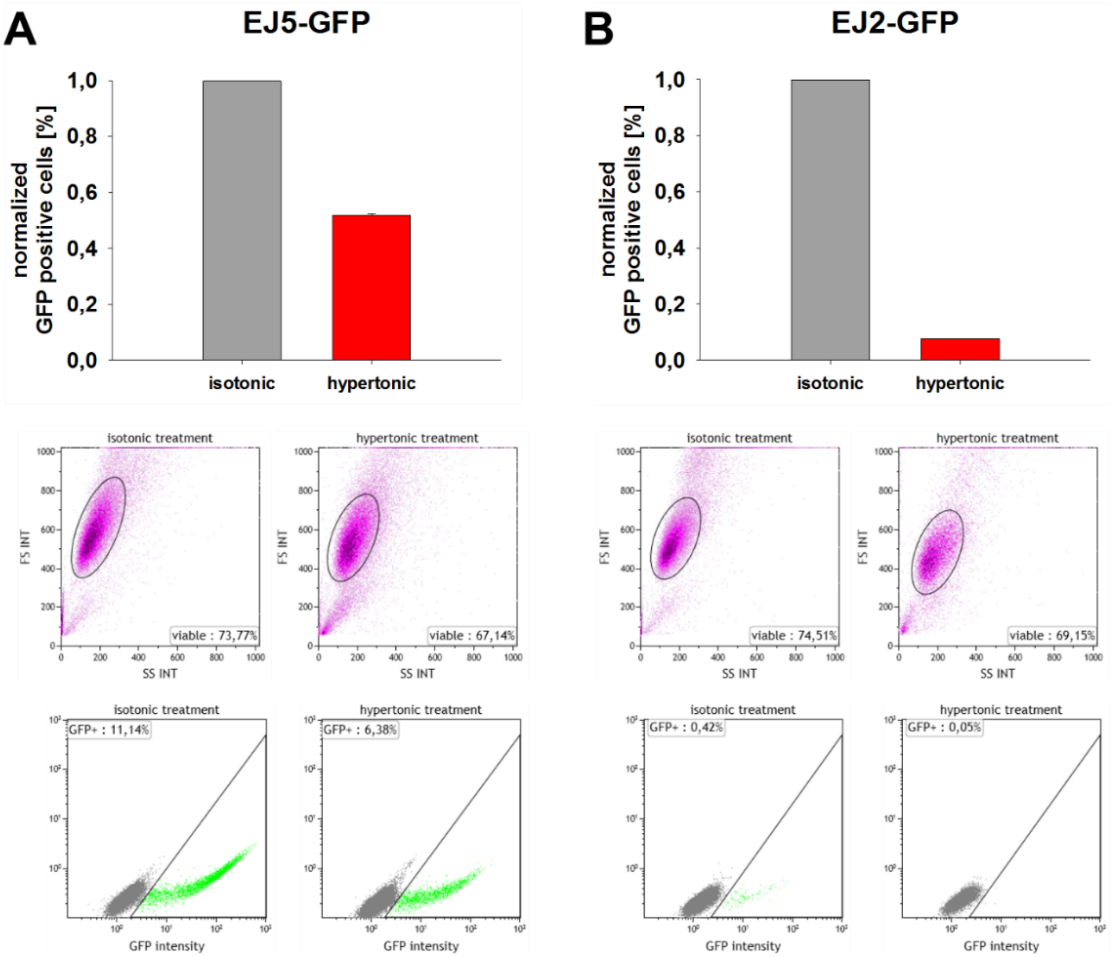

Figure 66 Effects of chromatin condensation on end joining events measured using the U2OS EJ5-GFP (A) and U2OS EJ2-GFP (B) reporter cell lines.
(A) Normalized GFP intensity of U2OS EJ5-GFP cells measured by FC 24 h after transfection with the I-*Sce*I expressing plasmid and treatment in isotonic or hypertonic medium. Graph shows means and SE of three independent experiments. Histograms of cell viability (upper panel) and GFP intensity (lower panel) of U2OS EJ5-GFP cells after transfection with I-*Sce*I and treatment in isotonic or hypertonic medium. (B) Same like in A, but for U2OS EJ2-GFP cells. Data for EJ2-GFP represent mean and SD from two independent experiments.

However, incubation in hypertonic medium drastically reduces the expression of GFP in the U2OS EJ2-GFP cell line and thereby the repair by microhomology dependent altEJ (see Figure 66 B). This repair pathway seems to be much more sensitive to chromatin condensation, which is in line with the findings of PFGE experiments (see Figure 62).

The fourth DSB repair pathway, SSA, is reported to function as back up to HRR. As HRR is completely abrogated when chromatin is globally condensed (see Figure 65) we wish to investigate a possible repair pathway switch to the more error prone repair pathway by using U2OS SA-GFP cells to specifically measure DSB repair events by SSA.

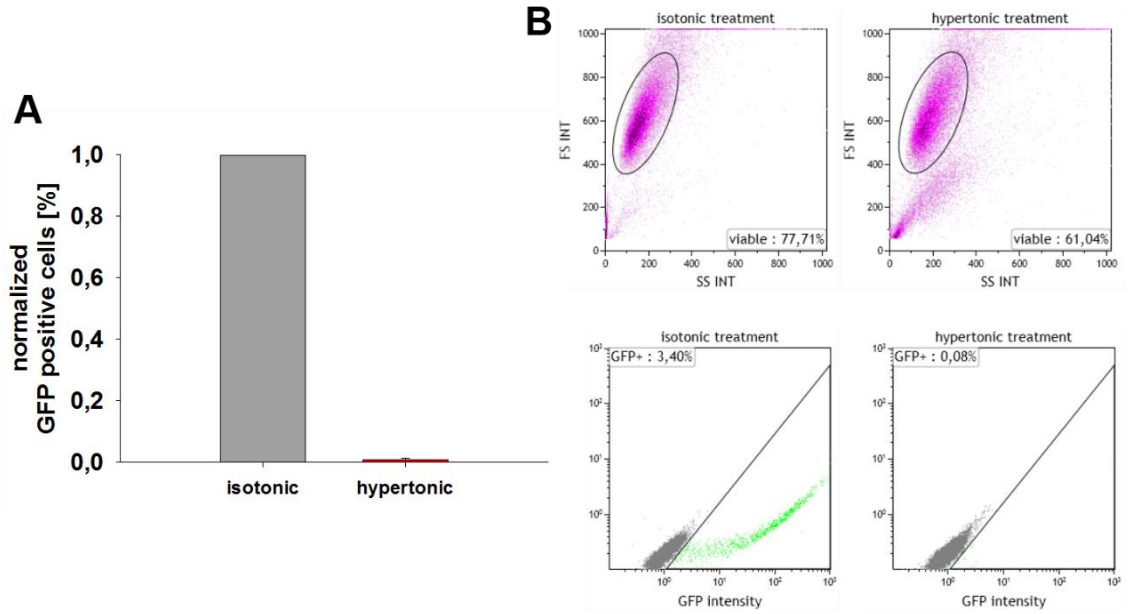

Figure 67 Effects of chromatin condensation on SSA repair measured by U2OS SA-GFP reporter assay.
(A) Normalized results of GFP intensity in U2OS SA-GFP cells measured by FC 24 h after transfection with an I-*Sce*I expressing plasmid and treatment in isotonic or hypertonic medium. Graph shows means ± SD of two independent experiments. (C) Histograms of cell viability (upper panel) and GFP intensity (lower panel) of U2OS SA-GFP cells after transfection with the I-*Sce*I expressing plasmid and treatment in isotonic or hypertonic medium.

However, when cells are incubated in hypertonic medium repair by SSA is completely abolished (see Figure 67 A).

It seems that global chromatin condensation induced by hypertonic treatment compromises DSB repair extensively. Only cNHEJ repair seems to tolerate this condition to a certain extent. As the other repair pathways benefit to different extents of chromatin relaxation in order to allow processes like DNA end resection and homology search, cNHEJ may be the only repair pathway left. In addition, chromatin compaction can be helpful to keep free DNA ends in close proximity and facilitate end joining.

7.3.5) Cells get radiosensitized when chromatin is globally condensed

The extensively compromising effect on DSB repair of chromatin condensation is further reflected in clonogenic survival experiments.

Plating efficiencies of cells treated continuously with hypertonic medium decrease to 0 % (see Figure 44 A), so that the treatment time for clonogenic survival assays

is adapted to only 6, 9, 16 and 24 h after IR. Subsequent to this treatment cells are plated in normal cell culture medium for colony formation.

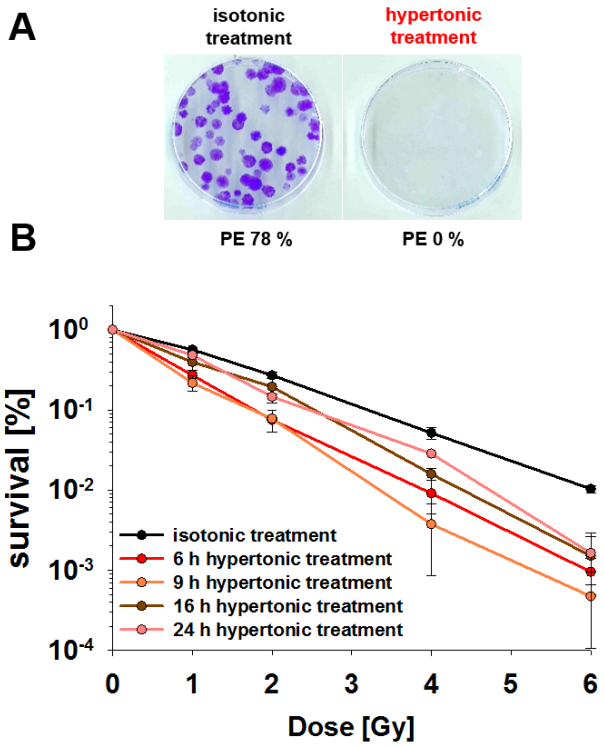

Figure 68 Clonogenic survival assay of RPE-1 cells.
(A) PE of cells treated continuously with isotonic or hypertonic medium for colony formation. Colonies are counted after 11 days of growth. (B) Cells are treated with isotonic (black line) or hypertonic (reddish lines) medium for 6, 9, 16 or 24 h immediately after IR before plating in isotonic medium for colony formation. Survival of control cells does not differ depending on treatment time (see supplementary Figure 73) so that here a representative curve is shown for isotonic treatment. Data shown here represent means ± SD from four determinations in two experiments.

Radiosensitization to killing of cells treated with hypertonic medium is dependent on the duration of treatment. Survival curves reveal the higher sensitization when cells are treated for 9 h instead of 6 h in chromatin condensing medium (see Figure 68 B). However, even longer treatment times do not further increase the radiosensitizing effect of global chromatin condensation but instead they reverse the radiosensitization observed. Indeed, 24 h of treatment with hypertonic medium increases the survival similar to that of untreated controls. Possibly, this is due to the reported adaptation of cells to chromatin condensing treatment (see 7.3.1). Nevertheless, long term treatment in hypertonic medium is toxic to the cells, as after 11 days of growth no cell survives.

Anyhow, the radiosensitizing effect of hypertonic treatment is not as marked as those on DDR signaling and DSB repair.

7.4) Radiosensitization after global chromatin condensation may result from recovery after transfer to normal growth conditions

Since, we only see a modest radiosensitizing effect in clonogenic survival assays after hypertonic treatment, we wonder how this fits to the large effects seen on DDR. A possible explanation could be that in survival experiments incubation in hypertonic medium is carried out only for a part of the experiment (up to plating for colony formation), whereas in DDR signaling and DSB repair experiments it is kept for the entire duration of the experiment. Therefore, we postulate that some of the effects generated under conditions of global chromatin condensation, are reversed when cells are returned to normal cell culture conditions.

To address this possibility experimentally, we measure γH2AX, pATM and 53BP1 foci development after returning cells to isotonic medium following a brief incubation in hypertonic medium.

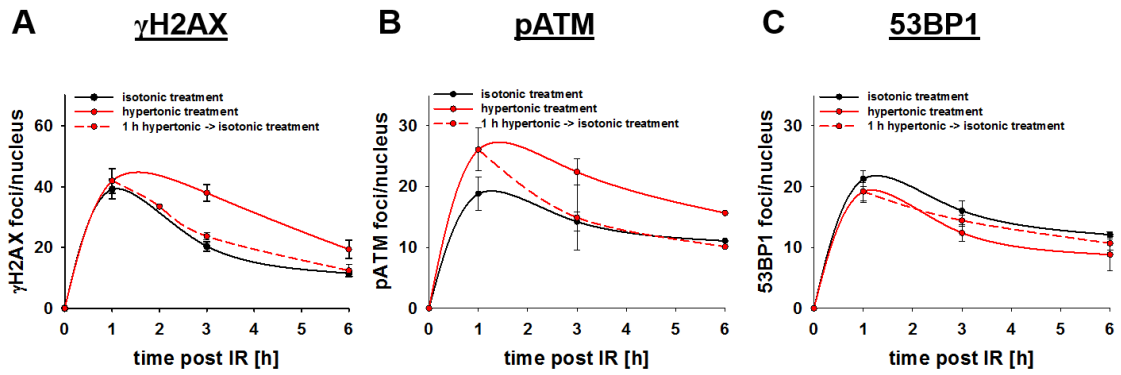

Figure 69 Reversibility of γH2AX (A), pATM (B) and 53BP1 (C) foci effects after short incubation in hypertonic medium.
Cells are either continuously incubated in isotonic (black plot) or hypertonic (red, solid plot) medium or treated in hypertonic medium for 1 h (red, dashed plot) before returning to isotonic conditions. Data for continuous treatment are the same as in Figure 58, Figure 59 and Figure 60. For reversible treatments means and SD of two (A and B) and one (C) independent experiments are shown.

When cells are incubated in hypertonic medium for only 1 h after IR and are then returned to normal growth conditions, γH2AX and pATM foci decrease to levels similar to those seen in the untreated controls (see Figure 69). Also 53BP1 foci numbers, which are slightly decreased in globally condensed chromatin,

approached normal levels. Thus, DDR signaling is indeed restored when global chromatin condensation is reversed by transfer to normal growth medium.

To gather supporting evidence for this effect, we investigate if also the condensation of chromatin is reversed by re-incubation in isotonic medium after 1 h treatment with hypertonic medium.

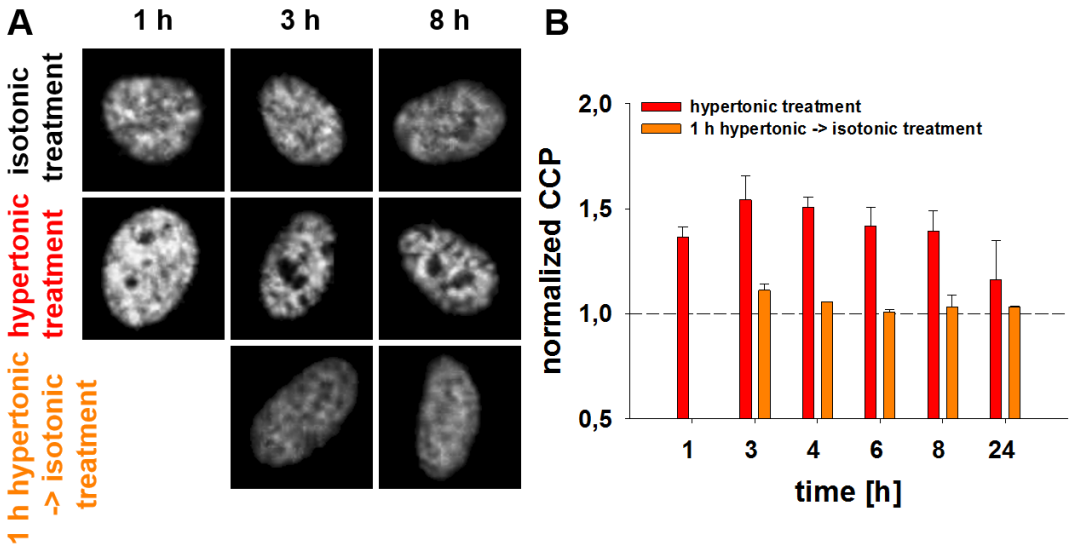

Figure 70 CCP of RPE-1 cells after either continuous incubation in hypertonic medium, or 1 h treatment in hypertonic medium followed by re-incubation under isotonic conditions.
(A) Representative images taken by CLSM of DAPI stained RPE-1 nuclei at different times of treatment with isotonic or hypertonic medium (continuously) or hypertonic medium for 1 h followed by return to isotonic conditions. (B) Data represent mean CCP values and SD of continuously hypertonically treated (red bars), and of only 1 h hypertonically treated (orange bars) cells calculated from two independent experiments.

CCP calculations show that chromatin relaxes when cells are returned to isotonic medium (see Figure 70). The recovery takes place within 2 h (see 3 h timepoint in Figure 70 B), matching to quick condensing effect on chromatin observed upon transfer of cells to hypertonic medium.

As shown in previous experiments the condensation induced by hypertonic treatment is also seen in metaphase chromosomes (see Figure 51) and its reversibility can also be documented in this endpoint. Cells treated in chromatin condensing medium for 1 h and then returned to isotonic medium form normally shaped chromosomes 3 h later (see Figure 71).

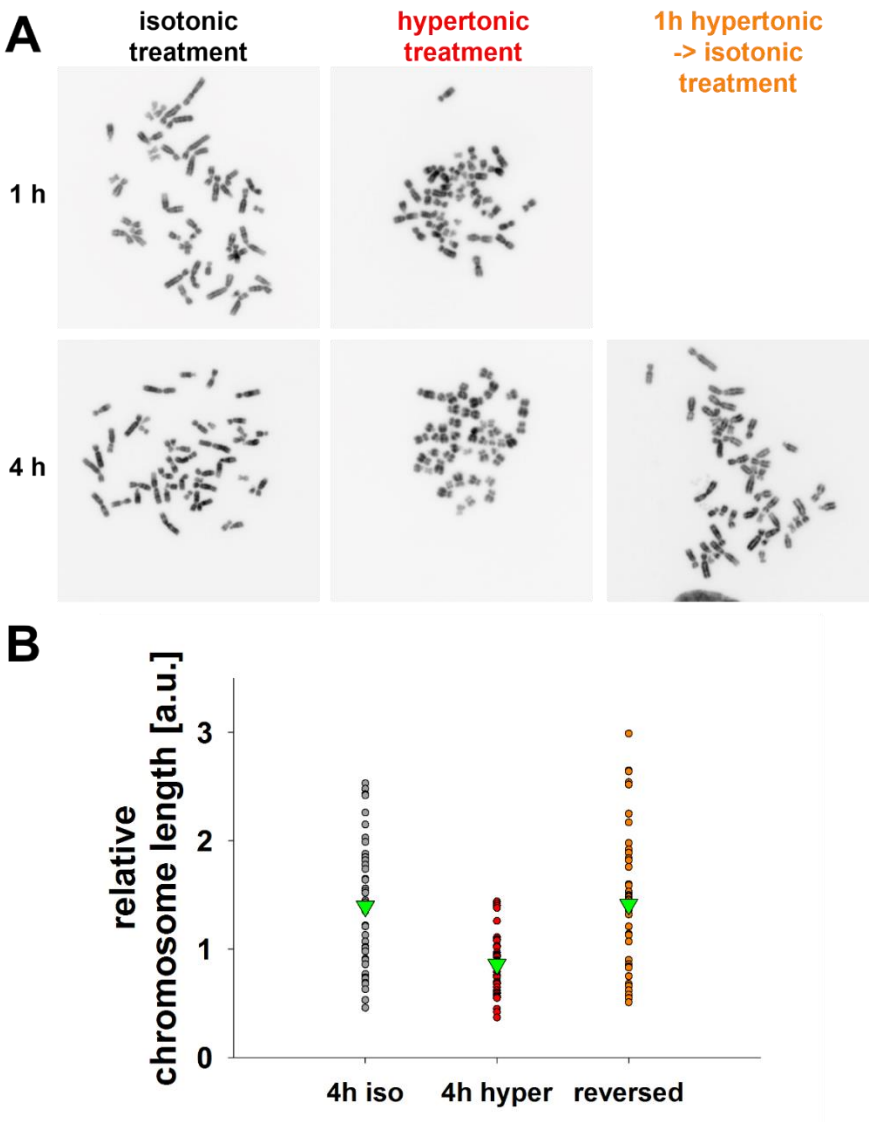

Figure 71 Representative images and length quantification of metaphases formed in hypertonically treated cells.
(A) Cells are incubated either in isotonic or hypertonic medium continuously or in hypertonic medium for 1 h and then in isotonic medium before a 30 min treatment with colcemid. DNA is stained with DAPI and is shown in inverted greyscale. The scale is the same in all images. (B) Length quantification of metaphase chromosome images shown in (A). Green triangles represent means.

Quantification of chromosome length confirms this finding, as mean length increases when cells are treated isotonically again after hypertonic incubation (see Figure 71 B). The spreading shows that there are even longer chromosomes which hints to an overreaction of processes counteracting strong condensation of chromosomes.

Another process strongly affected under conditions of global chromatin condensation is cell division. RPE-1 cells synchronized in G2-phase fail to progress

to mitosis when transferred in hypertonic medium (see Figure 55). Even after 24 h cells remained in G2-phase. We wish to investigate if this arrest in cell division is reversed upon transfer to isotonic medium.

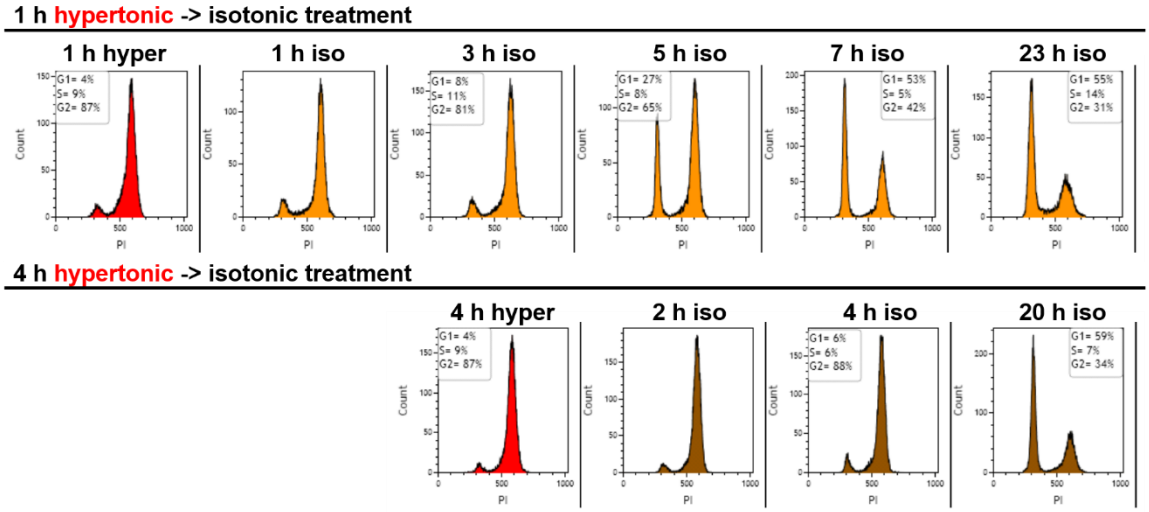

Figure 72 Cell cycle distribution of synchronous RPE-1 cells at different times after 1 or 4 h pretreatment in hypertonic medium.
Treatment of RPE-1 cells in hypertonic medium starts at 4 h after release of thymidine block when most cells have accumulated in G2-phase (see Figure 24 A). After 1 h (upper panel) and 4 h (low panel) of pretreatment in hypertonic medium, cells are incubated in normal cell culture medium and cell cycle distribution is measured by PI staining and FC as a function of time.

Indeed, when cells are treated in hypertonic medium for only 1 h before returning to normal cell culture medium, progression into mitosis and then to G1-phase is observed. 5 h after reinstating normal growth conditions, more than 20 % of cells divide (see Figure 72). After 7 h there a more than 50 % of cells in G1-phase and after 23 h the proportion of cells in S-phase is increased as well. When cells are treated longer in hypertonic medium (4 h), the inception of division takes longer. But even then after 20 h nearly 60 % of cells are in G1-phase (see Figure 72). Thus, also for this endpoint, the effect of global chromatin condensation achieved in medium containing 300 mM NaCl is reversible.

8) Discussion

The repair of DNA damage is of highest importance to the cell, as unrepaired damage, especially unrepaired DSBs, can lead to tumorigenesis, senescence and apoptosis. In eukaryotic cells the DNA is organized in chromatin whose structure is highly regulated. Different chromatin structures like EC or HC determine the usage of genes contained in the corresponding DNA segment, e.g. the silencing of gene expression within facultative HC.

Chromatin, particularly PTMs on histone tails, serves as binding platform for several proteins participating in DDR and DSB repair. There are several reports describing various effects of chromatin condensation status on DSB processing. Some studies report local chromatin relaxation upon damage induction to facilitate access for repair factors, while, on the other hand, chromatin condensation is considered to have a protective function.

To further elucidate the role of chromatin condensation status in DDR and DSB repair we utilized here hypotonic and hypertonic treatment to investigate responses to IR in globally relaxed and condensed chromatin, respectively.

8.1) Global chromatin relaxation impairs DDR signaling and DSB repair, but reveals a pathway switch to SSA

Hypotonic treatment is widely used to globally relax chromatin structure. In many studies it is used in comparison to other, more specific chromatin relaxing agents like Trichostatin A (TSA) or chloroquine. Though its function in relaxing chromatin is accepted, we wished to quantify its influence on chromatin compaction. Therefore we utilize measurements of CCP and demonstrate that indeed the relaxing effect of hypotonic medium can be quantified (see Figure 20).

Upon incubation in medium with low tonicity cells swell by taking up water in order to counterbalance changes in ion concentrations. This is a very fast response, as we showed by analyzing cell volume (see Figure 19); but we could also see a quick counter-regulation due to the activation of RVD processes. As we use relatively mild hypotonic conditions (75 mM NaCl), cells are able to adapt and survive.

When the ion concentration decreases too much, or processes that regulate RVD are compromised, the cell volume cannot get normalized and cells burst. This

approach is used during surgery for hepatocellular carcinoma or pancreatic cancers to avoid peritoneal metastasis. During tumor excision cancer cells float into the peritoneal cavity and can potentially produce recurrences. Therefore, peritoneal lavage with distilled water is applied to kill these tumor cells. As distilled water doesn't contain ions the osmotic difference is too large, and especially in combination with RVD inhibitors, tumor cells die (Nako et al. 2012; Kudou et al. 2016). Another advantageous application of low tonicity is also reported in the therapy of cancers of the abdominal cavity. Thus, the uptake of chemotherapeutic agents into tumor cells is increased when drugs are infused in solutions of lower osmolality (Stephen et al. 1990).

RPE-1 cells used in our studies are able to regulate their volume quickly in response to hypotonic treatment. Anyway, the aim of our investigations was to achieve chromatin relaxation and not cell death. In contrast to the fast regulation of cell volume, the relaxing effect of low tonicity on chromatin is not normalized quickly. Chromatin remains relaxed after several hours of treatment (see Figure 20), although recovery is evident after 24 h. This slower recovery of chromatin relaxation may be due to the altered ionic strength that occurs after incubation in hypotonic medium and that may need longer times to normalize. Changes in ionic strength perturb macromolecules within the cell, and affect chromatin organization. Especially investigation of chromosomes at metaphase shows the relaxing effect of hypotonic medium. In addition to their elongated shape the sister chromatids appear more apart from each other.

When DNA is replicated during S-phase, the generated pairs of sister chromatids become physically connected and remain connected through G2-phase; they only begin to separate during the transition from metaphase to anaphase during mitosis. This connection is established by cohesins which form ring-like structures around the replicated DNA and held the sister chromatids in close proximity (Brooker and Berkowitz 2014). In hypotonically treated cells this connecting function of cohesins seems to be at least partially disrupted. This might have severe consequences for genomic stability as it can lead to aneuploidy. Further it has been reported that cohesins are involved in the ATM DNA damage signal transduction pathway and are important for survival after irradiation (Brooker and Berkowitz 2014; Kim, Xu, and Kastan 2002).

Another possible explanation for the altered appearance of chromosomes in response to hypotonic treatment might be a functional disruption of condensins. Depletion of either condensin I or condensin II leads to a swollen or curly appearance of chromosomes, respectively, which is reminiscent to our observations (Hirano 2004).

However, to further investigate the influence of hypotonic treatment on chromatin condensation status we quantify also the levels of histone H1, as well as typical HC and EC markers. WB analysis reveals indeed a decrease in H1 levels, which further confirms a less condensed chromatin structure. In contrast, the observed increase in H3K27me3 (HC marker) and the decrease in H3K9ac (EC marker) are not expected in more open chromatin. As we outline above, the alteration in chromatin compaction is most probably occurring due to changes in ionic strength; so we conclude that the relaxed status of chromatin is not comparable with the open structure of well-defined EC. The definition of EC is not only based on the lower condensation status of chromatin, but is also connected to additional modification and functional changes allowing for example altered gene expression. Indeed, the PTMs at histone tails allow or restrict the binding of several proteins implicated in many cellular processes. Thus, we conclude that treatment with hypotonic medium indeed relaxes chromatin structure but not in ways that will make this form of chromatin relaxation equivalent to EC. Nevertheless, the changes of histone markers we observed might influence cellular processes by altering protein recruitment to chromatin.

In preparation for experiments investigating the effect of global chromatin relaxation on DDR and DSB repair, we find an initial stop in cell growth (persisting for 6 h after starting treatment), which recovers as cells adapt (see Figure 25). Further evidence along these lines comes from experiments with cells synchronized in G2-phase; but also investigation of MI shows that initially cells are arrested in G2 before progressing to M-phase - but adaptation in terms of MI recovery is seen as well (see Figure 26 and Figure 27).

With chromatin exhibiting its highest condensation status during mitosis, it is likely that this process is disrupted when chromatin is globally relaxed in hypotonic medium. Therefore, it is also difficult to get metaphase chromosomes at the 1 h time point and indeed we find only very few metaphases. However, chromatin

condensation in preparation for mitosis seems to be possible as soon as cells adapt to hypotonic treatment; but still chromosomes appear less condensed than in untreated controls (see Figure 22).

From the literature we know that ATM responds to changes in chromatin structure even in the absence of DNA damage (Bakkenist and Kastan 2003), and this activation may activate in turn a checkpoint in hypotonically treated cells. However, investigation of MI development in conditions with inhibited ATM does not show any influence of ATM in this recovery. In contrast, inhibition of ATR diminishes the transient decrease in MI upon global chromatin relaxation. ATR is usually activated by stalled and collapsed replication forks, but also by ssDNA and ssDNA/dsDNA junctions that occur upon DNA damage (Shiotani et al. 2013). Furthermore, one report describes a critical role of resection for ATR/Chk1 activation (You and Bailis 2010), but other studies show that resection (dependent on CtIP) is not needed for the initial activation of ATR but for maintaining intra-S- and G2-checkpoints (Kousholt et al. 2012). In order to investigate a possible checkpoint activation mediated by the ATR-Chk1 signaling branch in response to chromatin relaxation induced by hypotonic treatment, it would help to analyze Chk1 and CDC25A activation in future experiments.

Chromatin and its compaction status determines a multitude of processes the DNA is involved in. In our study we focus on the function of chromatin in DDR signaling and DSB repair. In the literature, there are several models describing the role of open, relaxed EC and of the more condensed HC in the cellular responses to DNA damage. Chromatin in general is considered to protect DNA against break induction. This protective function of chromatin is thought to be generated by physical shielding of DNA to exogenous insults (Elia and Bradley 1992; Warters and Lyons 1992; Takata et al. 2013).

Indeed, there are reports about the influence of HC and EC domains on genome instability in human somatic cells. Especially in cancer cells in which chromatin structure determines the mutation rate, DNA base substitutions are elevated predominantly in HC but less frequent in relaxed EC (Nair, Shoaib, and Sorensen 2017; Schuster-Böckler and Lehner 2012). Further, gene expression seems to be implicated in mutational outcome, as increased nucleosome occupancy coincides

with increased mutation rates (Sabarinathan et al. 2016) but higher transcription rates are connected to lower mutation events (Pleasance et al. 2010).

The response of chromatin to DNA damage induction is described in the "access-repair-restore" (ARR) model (Adam, Dabin, and Polo 2015). Herein, the initial response to DNA damage is a rapid relaxation of chromatin to allow detection of the damage and access for repair proteins (Khurana et al. 2014). In line with this model there are reports about the refractory characteristics of HC to initial DDR signaling in terms of H2AX phosphorylation (Cowell et al. 2007). Promoting this finding, the artificial relaxation of chromatin using HDAC inhibitors or by reducing levels of histone H1, enhances the signaling and the extent of γH2AX spreading (Iacovoni et al. 2010). Upon chromatin relaxation by hypotonic medium we find slightly reduced levels of H1, which might lead to an enhanced DDR signaling.

However, in our experiment the number of γH2AX foci decreases dramatically upon hypotonic treatment (see Figure 29), challenging the general model that open chromatin alone mediates/facilitates recruitment of DDR proteins to the damage sites. As we know that different chromatin structures respond differently to DNA damage induction, we start incubation in hypotonic medium always after DSB induction. Thus, we can assume that the same numbers of DSBs are induced as in control cells. Investigation of ATM, the main kinase for H2AX phosphorylation, reveals a decrease in pATM foci number in response to DSB induction as well (see Figure 30). This decrease is a possible explanation for low levels of γH2AX foci, but let's first ask why the ATM response is so weak? It is known, that especially ATM is activated by changes in chromatin even in the absence of DNA damage. Furthermore, the same study reports that under these conditions ATM is activated, as measured by the phosphorylation of ATM-S1981, but does not form discrete foci and does not result in H2AX phosphorylation (Bakkenist and Kastan 2003). As this effects occur in the absence of DNA damage, the observations are not directly applicable to our experiments as we induce DSBs by exposure to IR before analyzing the response. The unirradiated controls could help to reveal this activation of ATM by measuring differences in the overall signal of pATM. It would be useful to study further upstream signaling events like for example the formation of Mre11 foci in order to investigate the recruitment of MRN complex to sites of damage that are required for full ATM activation in the context of DSB induction. Possibly global

chromatin relaxation induced by hypotonic treatment interrupts the recruitment of the MRN complex at DSBs and thus the entire DDR signaling cascade is interrupted as well.

Further investigation of DDR signaling and of 53BP1 foci formation confirms the compromising effect of hypotonic treatment on DDR signaling (see Figure 31). As 53BP1 also responds to ATM activation, this is not surprising. However, Huyen et al. report that 53BP1 binds to methylated H3K79 which is exposed upon chromatin relaxation in response to DNA damage induction. They even show that chromatin changes induced by hypotonic treatment are sufficient to recruit 53BP1 in the absence of DNA damage (Huyen et al. 2004). However, a more recent study reports that 53BP1 accumulation at DSBs is dependent on H2AK15ub and H4K20me2. The disruption of one of the two sites completely abolishes 53BP1 foci formation. Possibly chromatin relaxation induced by hypotonic treatment interferes with either the ubiquitylation of H2AK15 mediated by RNF168 or with the methylation of H4K20 established by the methyl-transferases SETD8, SUV4-20H1 and SUV4-20H2 (Simonetta et al. 2018). Further investigation of the participating proteins would help to elucidate the disruption of 53BP1 foci formation we observed.

ATM plays a major role in checkpoint activation (Iliakis et al. 2003) and 53BP1 binding to DSBs is implicated in DSB repair pathway choice (Daley and Sung 2014), so we further investigate influence of chromatin relaxation on these outcomes.

The G2-checkpoint prevents the progression of G2-phase cells harboring DNA damages into mitosis, as this would have dramatic consequences for genomic stability. The activation of checkpoints is one consequence of DDR signaling in response to DNA damage. As we see dramatic reduction in DDR signaling upon global relaxation of chromatin by hypotonic treatment, we expect also a weakened checkpoint response. To our surprise, we see the same initial drop in MI in hypotonically treated cells as in control cells in response to IR (see Figure 32). Furthermore, irradiated cells do not recover within the time analyzed as controls do suggesting a potentiation of the checkpoint response.

The transient inhibition of cells progressing into M-phase due to hypotonic treatment does not allow us to discriminate between an IR-induced response and one due to the hypotonic treatment alone. However, when cells are pretreated in hypotonic medium to allow for adaptation that avoids this problematic, we still see a

strengthened checkpoint response upon irradiation (see Figure 32). Using ATM and ATR inhibitors we conclude that this checkpoint response is dependent on both kinases as inhibition of either ATM or ATR shows similar results, namely a reduction of the checkpoint (see Figure 34). The response is even completely abrogated when both kinases are inhibited at the same time. This leads us to postulate that one kinase can partly back up the function of the other in the checkpoint response.

However, the activation of ATM and ATR in response to DNA damage is not equivalent; as mentioned before ATR is activated by ssDNA and ssDNA/dsDNA junctions that occur e.g. upon DNA end resection at DSBs. Investigation of DNA end resection by measuring RPA70 recruitment to ssDNA, we observe indeed that end resection is active when chromatin is globally relaxed by hypotonic treatment (see Figure 38 A). This finding explains the activation of an ATR-dependent G2-checkpoint in this condition.

Now that we see a functional G2-checkpoint response in cells adapted to hypotonic conditions in terms of proliferation, we are interested if also other branches of DDR signaling are restored. But cells pretreated with hypotonic medium still show very low levels of γH2AX and 53BP1 foci formation (see Figure 35). Thus, not all parts of DDR signaling are restored upon adaption of cells to hypotonic conditions.

DSB repair is another outcome of DDR signaling, so that we investigated this response by different experimental approaches.

One major DSB repair pathway is HRR, which needs DNA end resection in preparation for homology search. In our experiments, we show that DNA end resection is not altered by hypotonic treatment; and in addition 53BP1 accumulation is decreased under these conditions, which further directs the DSB repair pathway choice to HRR. Surprisingly, investigation of Rad51 foci formation representing ongoing HRR shows dramatically reduced numbers upon treatment with hypotonic medium (see Figure 38 B). Further investigation of HRR repair using a cell line with a stably integrated reporter construct for evaluation specifically of repair events performed by HRR, confirms the abrogation of this repair pathway in globally relaxed chromatin (see Figure 40). Although chromatin initially relaxes in response to IR induced DNA damages, the subsequent recondensation of chromatin dependent on macroH2A1 is reported to facilitate repair mediated by HR (Khurana et al. 2014). In addition, chromatin condensation is reported to facilitate homology search by

reducing the spatial distance between sister chromatids (Sonoda et al. 2006), which is also a known function of cohesins (Wu and Yu 2012). As we assume a perturbation in cohesion function by hypotonic treatment (see above) this might be an explanation for the observed abrogation of HRR. In addition, also condensin II, whose absence leads to the formation of curly shaped chromosomes, as we observe in hypotonically treated cells, is involved in facilitating HRR (Wood et al. 2008). Taken together, several components that usually facilitate faithful HRR may be disturbed by global chromatin relaxation and thereby compromising HRR.

Besides HRR, cNHEJ is a main DSB repair pathway, which even repairs the majority of DSBs (Lobrich and Jeggo 2017). This mechanism, when compared to HRR, is quite simple, as it rejoins free DNA ends without needing a template. However, during cNHEJ, binding of Ku prevents DNA end resection and only minor processing of DNA ends occurs. In pathway choice, 53BP1 directs the repair to cNHEJ by inhibiting DNA end resection. The observed compromised recruitment of 53BP1 and the unchanged DNA end resection, lead us to speculate that cNHEJ is not favored under conditions of globally relaxed chromatin. Surprisingly, however, PFGE experiments show only small effects on cNHEJ under hypotonic conditions (see Figure 36). On the other hand, reporter cell lines reveal a reduction by 50 % in repair efficiency by cNHEJ (see Figure 41 A). For PFGE experiments cells are irradiated with 20 Gy, which produce many randomly distributed DSBs with higher complexity in terms of additional sugar and base lesions accompanying the DSBs. These lesions complicate the processing of DSBs (Schipler and Iliakis 2013). In reporter cell lines, the DSBs are induced enzymatically, which will result in clean DNA ends that are much easier to repair. Further cNHEJ may rather benefit from chromatin condensation than from relaxation as in condensed environment the free DNA ends may be held in closer proximity. Therefore, we conclude that cNHEJ is also negatively affected by global chromatin relaxation.

It is known that back up pathways can take over the repair of DSBs when the main repair pathways HRR and cNHEJ fail to work properly. The mechanisms of altEJ are still not completely understood, but at least some branches of altEJ benefit from resected DNA ends (Wang and Xu 2017). Indeed, PFGE experiments investigating repair by altEJ show no difference in repair efficiency when chromatin is globally relaxed (see Figure 37). However, the reporter assay cell line EJ2-GFP measuring

repair events mediated by MMEJ reveals a compromising effect of chromatin relaxation (see Figure 41 B). This is surprising as DNA end resection is still functional under hypotonic conditions and HRR is compromised, which would shift DSB processing to backup repair by altEJ. However, altEJ is not the only pathway that can backup HRR. Investigation of SSA indeed shows a three-fold increase in cells with globally relaxed chromatin (see Figure 43). The mechanism of SSA needs extensive DNA end resection (Muñoz et al. 2012) to uncover homologous DNA repeats that are then annealed to each other. Possibly, chromatin relaxation mediated by hypotonic treatment makes DNA repeats that are commonly located in compacted chromatin more accessible for DNA repair factors. The reported reduction in Rad51 foci formation is further promoting the pathway switch to SSA as disruption of Rad51 or its mediator proteins (e.g. BRCA2 and Rad54) increases this repair activity (Tutt et al. 2001). Further investigation of Rad52 recruitment to DSBs in hypotonically treated cells would help to also elucidate a possible pathway switch in response to IR. A very recent study shows that the interplay of 53BP1 and the ring finger protein RNF169 is participating in SSA regulation and pathway choice (An et al. 2018). Our previous results show that 53BP1 recruitment to DSBs is abrogated in relaxed chromatin, which might be an explanation for elevated SSA repair as An et al. reported increased SSA efficiency in 53BP1 knockout cells. However, they are able to restore levels of SSA by coinactivation of RNF169. In addition, overexpression of RNF169 in SA-GFP cell line stimulates SSA but not repair events in other reporter cell lines. Possibly RNF169 gets hyperactivated upon hypotonic treatment and thereby increases DSB repair mediated by SSA. Thus, investigation of RNF169 levels in hypotonically treated cells would help us to elucidate the elevated SSA efficiency observed. SSA is a highly mutagenic repair pathway and can produce large chromosomal rearrangements (Elliott, Richardson, and Jasin 2005; Manthey and Bailis 2010) which endanger genomic stability. It would be therefore interesting to investigate the formation of translocation in cells with this increased SSA activity.

However, in clonogenic survival experiments only modest effects on radiosensitization to killing are observed. Notably, the treatment time in hypotonic medium has to be reduced as continuous treatment is toxic (see Figure 44). The small effect on cell survival contrasts the dramatic reductions in DDR signaling and

DSB repair observed (obtained by less error-prone pathways). However, experiments investigating DDR signaling with cells that are only transiently incubated in hypotonic medium show that normal formation of γH2AX, pATM and 53BP1 occurs as soon as cells are returned to isotonic medium (see Figure 45). Also the relaxed chromatin structure is reversed when the treatment stops and cells are incubated in normal cell culture medium (see Figure 46), which is in line with reports showing that upon reversed treatment of prior hypotonically treated chondrocytes, the chromatin condensation level increases again (Irianto et al. 2013). These results clearly show that the effects of hypotonic treatment are completely reversible and that DDR signaling can be restored, which explains the modest effect on radiosensitization to killing.

8.2) Global chromatin condensation achieved by incubation in hypertonic medium arrests cells in G1-, G2- and M-phase and impairs resection-dependent DSB repair

Hypertonic treatment is used in several studies to globally condense chromatin structure (Albiez et al. 2006; Reitsema et al. 2005) and indeed we quantify a condensing effect of incubation in medium containing 300 mM NaCl by elevated CCP values on RPE-1 cells as well (see Figure 50). Images and length measurements of metaphase chromosomes of cells treated in high tonicity medium further confirms chromatin condensation (see Figure 51 and Figure 52). However, this response to hypertonic treatment is only transient, as we observe adaptation and normalization of these endpoints at 24 h.

Since we know that condensed HC is characterized by specific histone tail PTMs assisting in the repressive nature of chromatin, we investigated how histone markers change upon treatment in hypertonic medium. Indeed, we find elevated levels of H3K27me3 after hypertonic treatment (see Figure 53), which is usually connected to transcriptional repression (Ferrari et al. 2014) and is therefore abundant in facultative heterochromatin (Saksouk, Simboeck, and Dejardin 2015). In line with this finding is a decrease in H3K9ac levels (EC marker). However, also the levels of histone H1 are lower than in controls, which helps in chromatin condensation under normal conditions. Obviously, a condensation of chromatin mediated by hypertonic treatment is independent of H1 and might mainly derive from changes in ionic

strength. Further evaluation of other histone markers and proteins associated with HC (e.g. HP1, Kap1) will help to understand the mechanism of chromatin condensation by hypertonic medium.

Investigation of proliferation of cells treated in hypertonic medium reveals an inhibition of progression through the cell cycle. Asynchronous cell populations show that cells are blocked in G1-phase while experiments with cells synchronized in G2-phase demonstrate a G2 arrest (see Figure 54 and Figure 55). Cells even seem to be held in mitosis (see Figure 56), which promotes the appearance of highly condensed chromosomes in metaphase that are reminiscent to those treated with colcemid for long times (Miura et al. 2012). In the literature we find reports about a G2-block upon hypertonic treatment, which is independent of Chk1 activation (Burg, Ferraris, and Dmitrieva 2007). The signaling cascade resulting in the activation of G2-checkpoint mediated by Chk1, is initiated by ATR activation. However, ATR is usually activated by ssDNA and ssDNA/dsDNA junctions that result from stalled replication forks or upon DNA end resection at DSBs. Likely, hypertonic treatment-induced chromatin condensation does not lead to the formation of ssDNA, which would explain the Chk1-independency.

In addition to ATR, ATM is also able to mediate a G2-arrest via Chk2 phosphorylation and it is shown that ATM responds to changes in chromatin conformation. Thus, even in the absence of DNA damage, ATM still phosphorylates substrates like p53, which may explain the block in G1-phase seen in our experiments. Furthermore, p38 is reported to function in checkpoint activation especially in response to osmotic shocks. So it induces a G1/S-arrest by activating p53 and thereby inducing expression of the CDK inhibitor p21. With regard to G2-checkpoint activation upon hypertonic treatment, p38 is also playing a role through down-regulation of CDC25C expression (Kishi et al. 2001; Wang et al. 2000; Kurosu et al. 2005).

Interestingly, many years ago hypertonic treatment has been used as a method to enrich cells in M-phase, as investigators found cells to be blocked in mitosis, which is in line with our findings. However after longer treatment in hypertonic conditions cells die (Wheatley 1974).

Now that we see strong activation of cell cycle checkpoints in response to hypertonic treatment, we are curious how this treatment and its resulting condensation in

chromatin may influence DDR signaling and DSB repair. As mentioned before ATM is activated by changes in chromatin structure and indeed we see in addition to IR induced ATM activation increased numbers of pATM foci in hypertonically treated cells (see Figure 59). In line with this finding, also numbers of γH2AX foci are slightly increased and resolve slower than in untreated controls (see Figure 58). In the literature it is shown that DSB repair is slower in compacted HC than in open EC, and that γH2AX foci persist (Goodarzi et al. 2008). In addition, the foci size of γH2AX is increased at later time points further confirming perturbed DSB repair. In terms of 53BP1 accumulation at DSBs, we see almost no change upon chromatin condensation (see Figure 60). A former study in our laboratory also shows that 53BP1 prefers binding to HC over EC (Demond 2016), which might explain the unchanged formation of 53BP1 foci.

This strong response of initial DDR signaling to hypertonic treatment anticipates the strong checkpoint response to hypertonic stress. However, upon IR a checkpoint response in terms of decrease in MI cannot be observed (see Figure 57). As mentioned before, cells also arrest in M-phase, which explains why we don't find a decrease in MI upon IR. Obviously, checkpoints are activated already by hypertonic stress and mask the response of cells to IR.

Investigation of the DSB marker γH2AX shows a disturbed resolution of foci, which hints to impaired DSB repair. Therefore we examined the efficiency of DSB repair on several levels.

PFGE experiments reveal that chromatin condensation induced by hypertonic treatment has a moderate compromising effect on DSB repair by cNHEJ, as well as by altEJ (see Figure 61 and Figure 62). This effect is further confirmed by the reporter cell lines EJ5-GFP and EJ2-GFP that show 50 % reduction of cNHEJ and almost complete abrogation of MMEJ (see Figure 66). The mechanisms of altEJ are not necessarily dependent on end resection, which may explain the less pronounced effect seen in PFGE experiments, but the sub-pathway MMEJ needs resected DNA ends to anneal microhomologous DNA sequences to facilitate DSB repair. Indeed, DNA end resection in cells with globally condensed chromatin is severely compromised as measured by bound RPA70 (see Figure 63 A). Therefore we assumed an abrogating effect of hypertonic treatment on DSB repair mediated by HRR, and experiments measuring formation of Rad51 foci and HRR repair events

by using a reporter cell line confirm this (see Figure 63 B and Figure 65). In addition, SSA that is dependent on DNA end resection as well is completely abrogated in cells with condensed chromatin (see Figure 67). Therefore we conclude that DSB repair dependent on end resection is abrogated in cells treated with hypertonic medium. Most likely this massive compaction of chromatin restricts access of proteins involved in DNA end resection which is further promoting the loss of ATR activation we observe.

As DSB repair is massively disturbed when cells are treated in hypertonic medium it is not surprising that clonogenic survival assays reveal also radiosensitizing effects of globally condensed chromatin (see Figure 68). This result is in line with reported impaired survival upon chromatin compaction and the sensitizing effect of hypertonic treatment to chromosomal damage and killing by IR (Burgess et al. 2014; Dettor et al. 1972). As mentioned before cells die when treated in hypertonic medium for longer times, which we also see when cells are continuously incubated in medium containing 300 mM NaCl for colony formation. Therefore the protocol for survival experiments is adapted and treatment times are shortened. However, radiosensitivity is not as increased as one would expect from the dramatic perturbation observed for DSB repair. This might be due to the transient treatment applied in this experiment. Indeed, DDR signaling is completely restored when chromatin is relaxed after hypertonic shock (see Figure 69). Additionally, cell cycle arrests are abolished and cells start to proliferate after reversing hypertonic conditions and return cells to normal cell culture medium (see Figure 72). Indeed the reversibility of chromatin condensation by hypertonic medium has been reported by (Irianto et al. 2013).

We conclude that chromatin condensation induced by hypertonic treatment has severe effects on DSB repair and thereby on radiosensitization to killing. However, DDR signaling in terms of activating cell cycle checkpoints are functional and serve to protect cells from genomic instability. Notably, cells can only transiently survive hypertonic conditions and die after longer treatment times. Recently it is reported that hyperosmotic stress, especially applied in tumor microenvironment, can enhance cytotoxicity of tumor necrosis factor (TNF)-related apoptosis-inducing ligand (TRAIL) and other death receptor (DR) ligands. Thus hypertonic treatment can be beneficial in apoptosis-inducing cancer treatments (Sirtl et al. 2018).

9) Summary

The results of our experiments reveal that global changes in chromatin structure achieved by hypotonic or hypertonic treatment have severe consequences on DDR signaling and DSB repair and thereby endanger genomic stability.

Chromatin relaxation by itself results in transient arrest of cells in G2-phase, which might be due to ATM activation. However, in response to IR DDR signaling is reduced in terms of pATM, γH2AX and 53BP1 foci formation. Surprisingly, we still see a strong G2-checkpoint response upon DSB induction, which is dependent on ATR as well as on ATM. Further investigation of upstream signaling of ATM will help to understand these diverse responses mediated by ATM. Since we observe functional DNA end resection in globally relaxed chromatin, an ATR mediated checkpoint response is promoted. However, DSB repair by the main repair pathways is disturbed, as we see less cNHEJ and especially HRR. Also altEJ fails to backup cNHEJ and HRR, but SSA is three-fold increased upon hypotonic treatment. As this is seen in experiments utilizing reporter cell lines, it would be interesting to investigate the response of SSA to chromatin relaxation on IR-induced DSBs.

While impairments of faithful DSB repair are seen and in addition only mutagenic DSB repair is functional, the modest effects found in survival are unexpected. However, as continuous hypotonic treatment is toxic to the cells, the adaptation of the protocol to transient treatment explains the small radiosensitizing effect observed. DDR signaling experiments and also measurements of CCP show that effects of global chromatin relaxation mediated by hypotonic treatment are completely reversible.

Global chromatin condensation achieved by hypertonic treatment arrests cells in G1-, G2- and M-phase, while it enhances DDR signaling in terms of ATM activation and H2AX phosphorylation in response to IR. However, DSB repair efficiency of all investigated repair pathways is compromised (cNHEJ) or completely abrogated (HRR, altEJ and SSA). This might be explained by nonfunctional DNA end resection upon chromatin condensation, which is necessary for HRR, altEJ and SSA. However, activation of checkpoints may help to maintain genomic stability although DSB repair is inhibited. Chromatin condensation and also DDR signaling is restored

when cells are re-incubated in normal cell culture medium, which explains the moderate effects of hypertonic treatment on radiosensitization to killing observed.

Collectively, global changes in chromatin massively perturb responses to DNA damage and risk genomic integrity. The action of hypotonic and hypertonic medium in altering chromatin structure is rather unspecific. Thus, more specific treatments like inhibitors of proteins influencing chromatin structure or genetically modified cell lines with loss-of-proteins that are known to facilitate, for example, chromatin condensation will help to further elucidate the role of chromatin structure in DDR signaling, DSB repair and DSB repair pathway choice.

10) Zusammenfassung

Die Ergebnisse unserer Experimente zeigen, dass globale Veränderungen der Chromatinstruktur, die durch hypotone oder hypertone Behandlung hervorgerufen werden, schwerwiegende Auswirkungen auf die DDR Signalübertragung und die DSB Reparatur haben und somit die genomische Stabilität gefährden.

Chromatinrelaxation allein verursacht ein vorübergehendes Stoppen der Zellen in der G2-Phase, möglicherweise resultierend aus einer ATM Aktivierung. Allerdings ist die DDR Signalübertragung, gemessen an der Bildung von pATM, γH2AX und 53BP1 Foci, nach Bestrahlung reduziert. Überraschenderweise können wir trotzdem eine starke G2-Kontrollpunktaktivierung nach DSB Induktion beobachten, die sowohl von ATR als auch von ATM abhängig ist. Weitere Untersuchungen der Signalübertragungen, die ATM vorausgehen, werden uns helfen diese unterschiedlichen ATM-vermittelten Endpunkte zu verstehen. Die in global relaxiertem Chromatin zu beobachtende, funktionsfähige DNA Resektion ermöglicht eine Kontrollpunktaktivierung durch ATR. Trotzdem ist die DSB Reparatur gestört, wie wir an einer weniger effizienten cNHEJ und vor allem an weniger HRR sehen. Auch altEJ kann die beiden Mechanismen nicht ersetzen; SSA ist dagegen dreifach verstärkt sobald die Zellen hypoton behandelt werden. Dieser Effekt wurde mithilfe von Reporter Zelllinien entdeckt und es wäre interessant auch die Reaktion des SSA auf strahlungsinduzierte DSBs in relaxiertem Chromatin zu untersuchen.

Obwohl wir starke Beeinträchtigungen der Hauptreparaturwege beobachten und außerdem nur mutagene DSB Reparatur aktiv ist, sind die geringen Effekte der Chromatinrelaxation auf das Zellüberleben unerwartet. Da die kontinuierliche Behandlung der Zellen mit hypotonem Medium toxisch ist, erklärt die nach Anpassung des Protokolls nur noch vorübergehende Behandlung diese geringen Effekte auf das Überleben nach Bestrahlung. DDR Signalübertragungsexperimente und auch die Messungen des CCP zeigen, dass die Effekte der globalen Chromatinrelaxation, hervorgerufen durch hypotone Behandlung, komplett reversibel sind.

Globale Chromatinkondensierung, erzeugt durch hypertone Behandlung, hält die Zellen in der G1-, G2- und M-Phase an, während die DDR Signalübertragung gemessen an der ATM Aktivierung und der H2AX Phosphorylierung nach Bestrahlung verstärkt wird. Jedoch ist die Aktivität aller untersuchten DSB

Reparaturwege beeinträchtigt (cNHEJ) bzw. komplett unterbrochen (HRR, altEJ und SSA). Eine mögliche Erklärung könnte sein, dass die DNA Resektion in kondensiertem Chromatin nicht mehr funktioniert, welche aber notwendig für die Reparatur durch HRR, altEJ und SSA ist. Daher könnte die funktionelle Aktivierung der Kontrollpunkte helfen die genomische Stabilität zu bewahren, obwohl die DSB Reparatur inhibiert ist. Chromatinkondensierung und die DDR Signalübertragung wird wiederhergestellt, sobald die Zellen in normalem Zellkulturmedium inkubiert werden. Das könnte ebenfalls eine Erklärung für die nur moderaten Effekte der hypertonen Behandlung auf das Überleben nach Bestrahlung sein.

Zusammenfassend stören globale Änderungen der Chromatinstruktur massiv die Reaktionen der Zelle auf DNA-Schadensinduzierung und gefährden somit die genomische Integrität. Die chromatinverändernde Wirkung der hypotonen und hypertonen Medien ist eher unspezifischer Natur. Daher können spezifischere Behandlungen wie zum Beispiel das Nutzen von Inhibitoren bestimmter Chromatin beeinflussender Proteine oder genetisch modifzierte Zelllinien, denen Proteine fehlen, die an der Chromatinkondensierung beteiligt sind, helfen die Rolle der Chromatinstruktur hinsichtlich der DDR Signalübertragung, der DSB Reparatur und der Wahl des Reparaturweges weiter aufzuklären.

11) References

Adam, Salomé, Juliette Dabin, and Sophie E. Polo. 2015. 'Chromatin plasticity in response to DNA damage: The shape of things to come', *DNA Repair*, 32: 120-26.

Alberts, Bruce, Alexander Johnson, Julian Lewis, Martin Raff, Keith Roberts, and Peter Walter. 2008. *Molecular Biology of The Cell* (Garland Science, Taylor & Francis Group: New York).

Albiez, H., M. Cremer, C. Tiberi, L. Vecchio, L. Schermelleh, S. Dittrich, K. Kupper, B. Joffe, T. Thormeyer, J. von Hase, S. Yang, K. Rohr, H. Leonhardt, I. Solovei, C. Cremer, S. Fakan, and T. Cremer. 2006. 'Chromatin domains and the interchromatin compartment form structurally defined and functionally interacting nuclear networks', *Chromosome Res*, 14: 707-33.

Allen, Chris, Amanda K. Ashley, Robert Hromas, and Jac A. Nickoloff. 2011. 'More forks on the road to replication stress recovery', *Journal of Molecular Cell Biology*, 3: 4-12.

Allen, Christopher, Thomas B. Borak, Hirohiko Tsujii, and Jac A. Nickoloff. 2011. 'Heavy charged particle radiobiology: Using enhanced biological effectiveness and improved beam focusing to advance cancer therapy', *Mutation Research/Fundamental and Molecular Mechanisms of Mutagenesis*, 711: 150-57.

An, L., C. Dong, J. Li, J. Chen, J. Yuan, J. Huang, K. M. Chan, C. H. Yu, and M. S. Y. Huen. 2018. 'RNF169 limits 53BP1 deposition at DSBs to stimulate single-strand annealing repair', *Proc Natl Acad Sci U S A*.

Andres, Sara N., Alexandra Vergnes, Dejan Ristic, Claire Wyman, Mauro Modesti, and Murray Junop. 2012. 'A human XRCC4–XLF complex bridges DNA', *Nucleic Acids Res*, 40: 1868-78.

Arjunan, K. P., V. K. Sharma, and S. Ptasinska. 2015. 'Effects of atmospheric pressure plasmas on isolated and cellular DNA-a review', *Int J Mol Sci*, 16: 2971-3016.

Bakkenist, C.J., and M. B. Kastan. 2003. 'DNA damage activates ATM through intermolecular autophosphorylation and dimer dissociation', *Nature*, 421: 499-506.

Bakr, A., S. Kocher, J. Volquardsen, C. Petersen, K. Borgmann, E. Dikomey, K. Rothkamm, and W. Y. Mansour. 2016. 'Impaired 53BP1/RIF1 DSB mediated end-protection stimulates CtIP-dependent end resection and switches the repair to PARP1-dependent end joining in G1', *Oncotarget*.

Bekker-Jensen, Simon, and Niels Mailand. 2010. 'Assembly and function of DNA double-strand break repair foci in mammalian cells', *DNA Repair*, 9: 1219-28.

Bhargava, R., D. O. Onyango, and J. M. Stark. 2016. 'Regulation of Single-Strand Annealing and its Role in Genome Maintenance', *Trends Genet*, 32: 566-75.

Blackford, A. N., and S. P. Jackson. 2017. 'ATM, ATR, and DNA-PK: The Trinity at the Heart of the DNA Damage Response', *Mol Cell*, 66: 801-17.

Bodnar, A. G., M. Ouellette, M. Frolkis, S. E. Holt, C. P. Chiu, G. B. Morin, C. B. Harley, J. W. Shay, S. Lichtsteiner, and W. E. Wright. 1998. 'Extension of life-

span by introduction of telomerase into normal human cells', *Science*, 279: 349-52.

Bonner, William M., Christophe E. Redon, Jennifer S. Dickey, Asako J. Nakamura, Olga A. Sedelnikova, Stephanie Solier, and Yves Pommier. 2008. 'γH2AX and cancer', *Nat Rev Cancer*, 8: 957-67.

Brooker, A. S., and K. M. Berkowitz. 2014. 'The roles of cohesins in mitosis, meiosis, and human health and disease', *Methods Mol Biol*, 1170: 229-66.

Burg, M. B., J. D. Ferraris, and N. I. Dmitrieva. 2007. 'Cellular response to hyperosmotic stresses', *Physiol Rev*, 87: 1441-74.

Burg, M. B., E. D. Kwon, and D. Kultz. 1997. 'Regulation of gene expression by hypertonicity', *Annu Rev Physiol*, 59: 437-55.

Burgess, Rebecca C, Bharat Burman, Michael J Kruhlak, and Tom Misteli. 2014. 'Activation of DNA Damage Response Signaling by Condensed Chromatin', *Cell Reports*, 9: 1703-17.

Burma, Sandeep, Benjamin P. C. Chen, and David J. Chen. 2006. 'Role of non-homologous end joining (NHEJ) in maintaining genomic integrity', *DNA Repair*, 5: 1042-48.

Ceccaldi, Raphael, Jessica C. Liu, Ravindra Amunugama, Ildiko Hajdu, Benjamin Primack, Mark I. R. Petalcorin, Kevin W. O/'Connor, Panagiotis A. Konstantinopoulos, Stephen J. Elledge, Simon J. Boulton, Timur Yusufzai, and Alan D. D/'Andrea. 2015. 'Homologous-recombination-deficient tumours are dependent on Pol[thgr]-mediated repair', *Nature*, 518: 258-62.

Cheng, Qiao, Nadia Barboule, Philippe Frit, Dennis Gomez, Oriane Bombarde, Bettina Couderc, Guo-Sheng Ren, Bernard Salles, and Patrick Calsou. 2011. 'Ku counteracts mobilization of PARP1 and MRN in chromatin damaged with DNA double-strand breaks', *Nucleic Acids Res*, 39: 9605-19.

Chou, D. M., B. Adamson, N. E. Dephoure, X. Tan, A. C. Nottke, K. E. Hurov, S. P. Gygi, M. P. Colaiacovo, and S. J. Elledge. 2010. 'A chromatin localization screen reveals poly (ADP ribose)-regulated recruitment of the repressive polycomb and NuRD complexes to sites of DNA damage', *Proc Natl Acad Sci U S A*, 107: 18475-80.

Cook, Peter J., Bong Gun Ju, Francesca Telese, Xiangting Wang, Christopher K. Glass, and Michael G. Rosenfeld. 2009. 'Tyrosine dephosphorylation of H2AX modulates apoptosis and survival decisions', *Nature*, 458: 591-96.

Cowell, I.G., N.J. Sunter, P.B. Singh, C.A. Austin, B.W. Durkacz, and Michael J. Tilby. 2007. 'γH2AX foci form preferentially in euchromatin after ionising-radiation', *PLoS One*, 2: e1057.

Dabin, J., A. Fortuny, and S. E. Polo. 2016. 'Epigenome Maintenance in Response to DNA Damage', *Mol Cell*, 62: 712-27.

Daley, James M., and Patrick Sung. 2014. '53BP1, BRCA1, and the Choice between Recombination and End Joining at DNA Double-Strand Breaks', *Molecular and Cellular Biology*, 34: 1380-88.

Demond, M. 2016. 'The influence of chromatin structure on DNA double strand break repair pathway choice', *PhD thesis*.

Dettor, C.M., W.C. Dewey, L.F. Winans, and J.S. Noel. 1972. 'Enhancement of X-ray damage in synchronous Chinese hamster cells by hypertonic treatments.', *Radiat Res*, 52: 352-72.

Dmitrieva, N., D.V. Bulavin, and M.B. Burg. 2003. 'High NaCl causes Mre11 to leave the nucleus, disrupting DNA damage signaling and repair', *Am J Physiol Renal Physiol*, 285: F266-F74.

Dmitrieva, Natalia I., and Maurice B. Burg. 2005. 'Hypertonic stress response', *Mutation Research/Fundamental and Molecular Mechanisms of Mutagenesis*, 569: 65-74.

Dmitrieva, Natalia I., Qi Cai, and Maurice B. Burg. 2004. 'Cells adapted to high NaCl have many DNA breaks and impaired DNA repair both in cell culture and in vivo', *Proc Natl Acad Sci U S A*, 101: 2317-22.

Doil, Carsten, Niels Mailand, Simon Bekker-Jensen, Patrice Menard, Dorthe Helena Larsen, Rainer Pepperkok, Jan Ellenberg, Stephanie Panier, Daniel Durocher, Jiri Bartek, Jiri Lukas, and Claudia Lukas. 2009. 'RNF168 Binds and Amplifies Ubiquitin Conjugates on Damaged Chromosomes to Allow Accumulation of Repair Proteins', *Cell*, 136: 435-46.

Dueva, Rositsa, and George Iliakis. 2013. 'Alternative pathways of non-homologous end joining (NHEJ) in genomic instability and cancer', *Translational Cancer Research*, 2: 163-77.

Elia, M.C., and M.O. Bradley. 1992. 'Influence of chromatin structure on the induction of DNA double strand breaks by ionizing radiation.', *Cancer Research*, 52: 1580-86.

Elliott, Beth, Christine Richardson, and Maria Jasin. 2005. 'Chromosomal Translocation Mechanisms at Intronic Alu Elements in Mammalian Cells', *Mol Cell*, 17: 885-94.

Falk, Martin, Emilie Lukásová, and Stanislav Kozubek. 2008. 'Chromatin structure influences the sensitivity of DNA to γ-radiation', *Biochimica et Biophysica Acta (BBA) - Molecular Cell Research*, 1783: 2398-414.

Ferguson, D. O., J. M. Sekiguchi, S. Chang, K. M. Frank, Y. Gao, R. A. DePinho, and F. W. Alt. 2000. 'The nonhomologous end-joining pathway of DNA repair is required for genomic stability and the suppression of translocations', *Proc Natl Acad Sci U S A*, 97: 6630-33.

Ferrari, K. J., A. Scelfo, S. Jammula, A. Cuomo, I. Barozzi, A. Stutzer, W. Fischle, T. Bonaldi, and D. Pasini. 2014. 'Polycomb-dependent H3K27me1 and H3K27me2 regulate active transcription and enhancer fidelity', *Mol Cell*, 53: 49-62.

Finan, J. D., H. A. Leddy, and F. Guilak. 2011. 'Osmotic stress alters chromatin condensation and nucleocytoplasmic transport', *Biochem Biophys Res Commun*, 408: 230-5.

Fischereder, M., B. Michalke, E. Schmockel, A. Habicht, R. Kunisch, I. Pavelic, B. Szabados, U. Schonermarck, P. J. Nelson, and M. Stangl. 2017. 'Sodium storage in human tissues is mediated by glycosaminoglycan expression', *Am J Physiol Renal Physiol*, 313: F319-f25.

Fradet-Turcotte, Amelie, Marella D. Canny, Cristina Escribano-Diaz, Alexandre Orthwein, Charles C. Y. Leung, Hao Huang, Marie-Claude Landry, Julianne Kitevski-LeBlanc, Sylvie M. Noordermeer, Frank Sicheri, and Daniel Durocher. 2013. '53BP1 is a reader of the DNA-damage-induced H2A Lys[thinsp]15 ubiquitin mark', *Nature*, 499: 50-54.

Fyodorov, D. V., B. R. Zhou, A. I. Skoultchi, and Y. Bai. 2018. 'Emerging roles of linker histones in regulating chromatin structure and function', *Nat Rev Mol Cell Biol*, 19: 192-206.

Goldstein, Michael, Frederick A. Derheimer, Jacqueline Tait-Mulder, and Michael B. Kastan. 2013. 'Nucleolin mediates nucleosome disruption critical for DNA double-strand break repair', *Proc Natl Acad Sci U S A*, 110: 16874-79.

Goodarzi, Aaron A., Angela T. Noon, Dorothee Deckbar, Yael Ziv, Yosef Shiloh, Markus Löbrich, and Penny A. Jeggo. 2008. 'ATM signaling facilitates repair of DNA double-strand breaks associated with heterochromatin', *Mol Cell*, 31: 167-77.

Gunn, Amanda, and Jeremy M. Stark. 2012. 'I-SceI-based assays to examine distinct repair outcomes of mammalian chromosomal double strand-breaks', *Methods in Molecular Biology*, 920: 379-91.

Hall, Eric J., and Amato J. Giaccia. 2006. *Radiobiology for the Radiologist* (Lippincott Williams & Wilkins: Philadelphia, Baltimore, New York, London, Buenos Aires, Hong Kong, Sydney, Tokyo).

Hamilton, Charlotte, Richard L. Hayward, and Nick Gilbert. 2011. 'Global chromatin fibre compaction in response to DNA damage', *Biochem Biophys Res Commun*, 414: 820-25.

Hirano, T. 2004. 'Chromosome shaping by two condensins', *Cell Cycle*, 3: 26-8.

Hoffmann, E. K., I. H. Lambert, and S. F. Pedersen. 2009. 'Physiology of cell volume regulation in vertebrates', *Physiol Rev*, 89: 193-277.

Huertas, Pablo, and Stephen P. Jackson. 2009. 'Human CtIP Mediates Cell Cycle Control of DNA End Resection and Double Strand Break Repair', *Journal of Biological Chemistry*, 284: 9558-65.

Huyen, Y., O. Zgheib, R.A. DiTullio Jr., V. G. Gorgoulis, P. Zacharatos, T.J. Petty, E.A. Sheston, H.S. Mellert, E.S. Stavridi, and T.D. Halazonetis. 2004. 'Methylated lysine 79 of histone H3 targets 53BP1 to DNA double-strand breaks', *Nature*, 432: 406-11.

Iacovoni, Jason S., Pierre Caron, Imen Lassadi, Estelle Nicolas, Laurent Massip, Didier Trouche, and Gaelle Legube. 2010. 'High-resolution profiling of γH2AX around DNA double strand breaks in the mammalian genome', *EMBO Journal*, 29: 1446-57.

Iliakis, G., L. Metzger, N. Denko, and T.D. Stamato. 1991. 'Detection of DNA double strand breaks in synchronous cultures of CHO cells by means of asymmetric field inversion gel electrophoresis.', *International Journal of Radiation Biology*, 59: 321-41.

Iliakis, G., R. Okayasu, J. Varlotto, C. Shernoff, and Y. Wang. 1993. 'Hypertonic treatment during premature chromosome condensation allows visualization

of interphase chromosome breaks repaired with fast kinetics in irradiated CHO cells.', *Radiat Res*, 135: 160-70.

Iliakis, G., H. Wang, A.R. Perrault, W. Boecker, B. Rosidi, F. Windhofer, W. Wu, J. Guan, G. Terzoudi, and G. Pantelias. 2004. 'Mechanisms of DNA double strand break repair and chromosome aberration formation', *Cytogenetic and Genome Research*, 104: 14-20.

Iliakis, G., Ya Wang, Jun Guan, and Huichen Wang. 2003. 'DNA damage checkpoint control in cells exposed to ionizing radiation', *Oncogene*, 22: 5834-47.

Ip, Stephen C. Y., Ulrich Rass, Miguel G. Blanco, Helen R. Flynn, J. Mark Skehel, and Stephen C. West. 2008. 'Identification of Holliday junction resolvases from humans and yeast', *Nature*, 456: 357-61.

Irianto, J., D. A. Lee, and M. M. Knight. 2014. 'Quantification of chromatin condensation level by image processing', *Med Eng Phys*, 36: 412-7.

Irianto, J., J. Swift, R. P. Martins, G. D. McPhail, M. M. Knight, D. E. Discher, and D. A. Lee. 2013. 'Osmotic challenge drives rapid and reversible chromatin condensation in chondrocytes', *Biophys J*, 104: 759-69.

Iyengar, Sushma, and Peggy J. Farnham. 2011. 'KAP1 Protein: An Enigmatic Master Regulator of the Genome', *Journal of Biological Chemistry*, 286: 26267-76.

Jackson, Stephen P., and Jiri Bartek. 2009. 'The DNA-damage response in human biology and disease', *Nature*, 461: 1071-78.

Jakob, Burkhard, Jörn Splinter, Sandro Conrad, Kay-Obbe Voss, Daniele Zink, Marco Durante, Markus Löbrich, and Gisela Taucher-Scholz. 2011. 'DNA double-strand breaks in heterochromatin elicit fast repair protein recruitment, histone H2AX phosphorylation and relocation to euchromatin', *Nucleic Acids Res*, 39: 6489-99.

Jantsch, J., V. Schatz, D. Friedrich, A. Schroder, C. Kopp, I. Siegert, A. Maronna, D. Wendelborn, P. Linz, K. J. Binger, M. Gebhardt, M. Heinig, P. Neubert, F. Fischer, S. Teufel, J. P. David, C. Neufert, A. Cavallaro, N. Rakova, C. Kuper, F. X. Beck, W. Neuhofer, D. N. Muller, G. Schuler, M. Uder, C. Bogdan, F. C. Luft, and J. Titze. 2015. 'Cutaneous Na+ storage strengthens the antimicrobial barrier function of the skin and boosts macrophage-driven host defense', *Cell Metab*, 21: 493-501.

Jiang, Xu-Rong, G. Jimenez, E. Chang, M. Frolkis, B. Kusler, M. Sage, M. Beeche, A.G. Bodnar, G.M. Wahl, T.D. Tlsty, and Choy-Pik Chiu. 1999. 'Telomerase expression in human somatic cells does not induce changes associated with a transformed phenotype', *Nature Genetics*, 21: 111-14.

Khanna, Kum Kum, and S. P. Jackson. 2001. 'DNA double-strand breaks: signaling, repair and the cancer connection.', *Nature Genetics*, 27: 247-54.

Khurana, Simran, Michael J Kruhlak, Jeongkyu Kim, Andy D Tran, Jinping Liu, Katherine Nyswaner, Lei Shi, Parthav Jailwala, Myong-Hee Sung, Ofir Hakim, and Philipp Oberdoerffer. 2014. 'A Macrohistone Variant Links Dynamic Chromatin Compaction to BRCA1-Dependent Genome Maintenance', *Cell Reports*, 8: 1049-62.

Kim, Seong-Tae, Bo Xu, and M. B. Kastan. 2002. 'Involvement of the cohesin protein, Smc1, in Atm-dependent and independent responses to DNA damage', *Genes Dev*, 16: 560-70.

Kishi, H., K. Nakagawa, M. Matsumoto, M. Suga, M. Ando, Y. Taya, and M. Yamaizumi. 2001. 'Osmotic shock induces G1 arrest through p53 phosphorylation at Ser33 by activated p38MAPK without phosphorylation at Ser15 and Ser20', *J Biol Chem*, 276: 39115-22.

Kousholt, Arne Nedergaard, Kasper Fugger, Saskia Hoffmann, Brian D. Larsen, Tobias Menzel, Alessandro A. Sartori, and Claus Storgaard Sørensen. 2012. 'CtIP-dependent DNA resection is required for DNA damage checkpoint maintenance but not initiation', *Journal of Cell Biology*, 197: 869-76.

Krieger, L. M., and G. Iliakis. 2017. 'Wenn Stränge reißen - Wege der DNA-Doppelstrangbruch-Reparatur', *BIOspektrum*, 23: 502-08.

Kudou, M., A. Shiozaki, T. Kosuga, D. Ichikawa, H. Konishi, R. Morimura, S. Komatsu, H. Ikoma, H. Fujiwara, K. Okamoto, S. Hosogi, T. Nakahari, Y. Marunaka, and E. Otsuji. 2016. 'Inhibition of Regulatory Volume Decrease Enhances the Cytocidal Effect of Hypotonic Shock in Hepatocellular Carcinoma', *J Cancer*, 7: 1524-33.

Kurosu, T., Y. Takahashi, T. Fukuda, T. Koyama, T. Miki, and O. Miura. 2005. 'p38 MAP kinase plays a role in G2 checkpoint activation and inhibits apoptosis of human B cell lymphoma cells treated with etoposide', *Apoptosis*, 10: 1111-20.

Larsen, Dorthe Helena, Catherine Poinsignon, Thorkell Gudjonsson, Christoffel Dinant, Mark R. Payne, Flurina J. Hari, Jannie M. Rendtlew Danielsen, Patrice Menard, Jette Christensen Sand, Manuel Stucki, Claudia Lukas, Jiri Bartek, Jens S. Andersen, and Jiri Lukas. 2010. 'The chromatin-remodeling factor CHD4 coordinates signaling and repair after DNA damage', *Journal of Cell Biology*, 190: 731-40.

Lin, Y. C., J. H. Chen, K. W. Han, and W. C. Shen. 2005. 'Ablation of liver tumor by injection of hypertonic saline', *AJR Am J Roentgenol*, 184: 212-9.

Lindahl, T. 1993. 'Instability and decay of the primary structure of DNA.', *Nature*, 362: 709-15.

Lobrich, M., and P. Jeggo. 2017. 'A Process of Resection-Dependent Nonhomologous End Joining Involving the Goddess Artemis', *Trends Biochem Sci*, 42: 690-701.

Löbrich, Markus, and Penny A. Jeggo. 2007. 'The impact of a negligent G2/M checkpoint on genomic instability and cancer induction', *Nat Rev Cancer*, 7: 861-69.

Luger, Karolin, Mekonnen L. Dechassa, and David J. Tremethick. 2012. 'New insights into nucleosome and chromatin structure: an ordered state or a disordered affair?', *Nat Rev Mol Cell Biol*, 13: 436-47.

Luijsterburg, Martijn S., Christoffel Dinant, Hannes Lans, Jan Stap, Elzbieta Wiernasz, Saskia Lagerwerf, Daniel O. Warmerdam, Michael Lindh, Maartje C. Brink, Jurek W. Dobrucki, Jacob A. Aten, Maria I. Fousteri, Gert Jansen, Nico P. Dantuma, Wim Vermeulen, Leon H. F. Mullenders, Adriaan B.

Houtsmuller, Pernette J. Verschure, and Roel van Driel. 2009. 'Heterochromatin protein 1 is recruited to various types of DNA damage', *Journal of Cell Biology*, 185: 577-86.

Lukas, Jiri, Claudia Lukas, and Jiri Bartek. 2011. 'More than just a focus: The chromatin response to DNA damage and its role in genome integrity maintenance', *Nature Cell Biology*, 13: 1161-69.

Malumbres, M., and M. Barbacid. 2001. 'To cycle or not to cycle: a critical decision in cancer', *Nat Rev Cancer*, 1: 222-31.

Mansour, Wael Y., Sabine Schumacher, Raphael Rosskopf, Tim Rhein, Filip Schmidt-Petersen, Fruszina Gatzemeier, Friedrich Haag, Kerstin Borgmann, Henning Willers, and Jochen Dahm-Daphi. 2008. 'Hierarchy of nonhomologous end-joining, single-strand annealing and gene conversion at site-directed DNA double-strand breaks', *Nucleic Acids Res*, 36: 4088-98.

Manthey, Glenn M., and Adam M. Bailis. 2010. 'Rad51 Inhibits Translocation Formation by Non-Conservative Homologous Recombination in *Saccharomyces cerevisiae*', *PLoS One*, 5: e11889.

Matsunaga, H., J. T. Handa, A. Aotaki-Keen, S. W. Sherwood, M. D. West, and L. M. Hjelmeland. 1999. 'Beta-galactosidase histochemistry and telomere loss in senescent retinal pigment epithelial cells', *Invest Ophthalmol Vis Sci*, 40: 197-202.

Mattiroli, Francesca, Joseph H A. Vissers, Willem J van Dijk, Pauline Ikpa, Elisabetta Citterio, Wim Vermeulen, Jurgen A Marteijn, and Titia K Sixma. 2012. 'RNF168 Ubiquitinates K13-15 on H2A/H2AX to Drive DNA Damage Signaling', *Cell*, 150: 1182-95.

Mazin, Alexander V., Olga M. Mazina, Dmitry V. Bugreev, and Matthew J. Rossi. 2010. 'Rad54, the motor of homologous recombination', *DNA Repair*, 9: 286-302.

Meek, Katheryn , Shikha Gupta, Dale A. Ramsden, and Susan P. Lees-Miller. 2004. 'The DNA-dependent protein kinase: the director at the end', *Immunological Reviews*, 200: 132-41.

Melander, Fredrik, Simon Bekker-Jensen, Jacob Falck, Jiri Bartek, Niels Mailand, and Jiri Lukas. 2008. 'Phosphorylation of SDT repeats in the MDC1 N terminus triggers retention of NBS1 at the DNA damage-modified chromatin', *Journal of Cell Biology*, 181: 213-26.

Metzger, L., and G. Iliakis. 1991. 'Kinetics of DNA double strand breaks throughout the cell cycle as assayed by pulsed field gel electrophoresis in CHO cells.', *International Journal of Radiation Biology*, 59: 1325-39.

Misteli, Tom, and Evi Soutoglou. 2009. 'The emerging role of nuclear architecture in DNA repair and genome maintenance', *Nat Rev Mol Cell Biol*, 10: 243-54.

Miura, T, A Nakata, K Kasai, and M Yoshida. 2012. 'Effects of Colcemid-Block on Chromosome Condensation in Metaphase Analysis and Premature Chromosome Condensation Assays', *REM*, 1: 70-74.

Mladenov, E., and G. Iliakis. 2011. 'Induction and repair of DNA double strand breaks: the increasing spectrum of non-homologous end joining pathways', *Mutat Res*, 711: 61-72.

Mladenov, E., S. Magin, A. Soni, and G. Iliakis. 2016. 'DNA double-strand-break repair in higher eukaryotes and its role in genomic instability and cancer: Cell cycle and proliferation-dependent regulation', *Semin Cancer Biol*, 37-38: 51-64.

Mladenov, Emil, Simon Magin, Aashish Soni, and George Iliakis. 2013. 'DNA double-strand break repair as determinant of cellular radiosensitivity to killing and target in radiation therapy', *Frontiers in Oncology*, 3: Article 113.

Morrical, Scott W. 2015. 'DNA-Pairing and Annealing Processes in Homologous Recombination and Homology-Directed Repair', *Cold Spring Harbor Perspectives in Biology*, 7: a016444.

Moscariello, Mario, and George Iliakis. 2013. 'Effects of chromatin decondensation on alternative NHEJ', *DNA Repair*, 12: 972-81.

Moscariello, Mario, Radi Wieloch, Aya Kurosawa, Fanghua Li, Noritaka Adachi, Emil Mladenov, and George Iliakis. 2015. 'Role for Artemis nuclease in the repair of radiation-induced DNA double strand breaks by alternative end joining', *DNA Repair*, 31: 29-40.

Muñoz, Meilen C., Corentin Laulier, Amanda Gunn, Anita Cheng, Davide F. Robbiani, André Nussenzweig, and Jeremy M. Stark. 2012. 'Ring Finger Nuclear Factor RNF168 Is Important for Defects in Homologous Recombination Caused by Loss of the Breast Cancer Susceptibility Factor BRCA1', *Journal of Biological Chemistry*, 287: 40618-28.

Nair, N., M. Shoaib, and C. S. Sorensen. 2017. 'Chromatin Dynamics in Genome Stability: Roles in Suppressing Endogenous DNA Damage and Facilitating DNA Repair', *Int J Mol Sci*, 18.

Nako, Y., A. Shiozaki, D. Ichikawa, S. Komatsu, H. Konishi, D. Iitaka, H. Ishii, H. Ikoma, T. Kubota, H. Fujiwara, K. Okamoto, T. Ochiai, T. Nakahari, Y. Marunaka, and E. Otsuji. 2012. 'Enhancement of the cytocidal effects of hypotonic solution using a chloride channel blocker in pancreatic cancer cells', *Pancreatology*, 12: 440-8.

Nikpey, E., T. V. Karlsen, N. Rakova, J. M. Titze, O. Tenstad, and H. Wiig. 2017. 'High-Salt Diet Causes Osmotic Gradients and Hyperosmolality in Skin Without Affecting Interstitial Fluid and Lymph', *Hypertension*, 69: 660-68.

O'Hagan, Heather M., Helai P Mohammad, and Stephen B. Baylin. 2008. 'Double strand breaks can initiate gene silencing and SIRT1-dependent onset of DNA methylation in an exogenous promoter CpG Island', *PLoS Genetics*, 4: e1000155.

Ochi, Takashi, Andrew N. Blackford, Julia Coates, Satpal Jhujh, Shahid Mehmood, Naoka Tamura, Jon Travers, Qian Wu, Viji M. Draviam, Carol V. Robinson, Tom L. Blundell, and Stephen P. Jackson. 2015. 'PAXX, a paralog of XRCC4 and XLF, interacts with Ku to promote DNA double-strand break repair', *Science*, 347: 185-88.

Okada, Y., and E. Maeno. 2001. 'Apoptosis, cell volume regulation and volume-regulatory chloride channels', *Comp Biochem Physiol A Mol Integr Physiol*, 130: 377-83.

Paddock, M. N., A. T. Bauman, R. Higdon, E. Kolker, S. Takeda, and A. M. Scharenberg. 2011. 'Competition between PARP-1 and Ku70 control the decision between high-fidelity and mutagenic DNA repair', *DNA Repair*, 10: 338-43.

Paddock, S. W. 2000. 'Principles and practices of laser scanning confocal microscopy', *Mol Biotechnol*, 16: 127-49.

Pan, Mei-Ren, Guang Peng, Wen-Chun Hung, and Shiaw-Yih Lin. 2011. 'Monoubiquitination of H2AX Protein Regulates DNA Damage Response Signaling', *Journal of Biological Chemistry*, 286: 28599-607.

Paul, K. 2013. 'Function of DNA Ligase III in the Repair of Radiation induced DNA Double Strand Breaks via alternative Pathways of Non-homologous End-Joining functioning as Backup', *PhD thesis*.

Paul, Katja, Minli Wang, Emil Mladenov, Alena A. Bencsik-Theilen, Theresa Bednar, Wenqi Wu, Hiroshi Arakawa, and George Iliakis. 2013. 'DNA ligases I and III cooperate in alternative non-homologous end-joining in vertebrates', *PLoS One*, 8: e59505.

Peng, Guang, Eun-Kyoung Yim, Hui Dai, Andrew P. Jackson, Ineke van der Burgt, Mei-Ren Pan, Ruozhen Hu, Kaiyi Li, and Shiaw-Yih Lin. 2009. 'BRIT1/MCPH1 links chromatin remodelling to DNA damage response', *Nature Cell Biology*, 11: 865-72.

Pleasance, Erin D., R. Keira Cheetham, Philip J. Stephens, David J. McBride, Sean J. Humphray, Chris D. Greenman, Ignacio Varela, Meng-Lay Lin, Gonzalo R. Ordonez, Graham R. Bignell, Kai Ye, Julie Alipaz, Markus J. Bauer, David Beare, Adam Butler, Richard J. Carter, Lina Chen, Anthony J. Cox, Sarah Edkins, Paula I. Kokko-Gonzales, Niall A. Gormley, Russell J. Grocock, Christian D. Haudenschild, Matthew M. Hims, Terena James, Mingming Jia, Zoya Kingsbury, Catherine Leroy, John Marshall, Andrew Menzies, Laura J. Mudie, Zemin Ning, Tom Royce, Ole B. Schulz-Trieglaff, Anastassia Spiridou, Lucy A. Stebbings, Lukasz Szajkowski, Jon Teague, David Williamson, Lynda Chin, Mark T. Ross, Peter J. Campbell, David R. Bentley, P. Andrew Futreal, and Michael R. Stratton. 2010. 'A comprehensive catalogue of somatic mutations from a human cancer genome', *Nature*, 463: 191-96.

Polo, Sophie E., and Stephen P. Jackson. 2011. 'Dynamics of DNA damage response proteins at DNA breaks: a focus on protein modifications', *Genes Dev*, 25: 409-33.

Price, Brendan D, and Alan D D'Andrea. 2013. 'Chromatin Remodeling at DNA Double-Strand Breaks', *Cell*, 152: 1344-54.

Reitsema, T.J., J.P. Banath, S.H. MacPhail, and P.L. Olive. 2004. 'Hypertonic Saline Enhances Expression of Phosphorylated Histone H2AX after Irradiation', *Radiat Res*, 161: 402-08.

Reitsema, Tarren, Dmitry Klokov, Ban, x00e, Judit P. th, and Peggy L. Olive. 2005. 'DNA-PK is responsible for enhanced phosphorylation of histone H2AX under hypertonic conditions', *DNA Repair*, 4: 1172-81.

Roberts, Steven A., Natasha Strande, Martin D. Burkhalter, Christina Strom, Jody M. Havener, Paul Hasty, and Dale A. Ramsden. 2010. 'Ku is a 5'-dRP/AP

lyase that excises nucleotide damage near broken ends', *Nature*, 464: 1214-17.

Rosidi, B., Minli Wang, Wenqi Wu, Aparna Sharma, Huichen Wang, and G. Iliakis. 2008. 'Histone H1 functions as a stimulatory factor in backup pathways of NHEJ', *Nucleic Acids Res*, 36: 1610-23.

Sabarinathan, Radhakrishnan, Loris Mularoni, Jordi Deu-Pons, Abel Gonzalez-Perez, and Núria López-Bigas. 2016. 'Nucleotide excision repair is impaired by binding of transcription factors to DNA', *Nature*, 532: 264-67.

Saksouk, N., E. Simboeck, and J. Dejardin. 2015. 'Constitutive heterochromatin formation and transcription in mammals', *Epigenetics Chromatin*, 8: 3.

Sallmyr, A., and A. E. Tomkinson. 2018. 'Repair of DNA double-strand breaks by mammalian alternative end-joining pathways', *J Biol Chem*.

Sancar, A., L.A. Lindsey-Boltz, K. Ünsal-Kacmaz, and S. Linn. 2004. 'Molecular Mechanisms of Mammalian DNA Repair and the DNA Damage Checkpoints', *Annu Rev Biochem*, 73: 39-85.

Schipler, Agnes, and George Iliakis. 2013. 'DNA double-strand-break complexity levels and their possible contributions to the probability for error-prone processing and repair pathway choice', *Nucleic Acids Res*, 41: 7589-605.

Schuster-Böckler, Benjamin, and Ben Lehner. 2012. 'Chromatin organization is a major influence on regional mutation rates in human cancer cells', *Nature*, 488: 504-07.

Schwertman, Petra, Simon Bekker-Jensen, and Niels Mailand. 2016. 'Regulation of DNA double-strand break repair by ubiquitin and ubiquitin-like modifiers', *Nat Rev Mol Cell Biol*, 17: 379-94.

Shanbhag, Niraj M., Ilona U. Rafalska-Metcalf, Carlo Balane-Bolivar, Susan M. Janicki, and Roger A. Greenberg. 2010. 'ATM-Dependent Chromatin Changes Silence Transcription In cis to DNA Double-Strand Breaks', *Cell*, 141: 970-81.

Shechter, D., H. L. Dormann, C. D. Allis, and S. B. Hake. 2007. 'Extraction, purification and analysis of histones', *Nat Protoc*, 2: 1445-57.

Shi, Lei, and Philipp Oberdoerffer. 2012. 'Chromatin dynamics in DNA double-strand break repair', *Biochimica et Biophysica Acta (BBA) - Gene Regulatory Mechanisms*, 1819: 811-19.

Shiotani, Bunsyo, Hai Dang Nguyen, Pelle Håkansson, Alexandre Maréchal, Alice Tse, Hidetoshi Tahara, and Lee Zou. 2013. 'Two Distinct Modes of ATR Activation Orchestrated by Rad17 and Nbs1', *Cell Reports*, 3: 1651-62.

Simonetta, M., I. de Krijger, J. Serrat, N. Moatti, D. Fortunato, L. Hoekman, O. B. Bleijerveld, A. F. M. Altelaar, and J. J. L. Jacobs. 2018. 'H4K20me2 distinguishes pre-replicative from post-replicative chromatin to appropriately direct DNA repair pathway choice by 53BP1-RIF1-MAD2L2', *Cell Cycle*, 17: 124-36.

Singh, Satyendra K., Theresa Bednar, Lihua Zhang, Wenqi Wu, Emil Mladenov, and George Iliakis. 2012. 'Inhibition of B-NHEJ in Plateau-Phase Cells Is Not a

Direct Consequence of Suppressed Growth Factor Signaling', *International Journal of Radiation Oncology Biology Physics*, 84: e237-e43.

Singh, Satyendra K., Wenqi Wu, Lihua Zhang, Holger Klammer, Minli Wang, and George Iliakis. 2011. 'Widespread Dependence of Backup NHEJ on Growth State: Ramifications for the Use of DNA-PK Inhibitors', *International Journal of Radiation Oncology Biology Physics*, 79: 540-48.

Sinha, R. P., and D. P. Hader. 2002. 'UV-induced DNA damage and repair: a review', *Photochem Photobiol Sci*, 1: 225-36.

Sirbu, Bianca M., and David Cortez. 2013. 'DNA Damage Response: Three Levels of DNA Repair Regulation', *Cold Spring Harbor Perspectives in Biology*, 5: a012724.

Sirtl, Simon, Gertrud Knoll, Dieu Thuy Trinh, Isabell Lang, Daniela Siegmund, Stefanie Gross, Beatrice Schuler-Thurner, Patrick Neubert, Jonathan Jantsch, Harald Wajant, and Martin Ehrenschwender. 2018. 'Hypertonicity-enforced BCL-2 addiction unleashes the cytotoxic potential of death receptors', *Oncogene*, 37: 4122-36.

Smeenk, G., and H. van Attikum. 2013. 'The chromatin response to DNA breaks: leaving a mark on genome integrity', *Annu Rev Biochem*, 82: 55-80.

Soni, Aashish, Maria Siemann, Gabriel E. Pantelias, and George Iliakis. 2015. 'Marked cell cycle-dependent contribution of alternative end joining to formation of chromosome translocations by stochastically induced DNA double strand breaks in human cells', *Mutation Research*, 793: 2-8.

Sonoda, Eiichiro, Helfrid Hochegger, Alihossein Saberi, Yoshihito Taniguchi, and Shunichi Takeda. 2006. 'Differential usage of non-homologous end-joining and homologous recombination in double strand break repair', *DNA Repair*, 5: 1021-29.

Soutoglou, E., J.F. Dorn, K. Sengupta, M. Jasin, A. Nussenzweig, T. Ried, G. Danuser, and T. Misteli. 2007. 'Positional stability of single double-strand breaks in mammalian cells', *Nature Cell Biology*, 9: 675-82.

Stadler, J., and H. Richly. 2017. 'Regulation of DNA Repair Mechanisms: How the Chromatin Environment Regulates the DNA Damage Response', *Int J Mol Sci*, 18.

Stamato, T.D., and N. Denko. 1990. 'Asymmetric field inversion gel electrophoresis: A new method for detecting DNA double-strand breaks in mammalian cells.', *Radiat Res*, 121: 196-205.

Stephen, R. L., J. M. Novak, E. M. Jensen, C. Kablitz, and S. S. Buys. 1990. 'Effect of osmotic pressure on uptake of chemotherapeutic agents by carcinoma cells', *Cancer Res*, 50: 4704-8.

Sun, Yingli, Xiaofeng Jiang, Shujuan Chen, Norvin Fernandes, and Brendan D. Price. 2005. 'A role for the Tip60 histone acetyltransferase in the acetylation and activation of ATM', *Proc Natl Acad Sci U S A*, 102: 13182-87.

Sun, Yingli, Xiaofeng Jiang, Ye Xu, Marina K. Ayrapetov, Lisa A. Moreau, Johnathan R. Whetstine, and Brendan D. Price. 2009. 'Histone H3 methylation links DNA damage detection to activation of the tumour suppressor Tip60', *Nature Cell Biology*, 11: 1376-82.

Symington, L. S. 2002. 'Role of Rad52 epistasis group genes in homologous recombination and double-strand break repair', *Microbiology and Molecular Biology Reviews:MMBR*, 66: 630-70.

Symington, Lorraine S, and Jean Gautier. 2011. 'Double-Strand Break End Resection and Repair Pathway Choice', *Annual Review of Genetics*, 45: 247-71.

Takata, H., T. Hanafusa, T. Mori, M. Shimura, Y. Iida, K. Ishikawa, K. Yoshikawa, Y. Yoshikawa, and K. Maeshima. 2013. 'Chromatin compaction protects genomic DNA from radiation damage', *PLoS One*, 8: e75622.

Thorslund, Tina, Anita Ripplinger, Saskia Hoffmann, Thomas Wild, Michael Uckelmann, Bine Villumsen, Takeo Narita, Titia K. Sixma, Chunaram Choudhary, Simon Bekker-Jensen, and Niels Mailand. 2015. 'Histone H1 couples initiation and amplification of ubiquitin signalling after DNA damage', *Nature*, 527: 389-93.

Tutt, A., D. Bertwistle, J. Valentine, A. Gabriel, S. Swift, G. Ross, C. Griffin, J. Thacker, and A. Ashworth. 2001. 'Mutation in Brca2 stimulates error-prone homology-directed repair of DNA double-strand breaks occurring between repeated sequences', *EMBO Journal*, 20: 4704-16.

Valerie, K., and L. F. Povirk. 2003. 'Regulation and mechanisms of mammalian double-strand break repair', *Oncogene*, 22: 5792-812.

Wang, H., and X. Xu. 2017. 'Microhomology-mediated end joining: new players join the team', *Cell Biosci*, 7: 6.

Wang, H., Z-C. Zeng, T-A. Bui, E. Sonoda, M. Takata, S. Takeda, and G. Iliakis. 2001. 'Efficient rejoining of radiation-induced DNA double-strand breaks in vertebrate cells deficient in genes of the RAD52 epistasis group.', *Oncogene*, 20: 2212-24.

Wang, Hailong, Linda Z. Shi, Catherine C. L. Wong, Xuemei Han, Patty Yi-Hwa Hwang, Lan N. Truong, Qingyuan Zhu, Zhengping Shao, David J. Chen, Michael W. Berns, John R. Yates, III, Longchuan Chen, and Xiaohua Wu. 2013. 'The Interaction of CtIP and Nbs1 Connects CDK and ATM to Regulate HR–Mediated Double-Strand Break Repair', *PLoS Genetics*, 9: e1003277.

Wang, Huichen, A.R. Perrault, Y. Takeda, Wei Qin, Hongyan Wang, and G. Iliakis. 2003. 'Biochemical evidence for Ku-independent backup pathways of NHEJ', *Nucleic Acids Res*, 31: 5377-88.

Wang, Minli, Weizhong Wu, Wenqi Wu, B. Rosidi, Lihua Zhang, Huichen Wang, and G. Iliakis. 2006. 'PARP-1 and Ku compete for repair of DNA double strand breaks by distinct NHEJ pathways', *Nucleic Acids Res*, 34: 6170-82.

Wang, X., C. H. McGowan, M. Zhao, L. He, J. S. Downey, C. Fearns, Y. Wang, S. Huang, and J. Han. 2000. 'Involvement of the MKK6-p38gamma Cascade in gamma-Radiation-Induced Cell Cycle Arrest', *Molecular and Cellular Biology*, 20: 4543-52.

Warters, R. L., and B. W. Lyons. 1992. 'Variation in radiation-induced formation of DNA double-strand breaks as a function of chromatin structure', *Radiat Res*, 130: 309-18.

Wheatley, D. N. 1974. 'Hypertonicity and the arrest of mammalian cells in metaphase: A synchrony technique for HeLa cells', *J Cell Sci*, 15: 221-37.

Wood, Jamie L., Yulong Liang, Kaiyi Li, and Junjie Chen. 2008. 'Microcephalin/MCPH1 Associates with the Condensin II Complex to Function in Homologous Recombination Repair', *Journal of Biological Chemistry*, 283: 29586-92.

Wu, N., and H. Yu. 2012. 'The Smc complexes in DNA damage response', *Cell Biosci*, 2: 5.

Wu, Wenqi, Minli Wang, Weizhong Wu, Satyendra K. Singh, Tamara Mussfeldt, and George Iliakis. 2008. 'Repair of radiation induced DNA double strand breaks by backup NHEJ is enhanced in G2', *DNA Repair*, 7: 329-38.

Xing, Mengtan, Mingrui Yang, Wei Huo, Feng Feng, Leizhen Wei, Wenxia Jiang, Shaokai Ning, Zhenxin Yan, Wen Li, Qingsong Wang, Mei Hou, Chunxia Dong, Rong Guo, Ge Gao, Jianguo Ji, Shan Zha, Li Lan, Huanhuan Liang, and Dongyi Xu. 2015. 'Interactome analysis identifies a new paralogue of XRCC4 in non-homologous end joining DNA repair pathway', *Nature Communications*, 6: 6233.

Xu, Ye, Yingli Sun, Xiaofeng Jiang, Marina K. Ayrapetov, Patryk Moskwa, Shenghong Yang, David M. Weinstock, and Brendan D. Price. 2010. 'The p400 ATPase regulates nucleosome stability and chromatin ubiquitination during DNA repair', *Journal of Cell Biology*, 191: 31-43.

You, Zhongsheng, and Julie M. Bailis. 2010. 'DNA damage and decisions: CtIP coordinates DNA repair and cell cycle checkpoints', *Trends in Cell Biology*, 20: 402-09.

Zhang, Y., and D. Reinberg. 2001. 'Transcription regulation by histone methylation: interplay between different covalent modifications of the core histone tails', *Genes Dev*, 15: 2343-60.

12) Supplementary data

12.1) Calculation of CCP

12.1.1) Image processing by ImageJ

For generating single nuclei images out of microscopy images, lif-files were imported to ImageJ, maximum intensity images in grey scale were generated for each stack and from those single nuclei images using the following macro code were produced.

```
requires("1.51w");
dir = getDirectory("Where to save the nuclei");
setBatchMode( true );
orig = getImageID();
img = split(getTitle(), ".");
run("Duplicate...", " ");
nme = getTitle();
run("Split Channels");
close(nme+" (green)");
close(nme+" (red)");
selectImage(nme+" (blue)");
blue = getImageID();
setAutoThreshold("Mean dark");
setOption("BlackBackground", false);
run("Convert to Mask");
run("Median...", "radius=1");
run("Fill Holes");
run("Watershed");
imageCalculator("Multiply create 32-bit", blue, orig);
rslt = getImageID();
selectImage(blue);
close();
selectImage(orig);
close();
selectImage(rslt);
run("8-bit");
setAutoThreshold("Mean");
run("Analyze Particles...", "size=0-10000 show=Nothing exclude add");
resetThreshold();
run("Invert LUT");
cnt = roiManager("count");
for ( i=0; i<cnt; i++ ) {
        roiManager("select", i);
        run("Duplicate...", " ");
        run("Clear Outside");
        run("Remove Overlay");
        save( dir+img[0]+"_nuc-"+(i+1)+".tif" );
        close();}
setBatchMode( false );
exit();
```

12.1.2) MatLab codes for calculating CCP

In order to calculate CCP based on single nuclei images produced by ImageJ following MatLab codes were taken by Irianto et al (Irianto, Lee, and Knight 2014) and adapted.

12.1.2.1) ApplyThresh

```
function [IThresh] = ApplyThresh(I,T)

%%%%%%%%%%%%%%%%%%%%%%%%%%%%%%%%%%%%%%%%%%%%%%%%%
%%%%%%%%%%%%%%%%%%%%%%%%%%
%This function receive the image to be thresholded and the threshold value.
%This function then produce a thresholded image.
%I: image to be thresholded
%T: threshold value
%%%%%%%%%%%%%%%%%%%%%%%%%%%%%%%%%%%%%%%%%%%%%%%%%
%%%%%%%%%%%%%%%%%%%%%%%%%%

clear row column int S sizerow sizecolumn R C

[row,column,int] = find(I>T);
S = length(row);
[sizerow,sizecolumn] = size(I);
IThresh = zeros(sizerow,sizecolumn);
for i = 1:S
   R = row(i,1);
   C = column(i,1);
   IThresh(R,C) = 1;
end
```

12.1.2.2) ExtractImage

```
function [IExtract] = ExtractImage(I,In)

%%%%%%%%%%%%%%%%%%%%%%%%%%%%%%%%%%%%%%%%%%%%%%%%%
%%%%%%%%%%%%%%%%%%%%%%%%%%
%This function receive the image to be extracted to a black background and
%the thresholded image (having the pixels locating where the target is).
%This function then produce a target image with black background.
%I:    target image
%In:   thresholded image
%%%%%%%%%%%%%%%%%%%%%%%%%%%%%%%%%%%%%%%%%%%%%%%%%
%%%%%%%%%%%%%%%%%%%%%%%%%%

clear row column int S sizerow sizecolumn R C

[row,column,int] = find(In>0);
S = length(row);
[sizerow,sizecolumn] = size(In);
IExtract = zeros(sizerow,sizecolumn);
for i = 1:S
   R = row(i,1);
   C = column(i,1);
   IExtract(R,C) = I(R,C);
end
```

12.1.2.3) GeneratingPrint

```
function [PrintList] = GeneratingPrint(PrintIndex,q,PrintNameList,I2,I3,I4,I5,I6,I7,A1,I8,I9,I10,I11,I12,I13)

%%%%%%%%%%%%%%%%%%%%%%%%%%%%%%%%%%%%%%%%%%%%%%%%%%%%%%%%%%%%%%%%%%%%%%%%%%%%%%%%%
%This function receive an Index, which show the chosen matrices, and the
%q-th image being processed.
%This function then produce prints of the chosen matrices
%PrintIndex:    The index of chosen matrices (m x 1)
%q:             The q-th image being processed
%%%%%%%%%%%%%%%%%%%%%%%%%%%%%%%%%%%%%%%%%%%%%%%%%%%%%%%%%%%%%%%%%%%%%%%%%%%%%%%%%

Index = find(PrintIndex>0);
Cond = isempty(Index);

if Cond == 0
   for i = 1:size(Index,1)
      ImageChosen = Index(i,1);
      if ImageChosen == 1
         imwrite(I2,PrintNameList(q,i).name,'tif');
      elseif ImageChosen == 2
         imwrite(I3,PrintNameList(q,i).name,'tif');
      elseif ImageChosen == 3
         imwrite(I4,PrintNameList(q,i).name,'tif');
      elseif ImageChosen == 4
         imwrite(I5,PrintNameList(q,i).name,'tif');
      elseif ImageChosen == 5
         imwrite(I6,PrintNameList(q,i).name,'tif');
      elseif ImageChosen == 6
         imwrite(I7,PrintNameList(q,i).name,'tif');
      elseif ImageChosen == 7
         imwrite(A1,PrintNameList(q,i).name,'tif');
      elseif ImageChosen == 8
         imwrite(I8,PrintNameList(q,i).name,'tif');
      elseif ImageChosen == 9
         imwrite(I9,PrintNameList(q,i).name,'tif');
      elseif ImageChosen == 10
         imwrite(I10,PrintNameList(q,i).name,'tif');
      elseif ImageChosen == 11
         imwrite(I11,PrintNameList(q,i).name,'tif');
      elseif ImageChosen == 12
         imwrite(I12,PrintNameList(q,i).name,'tif');
      elseif ImageChosen == 13
         imwrite(I13,PrintNameList(q,i).name,'tif');
      end
   end
   PrintList = size(Index,1);
else
   PrintList = 0;
end
```

12.1.2.4) GeneratingPrintName

```
function [PrintNameList] = GeneratingPrintName(PrintIndex,s)
```

```
%%%%%%%%%%%%%%%%%%%%%%%%%%%%%%%%%%%%%%%%%%%%%%%%%%%%%%%%%%%%%%%%%%%%%%%%%%%%
%This function receive an Index, which show the chosen matrices, and the
%number of images being processed.
%This function then produce the list of names of the chosen matrices
%PrintIndex:    The index of chosen matrices (m x 1)
%s:             The number of images being processed (1 x 1)
%%%%%%%%%%%%%%%%%%%%%%%%%%%%%%%%%%%%%%%%%%%%%%%%%%%%%%%%%%%%%%%%%%%%%%%%%%%%

Index = find(PrintIndex>0);
Cond = isempty(Index);

if Cond == 0
   for i = 1:size(Index,1)
      ImageChosen = Index(i,1);
      if ImageChosen == 1
         PName = 'I2';
      elseif ImageChosen == 2
         PName = 'I3';
      elseif ImageChosen == 3
         PName = 'I4';
      elseif ImageChosen == 4
         PName = 'I5';
      elseif ImageChosen == 5
         PName = 'I6';
      elseif ImageChosen == 6
         PName = 'I7';
      elseif ImageChosen == 7
         PName = 'A1';
      elseif ImageChosen == 8
         PName = 'I8';
      elseif ImageChosen == 9
         PName = 'I9';
      elseif ImageChosen == 10
         PName = 'I10';
      elseif ImageChosen == 11
         PName = 'I11';
      elseif ImageChosen == 12
         PName = 'I12';
      elseif ImageChosen == 13
         PName = 'I13';
      end
      for j = 1:s
         PrintName = sprintf('%s-%03d.tif',PName,j);
         PrintNameList(j,i).name = PrintName;
      end
   end
else
   PrintNameList = 'NO PRINT CHOSEN';
end
```

12.1.2.5) Main

```
clear all;
clc

%% ================== List of image matrices ==========================
%I  = original image
```

```
%I2 = original image smoothed by mean filter (6x)
%I3 = image of pixels that above the threshold (T)
%I4 = image of pixels that above the threshold with the holes filled
%I5 = image of the thresholded nucleus in black background plus intensity
%     redistributed
%I6 = downsampled I5 into 128x128 (by a factor of 4)
%I7 = SOBEL image (logical)
%A1 = SOBEL image (uint8)
%I8 = image of pixels that above the threshold from 128x128 image (I6)
%I9 = image of pixels that above the threshold from 128x128 image with the
%     holes filled
%I10 = the inner part of the nucleus (Region of Interest or ROI)
%I11 = perimeter of the ROI
%I12 = image of the SOBEL edge within the ROI
%I13 = image of the SOBEL edge within the ROI (I12) plus the perimeter of
%      previous ROI (I11)

%% ================= INPUT ============================================
%These are the required inputs for the algorithm.
%XLfilename:    The name given to the EXCEL file to be produced, this will
%               contain the area, edge count and edge density from each
%               image.
%filenames:     This will search the folder for the images name specified.
%
%If you want to print out an image matrix, give the value 1. If not
%required, give the value 0.
%
%PixRedFaxtor:  Image reduction factor.
%SobelThresh:   The threshold value for the SOBEL edge detection.
%=====================================================================

XLfilename = 'Results AREA EDGECOUNT EDGEDENSITY.xls';
filenames = dir('*.tif');

PrintI2 = 0;
PrintI3 = 0;
PrintI4 = 0;
PrintI5 = 0;
PrintI6 = 0;
PrintI7 = 0;
PrintA1 = 0;
PrintI8 = 0;
PrintI9 = 0;
PrintI10 = 0;
PrintI11 = 0;
PrintI12 = 0;
PrintI13 = 0;

PixRedFactor = 8;
SobelThresh = 0.09;

%% ===== Producing file names for image matrices to be printed out =======

PrintIndex = [PrintI2;PrintI3;PrintI4;PrintI5;PrintI6;PrintI7;PrintA1;...
   PrintI8;PrintI9;PrintI10;PrintI11;PrintI12;PrintI13];
s = numel(filenames);
[PrintNameList] = GeneratingPrintName(PrintIndex,s);

%% ================== CORE algorithm ==================================

Arealist = zeros(s,1);
```

```
edgecountlist = zeros(s,1);
edgedenlist = zeros(s,1);

for q=1:numel(filenames)
    %Load image
    I = imread(filenames(q).name);

    %Acquire threshold value for I
    [T] = ThreshMode(I);

    %Image average smoothening by (i)th times
    I2 = I;
    for i = 1:6
        h = fspecial('average');
        I2 = imfilter(I2,h);
    end

    %Thereshold application to I2
    [I3] = ApplyThresh(I2,T);
    I3 = logical(I3);

    %Hole-filling algorithm
    I4 = imfill(I3,'holes');

    %Extract the nucleus from the original image to a black background
    [I5] = ExtractImage(I,I4);
    I5 = uint8(I5);

    %Intensity redistribution for I5
    A = max(max(I5));
    B = double(I5);
    C = double(A);
    I5 = (B/C)*255;
    I5 = uint8(I5);

    %Image reduction by a factor of 4 (1/4 = 0.25)
    PixRed = 1/PixRedFactor;
    I6 = imresize(I5,PixRed);

    %Intensity redistribution for I6
    A = max(max(I6));
    B = double(I6);
    C = double(A);
    I6 = (B/C)*255;
    I6 = uint8(I6);

    %SOBEL edge detection application
    I7 = edge(I6,'sobel',SobelThresh);
    A1 = uint8(I7);
    A1 = A1*255;

    %Acquire threshold value for I6
    clear T
    [T] = ThreshMode(I6);

    %Threshold application to I6
    [I8] = ApplyThresh(I6,T);
    I8 = logical(I8);

    %Hole-filling algorithm
    I9 = imfill(I8,'holes');
```

```
    %Perimeter subtraction by (n)th times
    I10 = I9;
    n = 2;
    for i = 1:n
        I11 = bwperim(I10);
        I10 = I10-I11;
        I10 = logical(I10);
    end

    %Extract the SOBEL edge inside the nucleus into a black background
    [I12] = ExtractImage(I7,I10);
    I12 = logical(I12);
    I13 = I12+I11;
    I13 = uint8(I13);
    I13 = I13*255;

    %Nucleus area
    [row,column,int] = find(I10>0);
    S = length(row);
    Area = S;
    Arealist(q,1) = Area;

    %Edge count
    edgecount = sum(sum(I12));
    edgecountlist(q,1) = edgecount;

    %Edge density (i.e. chromatin condensation parameter)
    edgeden = (edgecount/Area)*100;
    edgedenlist(q,1) = edgeden;

    I12 = uint8(I12);
    I12 = I12*255;
    [PrintList] = GeneratingPrint(PrintIndex,PrintNameList,I2,I3,I4,...
        I5,I6,I7,A1,I8,I9,I10,I11,I12,I13);
end

xlswrite(XLfilename,Arealist,1);
xlswrite(XLfilename,edgecountlist,2);
xlswrite(XLfilename,edgedenlist,3);
```

12.1.2.6) ThreshMode

```
function [Thresh] = ThreshMode(I)

%%%%%%%%%%%%%%%%%%%%%%%%%%%%%%%%%%%%%%%%%%%%%%%%%%%%%%%%%%%%%%%%%%%%%%%%%%%%
%This function receive the image to be thresholded.
%This function then produce a threshold value by the mode method.
%I: image to be thresholded
%%%%%%%%%%%%%%%%%%%%%%%%%%%%%%%%%%%%%%%%%%%%%%%%%%%%%%%%%%%%%%%%%%%%%%%%%%%%

I = double(I);
MaxInt = max(max(I));
MaxInt = single(MaxInt);

H = hist(I(:),0:MaxInt);
```

```
Iteration = 0;
Cond = 0;
Thresh = 0;

while Cond == 0
    F = ones(1,3)/3;
    H = conv2(H,F,'same');

    Sy = size(H,2);
    Peak = 0;

    for i = 2:Sy-1
        if Peak < 3
            if H(i-1)<H(i) && H(i+1)<H(i)
                Peak = Peak+1;
            end
        end
    end

    if Peak > 2
        Cond = 0;
    else
        Cond = 1;
    end

    Iteration = Iteration + 1;

    if Iteration > 10000
        Thresh = 0;
        return
    end
end

for j = 2:MaxInt
  if H(j-1)>H(j) && H(j+1)>H(j)
    Thresh = j-1;
  end
end
```

12.2) Clonogenic survival assays

When RPE-1 cells were treated in isotonic medium for different times before plating cells for colony formation, the survival curves were not affected (see Figure 73).

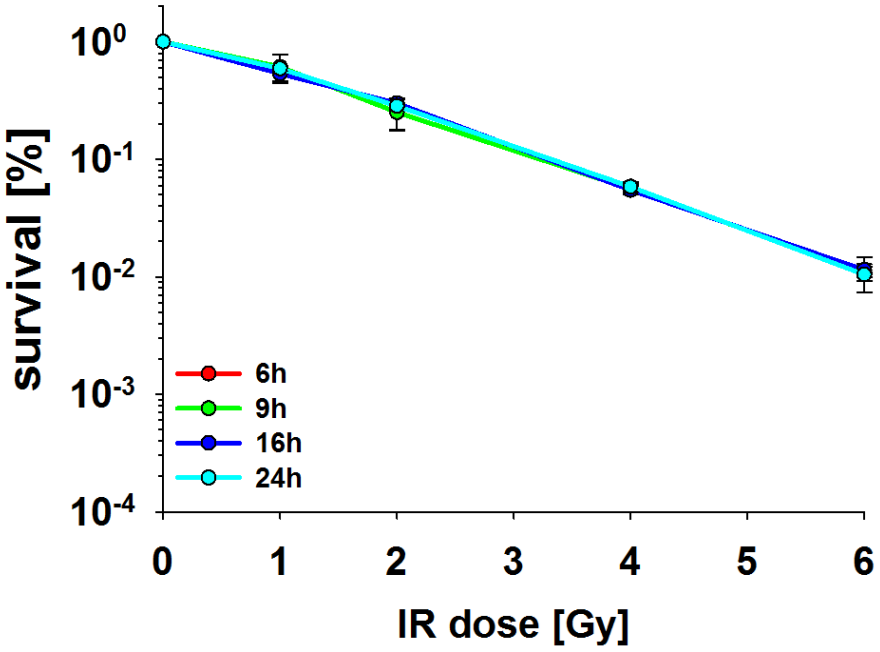

Figure 73 Survival of RPE-1 cells treated in isotonic medium for different times. Cells were treated with isotonic medium for 6, 9, 16 or 24 h immediately after IR before plating in normal cell culture medium for colony formation. Colonies were counted after 11 days of growth. Data shown here represent means and standard errors from four determinations in two experiments

13) Acknowledgements

First and foremost, I would like to express my thanks to my supervisor, Prof. Dr. George Iliakis, for giving me the opportunity to perform my Ph.D. at his Institute of Medical Radiation Biology. I could always count on his support, not only in scientific but also in personal matters. Also it made me proud to receive from him the confidence in overtaking responsible tasks and I want to thank him for always being patient and reassuring in times I became troubled.

My project was funded from Bundesministerium für Bildung und Forschung (BMBF) 02NUK037B entitled „VERCHROMT: Erkennung, Verarbeitung und biologische Konsequenzen von Chromatinschäden nach Teilchenbestrahlung“.

I am also grateful to Dr. Emil Mladenov who trained me during the start and was always helpful in solving technical and experimental problems.

Special thanks go to Marcel Thissen for helping me in all IT concerns and especially in establishing CCP measurements. Without him this wouldn’t have been possible.

I am grateful to Dr. Katja Konietzko, Dr. Marilen Demond and Dr. Tamara Murmann-Konda for having a great time in the lab at least during my first two years and for becoming friends, which is even better.

Of course also Tamara Mußfeldt, Anna Broich, Dr. Veronika Mladenova, Dr. Aashish Soni and Dr. Fanghua Li should not be forgotten. All of them brightened up my everyday life and were always there for a chat, of scientific nature or not.

Last but not least I would like to thank all my friends and my family. My parents, particularly my mother, who always supported and encouraged me and Laura Lahme for sharing and sustaining also stressful times with me.

Special thanks go to Daniel Weber for going through hard times and good times by my side. He is my greatest supporter and always very patient; to know him behind me is invaluable.

14) Curriculum vitae

Der Lebenslauf ist in der veröffentlichten Version aus Gründen des Datenschutzes nicht enthalten.

Der Lebenslauf ist in der veröffentlichten Version aus Gründen des Datenschutzes nicht enthalten.

15) Declarations

Erklärung:

Hiermit erkläre ich, gem. §7 Abs. (2) d) + f) der Promotionsordnung der Fakultät für Biologie zur Erlangung des Dr. rer. nat., dass ich die vorliegende Dissertation selbstständig verfasst und mich keiner anderen als der angegebenen Hilfsmittel bedient, bei der Abfassung der Dissertation nur die angegebenen Hilfsmittel benutzt und alle wörtlich oder inhaltlich übernommenen Stellen als solche gekennzeichnet habe.

Essen, den _____ _____
Unterschrift der Doktorandin

Erklärung:

Hiermit erkläre ich, gem. § 7 Abs. (2) e) + g) der Promotionsordnung der Fakultät für Biologie zur Erlangung des Dr. rer. nat., dass ich keine anderen Promotionen bzw. Promotionsversuche in der Vergangenheit durchgeführt habe und dass diese Arbeit von keiner anderen Fakultät/Fachbereich abgelehnt worden ist.

Essen, den _____ _____
Unterschrift der Doktorandin

Erklärung:

Hiermit erkläre ich, gem. § 6 Abs. (2) g) der Promotionsordnung der Fakultät für Biologie zur Erlangung des Dr. rer. nat., dass ich das Arbeitsgebiet, dem das Thema *„Global chromatin changes induced by altered tonicity interferes with DNA damage response signaling and DNA double-strand break repair“* zuzuordnen ist, in Forschung und Lehre vertrete und den Antrag von Lisa Marie Krieger befürworte und die Betreuung auch im Falle eines Weggangs, wenn nicht wichtige Gründe dem entgegenstehen, weiterführen werde.

Essen, den _____ _____
Unterschrift eines Mitgliedes der Universität Duisburg-Essen